OCS Study
BOEM 2023-080

Development of a Monitoring Program for Water Quality and Biogeochemical Processes of Louisiana Sediment Borrow Areas

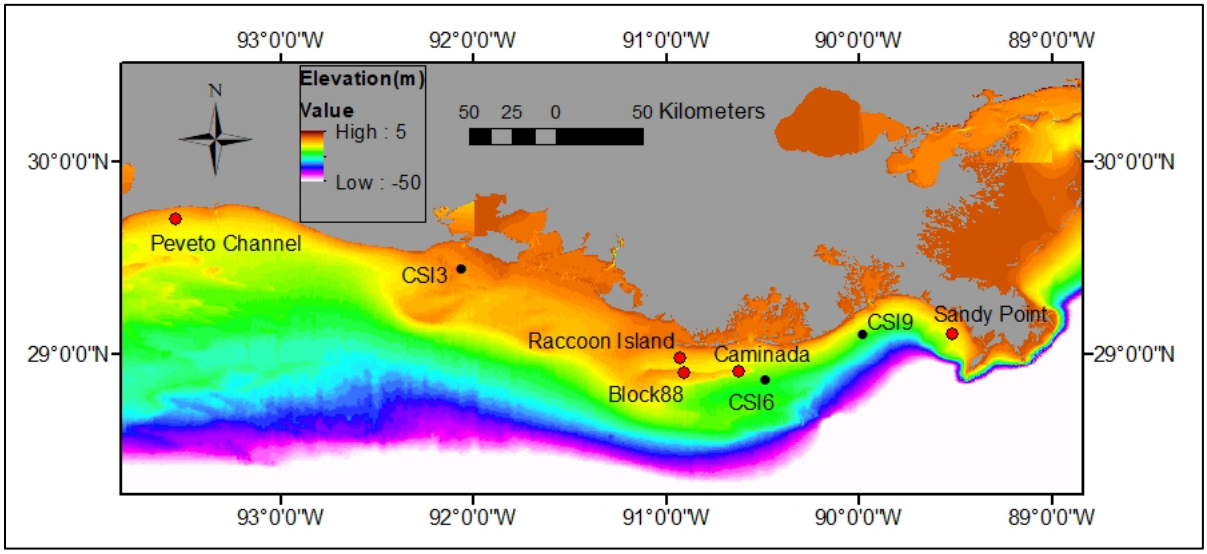

US Department of the Interior
Bureau of Ocean Energy Management
Gulf of Mexico Regional Office
New Orleans, LA

BOEM
Bureau of Ocean Energy Management

OCS Study
BOEM 2023-080

Development of a Monitoring Program for Water Quality and Biogeochemical Processes of Louisiana Sediment Borrow Areas

October 2023

Authors:
Kehui Xu, Kanchan Maiti, Sibel Bargu Ates, Samuel J. Bentley, John White, Carol Wilson, George Z. Xue, Robert Bales, Matthew Barley, Monique Boudreaux, Laura Thompson, Yanda Ou

Prepared under M17AC00019
by
Louisiana State University

93 South Quad Drive
Suite 1002
Baton Rouge, LA 70803

US Department of the Interior
Bureau of Ocean Energy Management
Gulf of Mexico Regional Office
New Orleans, LA

BOEM
Bureau of Ocean Energy Management

DISCLAIMER

Study collaboration and funding were provided by the US Department of the Interior, Bureau of Ocean Energy Management (BOEM), Environmental Studies Program, Washington, DC, under Agreement Number M17AC00019 with Louisiana State University. This report has been technically reviewed by BOEM, and it has been approved for publication. The views and conclusions contained in this document are those of the authors and should not be interpreted as representing the opinions or policies of the US Government, nor does mention of trade names or commercial products constitute endorsement or recommendation for use.

REPORT AVAILABILITY

Download a PDF file of this report at https://espis.boem.gov/Final%20Reports/BOEM_2023-080.pdf.

To search for other Environmental Studies Program ongoing and completed studies, visit https://www.boem.gov/environment/environmental-studies/environmental-studies-information/.

CITATION

Xu K, Maiti K, Bargu Ates S, Bentley S, White J, Wilson C, Xue ZG, Bales R, Barley M, Boudreaux M, Thompson L, Ou Y. 2022. Development of a monitoring program for water quality and biogeochemical processes of Louisiana sediment borrow areas. New Orleans (LA): US Department of the Interior, Bureau of Ocean Energy Management. Obligation No.: M17AC00019. Report No.: BOEM 2023-080. 71 p.

ABOUT THE COVER

Map showing the locations of three mud-capped dredge pits at Peveto Channel, Raccoon Island and Sandy Point and two sandy dredge pits at Caminada and Block 88 in Ship Shoal area. Black dots are LSU WAVCIS (wave-current information system) stations, including CSI3, CSI6, and CSI9.

Contents

List of Figures

List of Tables

List of Abbreviations and Acronyms

Short form	Long form
ADCP	Acoustic Doppler Current Profiler
ADV	Acoustic Doppler Velocimeter
BBB	borrow area biology and biogeochemistry
BOEM	Bureau of Ocean Energy Management
CA	Caminada dredge pit
CDOM	colored dissolved organic matter
chl a	chlorophyll a
COAWST	Coupled-Ocean-Atmosphere-Wave-Sediment Transport Modeling System
CTD	conductivity, temperature, and depth
DO	dissolved oxygen
EPA	Environmental Protection Agency
Gulf	Gulf of Mexico
HPLC	High-Performance Liquid Chromatography
LOI	Loss-on-ignition
LSU	Louisiana State University
MCDP	mud capped dredge pit
MPB	Microphytobenthos
NEMURO	North Pacific Ecosystem Model for Understanding Regional Oceanography
NTU	nephelometric turbidity unit
OCS	Outer Continental Shelf
RFU	relative fluorescent unit
ROMS	Regional Ocean Modeling System
SOC	sediment oxygen consumption
SP	Sandy Point dredge pit
SRP	soluble reactive phosphorus
SSBA	Ship Shoal borrow area
SSC	suspended sediment concentration
TN	total nitrogen
TOC	total organic carbon
WOD	world ocean database

1 Introduction

Barrier islands are elongated, sandy structures that are separated from the mainland by coastal bodies of water. These sandy deposits are critical for protecting wetlands from wave impact (Stone and McBride, 1998) and assisting in the regulation of salinity in back-barrier environments (Otvos, 2011). The combination of natural processes and anthropogenic operations is resulting in devastating environmental changes and land loss of coastal Louisiana (Khalil et al., 2010; Couvillion, 2017). Because barrier islands are highly sensitive to fluctuations in environmental conditions like sea-level and sediment supply, they are placed at high risk of erosion and submergence (Penland et al., 1988; Moore et al., 2014).

In response to the alarming and accelerated erosion of coastal Louisiana, almost 20 billion dollars has been devoted to coastal nourishment projects (CPRA, 2017). Coastal nourishment consists of the removal, or dredging, of sediment from a borrow site, and the delivery of that dredged sediment to another location experiencing erosion. This coastal protection method has proven to be more cost-effective for barrier island preservation and other landward nourishment operations in comparison to the construction of jetties, dikes, and seawalls (Penland and Suter, 1988). As a result, coastal nourishment projects place a demand for large quantities of sand for barrier island restoration and mud for marsh creation (Penland and Suter, 1988). Dredging processes result in unnatural pits and studies have shown these pits may directly or indirectly affect local and adjacent environments (Nairn et al., 2004). This is a concern for scientists, engineers, and decision makers, especially with the implementation of further dredging operations in the northern Gulf of Mexico (Gulf).

Environmental consequences of dredging include alterations of seabed characteristics, morphodynamics, and hydrodynamics which impact water quality and biological communities (Nairn et al., 2004). The most immediate biological effect is benthic habitat disturbance that results from the excavation of sediment. Not only does this impact benthic communities, but also fish and diving birds (Szymelfenig et al., 2006). The dredging processes also result in immediate, temporary increased turbidity from the resuspension of sediment (Palmer et al., 2008) that may impact primary productivity from the interference of light intensity throughout the water column (Nairn et al., 2004; Lehrter et al., 2009). These resuspended sediments may contain contaminants that impact water quality and result in bioaccumulation (Manap and Voulvoulis, 2016). The morphology of a dredge pit can affect hydrodynamic processes like waves and currents (Wang et al., 2018). Alterations of these processes may affect grain size distribution of infilling material, turbidity levels in bottom waters, and enhance stratification (Nairn et al., 2004). Due to possible enhanced stratification, the unnatural depressions may develop hypoxic or anoxic conditions (Palmer et al., 2008) resulting in less productive or uninhabitable environments.

Commonly referred to as the “dead zone,” coastal waters of the northern Gulf develop the largest zone of hypoxia in the western hemisphere, reaching up to 22,000 km^2 during summer (Turner et al., 2008; Bianchi et al., 2010). Defined by waters with dissolved oxygen (DO) levels below 2 mg of O_2 L^{-1}, hypoxia is primarily formed in late spring and summer (Bianchi et al., 2010). This condition results from the combination of (1) enhanced stratification, which limits DO diffusion throughout the water column, and (2) increased respiration in bottom waters due to increased downward flux of organic matter driven by higher primary production in surface waters (Bianchi et al., 2010). Due to high nutrient loading, the development of hypoxia in the northern Gulf is enhanced (Turner et al., 2008). Many dredge pits on the Louisiana shelf, like Caminada and Sandy Point, are located within the general area of seasonal hypoxia and may further amplify the development of the low oxygen condition (Figure 1).

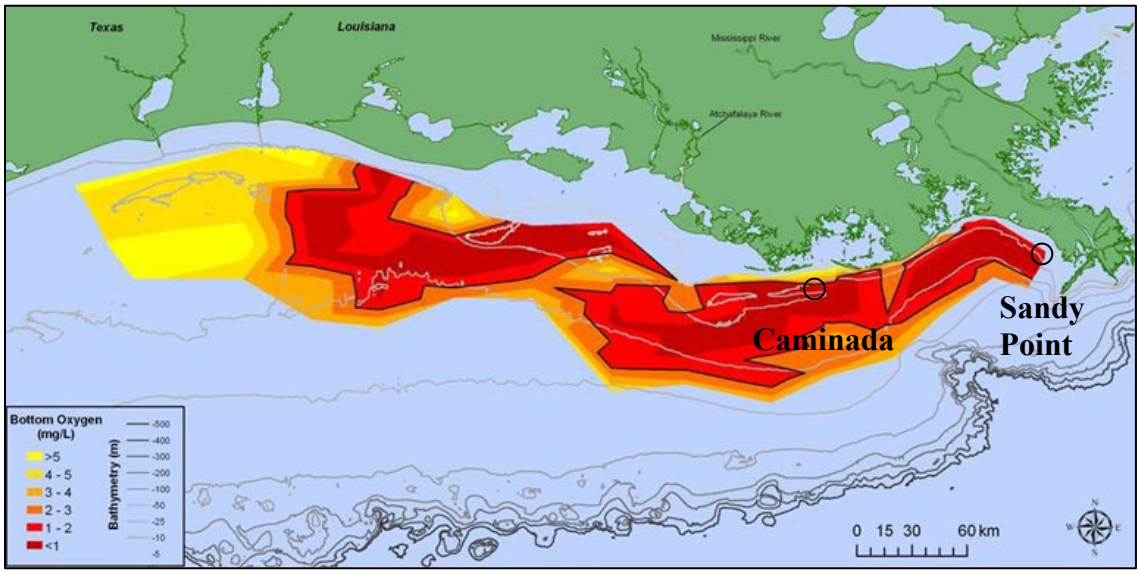

Figure 1. Hypoxia map.

Distribution of bottom water dissolved oxygen July–August 2015 west of the Mississippi River delta. The black line denotes dissolved oxygen less than 2 mg/L. Sandy Point and Caminada dredge pits are marked as blue circles. The map was downloaded from http://www.gulfhypoxia.net/Research/Shelfwide%20Cruises/2015/.

Because the Louisiana seabed is primarily muddy, sand excavation is restricted to sandy shoals and buried paleo river channels (Stone et al., 2004). This results in two primary types of dredge pits on the Louisiana shelf: (1) mud-capped dredge pits (MCDPs), like Sandy Point, and (2) sandy pits, like Caminada. MCDPs result from the excavation of sediment from buried paleo river channels and receive this name due to thick and muddy deposits that commonly cover the ancient channels in the northern Gulf (Robichaux et al., 2020). Sandy pits are dredge sites located in sandy settings like shoals, with Ship Shoal on the Louisiana shelf being a dominant sand resource. Characterized by coarser grain size, it is believed that sandy pits are in more "energetic" environments in comparison to MCDPs. A recent study at Sandy Point dredge pit discovered that current velocities were sluggish in bottom waters of the pit and wave heights were much smaller than those observed outside the pit (Wang et al., 2018). The lower energy conditions of MCDPs may exacerbate hypoxia more severely than sandy pits; however, before this project, limited studies existed to test this hypothesis. The results from this project are used to evaluate post dredging impacts on local water quality and biogeochemical processes.

Nairn et al. (2005) developed a theoretical model illustrating the physical and geological changes impacted by pit morphology. Figure 2 shows the conceptual diagram by Nairn et al. (2005) depicting pit infilling and erosional processes associated with a hypothetical dredge pit. Due to the increase in depth, current velocities decrease directly over the pit. Because sediment load capacity is proportional to flow velocity, sedimentation occurs inside the pit and results in pit infilling and a decrease in sediment load of the flow. As the flow exits the pit, a reduction in water depth causes the flow velocity to increase due to the conservation of mass. Thus, the sediment capacity increases. As a result, the outgoing margin of the pit is eroded to bring the suspended sediment concentration and sediment load capacity to an equilibrium.

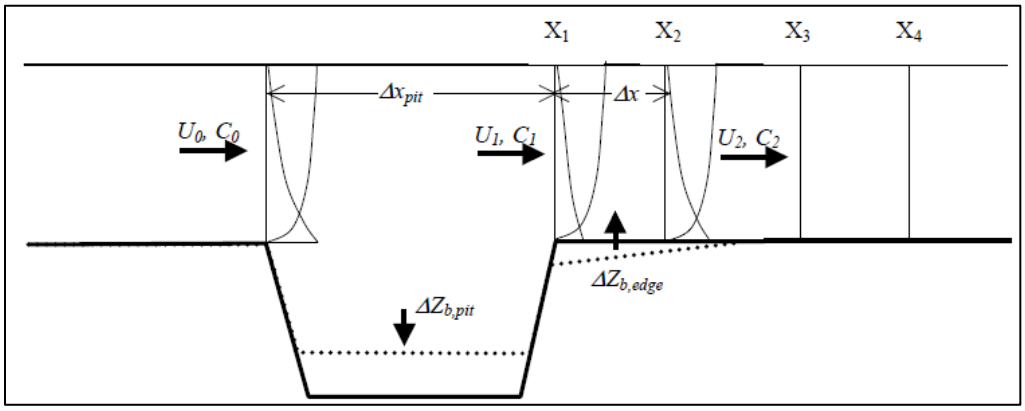

Figure 2. Pit infilling diagram.

Pit infilling and pit margin erosion processes conceptual diagram (from Nairn et al., 2005). U is velocity, C is sediment concentration, X is distance from pit edge and Z is elevation change.

Changes in hydrologic and geologic processes associated with pit morphology shown in Figure 2 likely impact changes in the water column and seafloor of a dredge pit. The impacts may be harmful to the local ecosystem. We developed a preliminary conceptual model depicting these potential changes and conducted various studies to improve the model. Figure 3 illustrates that the hydrologic processes associated with the increased depth of a pit (decreased current velocities and wave orbit) may limit vertical mixing throughout the water column. The limited mixing and general increased depth will likely enhance water column stratification and prohibit oxygen diffusion and reduce oxygen transport from surface to bottom water columns. As a result, hypoxic conditions will form. Hydrologic processes may develop a slower flow inside the dredge pit, resulting in finer grained material infilling it (Johnston, 1981). Previous studies verify the deposition of finer grained material inside dredge pits in comparison to adjacent seafloors (Jutte et al., 2002; Wang et al., 2018). A change in surficial sediment grainsize may impact benthic communities because of habitat alteration (Nairn et al., 2004; Palmer et al., 2008). Moreover, finer grained material contains relatively higher concentrations of heavy metals (Cu, Pb, Hg, etc.) and organic contaminates (PAHs, DDTs, PCBs) when comparing to coarser sediment because of their greater surface areas and organic matter content (Stantschi et al., 2001). Shown in Figure 3, a flux of organic matter inside dredge pits has also been observed in previous studies (Graca et al., 2004; Wang et al., 2018). The deposition of organic matter enhances hypoxic or anoxic conditions of a dredge pit's bottom waters. Such changes in sedimentation and water chemistry can also impact the sediment biogeochemical and microbial processes and introduce variability in benthic fluxes and organic matter preservation potential (Figure 3). We thus expect increased benthic fluxes of redox sensitive species, higher sediment oxygen demand and denitrification rates, and enhanced microbial activity in the dredge pits.

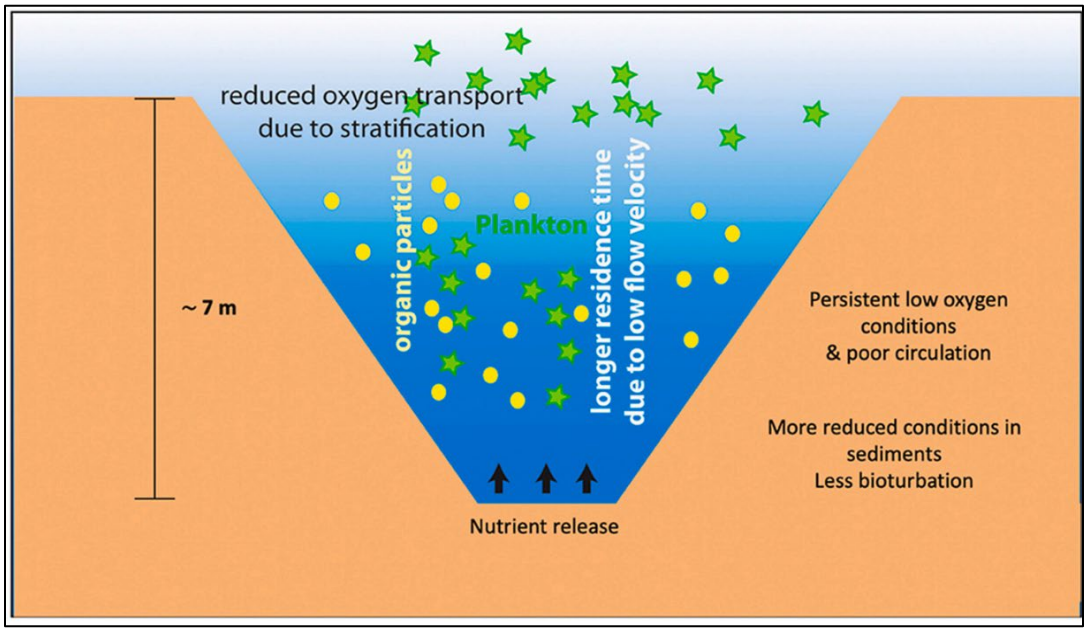

Figure 3. Pit Conceptual Model.

A preliminary conceptual model of biogeochemical processes in a dredge pit (from Thompson et al., 2021).

2 Objectives

This project, *Development of a Monitoring Program for Water Quality and Biogeochemical Processes of Louisiana Sediment Borrow Areas* (abbreviated as Borrow area Biology and Biogeochemistry, BBB), was built on two previous BOEM-funded dredge pit studies: *Assessment of Mud-Capped Dredge Pit Evolution on the Outer Continental Shelf of northern Gulf of Mexico* (MCDP; BOEM OCS Study 2022-006) and *Assessment of Ship Shoal Borrow Areas for Coastal Restoration of Louisiana Barrier Islands* (SSBA; agreement M16AC00018). The MCDP project (2014–2018) focused on Peveto Channel, Raccoon Island, and Sandy Point dredge pits (locations in Figure 4) to observe the long-term morphologic evolution of mud-capped dredge pits. The SSBA project (2016–2021) focused on Caminada and Block 88 (locations in Figure 4) to evaluate physical and geological processes of two sandy pits on Ship Shoal.

The BBB project leveraged resources from previous projects and expanded upon the effects that physical changes may have on hydrodynamics, water quality, and biogeochemical processes at Caminada and Sandy Point dredge pits. Caminada pit has been dredged in multiple increments and the most recent excavation was in 2016 (Liu et al., 2019). The primary goal of this study was to observe the early stages of post dredging impacts on water quality and biogeochemistry. Because Nairn et al. (2005) predicted that it takes only three to five years to fill some sandy pits, this project was time-sensitive and data collection was completed within a short period (spring 2018–summer 2019).

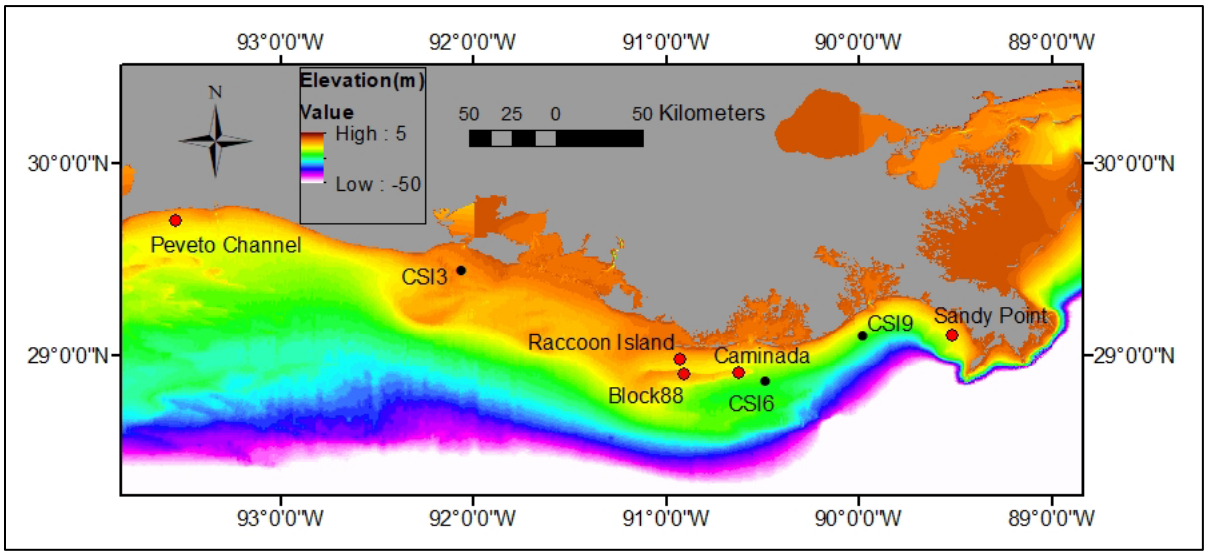

Figure 4. Base map.

Map showing the locations of three mud-capped dredge pits at Peveto Channel, Raccoon Island and Sandy Point and two sandy dredge pits at Caminada and Block 88 in Ship Shoal area. Black dots are LSU WAVCIS (wave-current information system) stations, including CSI3, CSI6, and CSI9.

3 Methods

There are two main study areas in this project: inside and outside of Sandy Point (SP) dredge pit as well as inside and outside of Caminada (CA) dredge pit. The dredge pit in South Pelto Blocks 12 & 13 on eastern Ship Shoal was used for Caminada-Moreau Headland restoration project (Figure 5). Thus Caminada pit is also called South Pelto pit in some recent publications. Sandy Point pit was used for the Pelican Island restoration project in the eastern shelf of Louisiana (Figure 6). Stations inside the pits are generally labeled with "IN" for easier identification. The names of two tripod stations are T1 and T2 for both CA and SP pits.

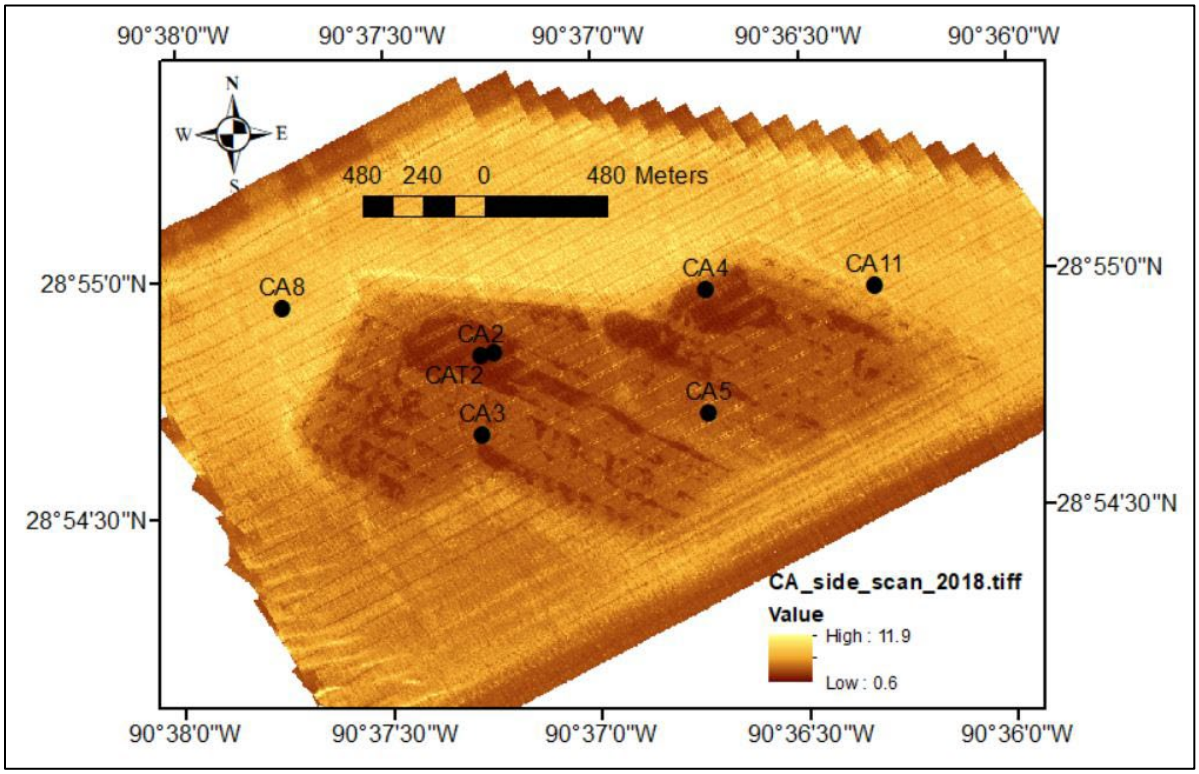

Figure 5. Caminada dredge pit.

Coring locations for Caminada dredge pit overlying sidescan sonar imagery taken in 2018.

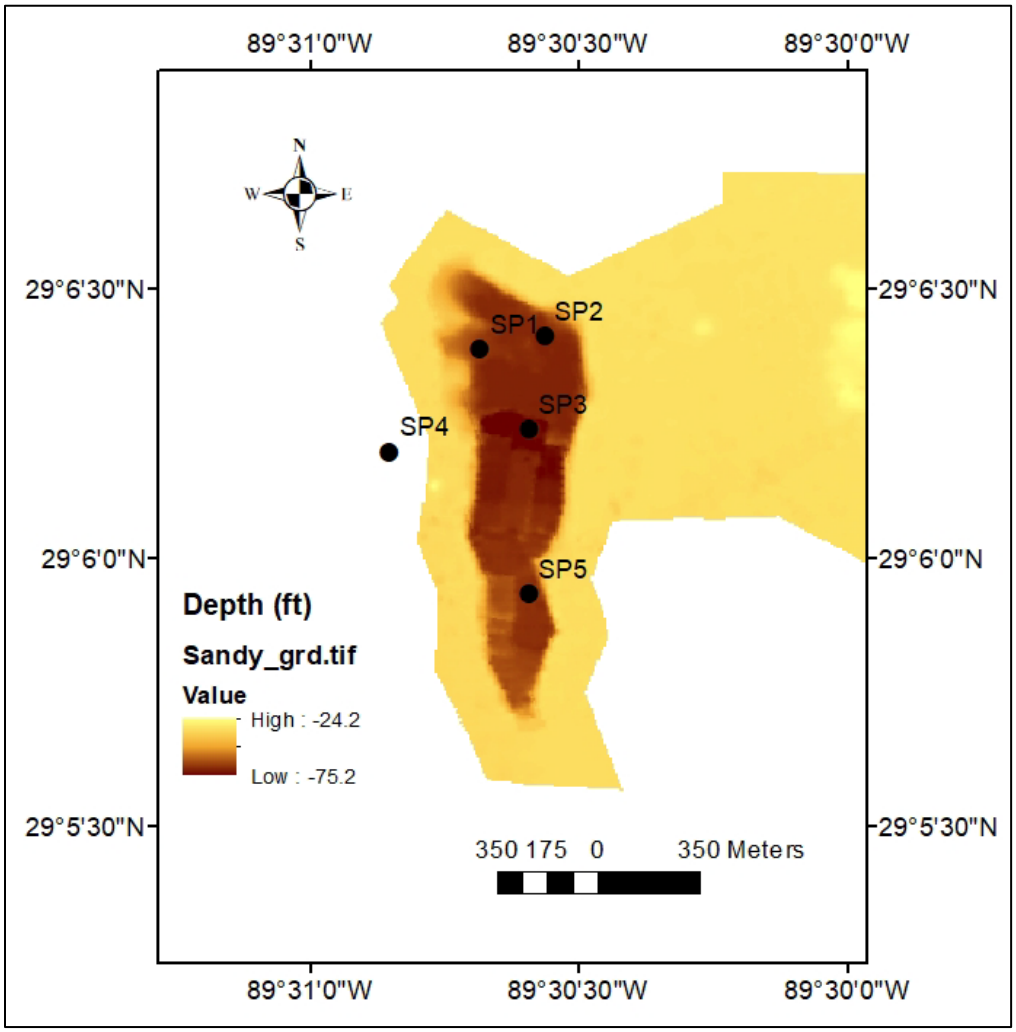

Figure 6. Sandy Point dredge pit.

Coring locations of Sandy Point pit and bathymetric map. Bathymetric data were collected in 2012 after sand excavation.

3.1 Vessel-based Water Sampling and Profiling

3.1.1 CTD Profiling

Vertical profiles of dissolved oxygen (DO), temperature, salinity, turbidity, and chlorophyll a were recorded during two fieldtrips to Caminada pit in 2018 and 4 trips to Sandy Point pit in 2019. The location, date, and sampling parameters of these profiling casts are in Tables 1 and 2.

3.1.2 Water Sampling

The Caminada pit was sampled inside and outside of the dredge pit during spring (May) and summer (July) of 2018 and Sandy Point borrow pit was sampled during spring (May) and late summer (September) of 2019 for determining environmental conditions and collect water and sediment core samples. Samples were taken at four stations, two within the borrow area (inside - IN stations) and two outside of the borrow area.

Water samples were collected using a five-liter Niskin bottle at each station at surface (one meter below the surface) and bottom (one meter above the seafloor) water depths and stored in clean one-liter polypropylene bottles in the dark on ice for later chemical and biological analyses in a laboratory.

Fifteen milliliter subsamples were taken from each one-liter bottle at each depth for analysis of NO_2 + NO_3, NH_4, PO_4 (soluble reactive phosphorus or SRP). A Ponar grabber was used to collect surficial sediment in both CA and SP pits. Intact sediment cores were collected via a multicorer using 10 cm diameter polycarbonate core tubes (with length of 58 cm) from inside and outside stations. A box corer was utilized when substrate was mostly sand and could not be penetrated with a multicorer; the same core tubes were used to collect subsamples from box corer.

Loss on ignition (LOI) was performed in a lab on sediment samples to estimate organic matter (Heiri et al., 1999). A grain size analysis was conducted on 12 subsamples of collected sediments from corresponding tripod locations following the method of Xu et al. (2016). HydroCAT turbidity data were calibrated from Nephelometric Turbidity Unit (NTU) to mg L^{-1}, providing suspended sediment concentration (SSC). Lastly, water samples were collected at sea surface using 2-L bottles during tripod deployments and retrievals at both CA and SP pits. Water samples were transferred to a lab and later filtered to calculate suspended sediment concentration (SSC).

Over the lifespan of this project, a total of 26 pairs of cores were extracted for radionuclide and grain size analysis from CA and SP borrow areas from September 2018 through September 2019 using the R/V *Coastal Profiler* from LSU and R/V *Acadiana* from LUMCON. Five coring locations were targeted at CA and six coring locations targeted at SP, including multiple sites located inside the pits along with 1-2 sites located outside the pits (Figures 5 and 6). Of these pairs, one was selected for radionuclide and grain size analysis and the other for x-ray analysis of sedimentary structures. Methods for radionuclide and grain size analysis is briefly outlined below; details can be found within Zehao Xue's M.S. thesis (2019) and Matthew Barley's M.S. thesis (2020).

Cores were extracted using an Ocean Instruments MC400 multicorer, which extracts sediment cores to ~ 0.5 m below the sediment-water interface. One core was extruded into 2 cm sections on deck (sealed in plastic Whirl-Paks ®) and samples were transported to LSU where they were subsampled for grain size and radiochemical analysis, weighed for water content, and refrigerated. The second core was sampled for x-radiography (methods described in subsequent section). Short-term sedimentation rates were calculated using the radionuclide Beryllium-7 (^{7}Be) which has a half-life of 53.3 days (Kaste and Baskaran, 2011). Once deposited on the Earth's surface, ^{7}Be forms strong bonds with oxygen atoms, so it adsorbs rapidly onto organic and inorganic solids in terrestrial environments, making it an excellent tracer of fluvial-derived, short term (< 6 months) sediment accumulation in shallow marine environments (Baskaran et al., 1993; Kaste and Baskaran, 2011), including the Louisiana continental shelf (Keller et al., 2016; Restreppo et al., 2019). For this analysis, core samples were immediately weighed and subsequently dehydrated to determine water saturation. Samples were then pulverized using a mortar and pestle and packed into petri dishes (50 × 9 mm) to be analyzed for approximately 24 hours on Canberra BEGe, LEGe, and REGe low-background planar gamma detectors housed at LSU. The presence of ^{7}Be was distinguished by a peak at 477 keV. Inventory of ^{7}Be for each core (disintegrations per minute per square centimeter, or dpm cm^{-2}) and short-term sedimentation rates (cm yr^{--1}) were then calculated. More detailed information can be found in two M.S. theses that were produced from this study, from Zehao Xue (2019) and Matthew Barley (2020).

Grain size analysis was performed on samples after deflocculation using a Beckman Coulter Laser Diffraction Particle Size Analyzer housed at LSU. SigmaPlot was used to generate volume-frequency contour plots for distribution of grain size in microns for all samples from all cores. The software Strater

4 was used to make stratigraphic columns that correlate with grain size volume-frequency plots for each multicore.

3.1.3 Core Biological Analysis

Samples for total organic carbon and total nitrogen were collected and analyzed via a Costech 1040 Elemental Combustion Analyzer according to EPA method 440 using high temperature combustion. The top 10 cm of each core was sliced into two-centimeter increments and each increment of sediment was used for the analysis to determine percent contribution of carbon and nitrogen to the total sample. Each 2 cm section was analyzed, and the average was used due to no significant differnce found. Subsamples from each slice were dried at 50 °C using a Fisher Scientific Isotemp Incubator. Weights were recorded for each sediment subsample prior drying and removed from the drying oven once a constant weight was reported after at least a 24-hour period to ensure all moisture was removed from the sample. Sample weights were recorded after constant weight was achieved. Dried sediment samples were grounded using a traditional mortar and pestle and homogenized using a 125 µm sieve. Samples were weighed out into Costech silver capsules and fumigated in a vacuum-sealed glass desiccator alongside 12N hydrochloric acid (HCl) for 12 hours to remove all inorganics (Hedges et al. 1984).

Sediment cores were taken at each station and the top 0.5 cm sliced were placed into 50-mL centrifuge tubes, placed on ice, and kept in the dark. Samples were preserved in 2% glutaraldehyde upon arrival to laboratory and kept at 4°C until further microscopy and chl a analysis. Sediment chl a concentrations were determined at all stations as an estimate of microphytobenthos (MPB) biomass. Samples were frozen at -20°C upon arrival to the lab for further analysis. Once thawed, the samples were mixed well using a small spatula and weighed so that each sample is ~ 3-4 grams. For extraction, 92% acetone was added to each sample and shaken to mix well. Each sample was sonicated at an amplitude intensity of 25% for 30 seconds and allowed to rest for ~16 hours in the refrigerator. Fluorescence was measured in extracted samples before and after acidification with HCl using a Turner 10-AU fluorometer in low light according to adapted from Dalsgaard et al. (2000). Microscopy observations were performed using an Axio Observer – A1 inverted microscope (Axiovert 135, Zeiss) using a Sedgewick-Rafter slide to identify the most dominant MPB species.

3.1.4 Core Biogeochemical Analysis

Temperature-controlled, continuous-flow intact sediment core incubations were used to evaluate sediment-water interface exchanges of nutrients for each station. Sediment cores were carefully filled along the sidewall, for minimum disturbance, with in situ filtered water until it overflowed the top of the core tube and no air bubbles were visible. Each tube was capped with custom designed PVC lids and brought to an adjusted water height of 20–25 cm from the sediment surface to ensure a uniform water column volume among all cores. The custom PVC lids are fitted with two O-rings for gas tight incubations and include one tube attachment for the corresponding water reservoir, one tube attachment for sample extraction, and two tube attachments that connect to each other in a peristaltic pump, allowing continuous flow and circulation in the core for the entire duration of the incubation (Upreti et al., 2019; Ghaisas et al., 2019). Sediment cores were then immediately submerged into the temperature-controlled water baths. Reservoir tanks along with the incubation water bath were covered to ensure no allowance of primary production (i.e., dark incubation). The incubation continued until dissolved O_2 in the cores fell below 1.0 mg L^{-1}, and total incubation periods ranged from 16–60 hours depending on dissolved O_2 concentrations which was associated with substrate quality.

Water samples were collected every 4–6 hours by releasing ~10 mL of the “dead volume” water in the tubing at each time interval before collecting samples. Gravity-driven water replenishment from the reservoir allowed the simultaneous collection of water sample and water refill within the core without any introduction of O_2 (Hopkinson et al. 1999; Upreti et al. 2019). Both N_2 and O_2 samples were collected

using Labco septa vials, where water could overflow the vial in order to remove air bubbles, and O_2 was immediately measured at collection using a Presens Microx 4 O_2 sensor. Nutrient samples were collected by filtration (GF/F syringe filter 0.45 μm) into 20 mL plastic scintillation vials and stored in a freezer until analysis. Nutrients NH_4 (EPA method 350.1; USEPA, 1993), NO_2+NO_3 (EPA method 353.4; Zhang et al., 1997), and PO_4 (EPA method 365.1; USEPA, 1993) were analyzed using a Seal Analytical auto analyzer. Dissolved silica was processed using the silico-molybdate colorimetric method outlined in Strickland and Parsons (1968) and analyzed using an ultraviolet-visible spectrophotometer. All nutrient concentrations were corrected during flux calculations for minor sample volume withdrawn during sampling intervals. Positive fluxes indicate a flux from the sediments to the overlying water column, while negative fluxes indicate nutrients being taken from the overlying water column. Sediment oxygen consumption (SOC) is presented as a positive flux.

Total organic carbon analysis (TOC) of top 10 cm from the sediment slices were subsampled, weighed, and dried at 50 °C using a Fisher Scientific Isotemp Incubator. The dried sediment samples were then homogenized by sieve after grinding using a traditional mortar and pestle. Samples were weighed into Costech silver capsules and placed in a vacuum glass desiccator for fumigation with 12N hydrochloric acid (HCl) for 12 hours to remove inorganic carbon (Hedges et al 1984). Samples were then repacked into tin capsules to ensure no loss of sample and analyzed on a Costech 1040 CHNOS Elemental Combustion system (EPA method 440.0) using high temperature combustion.

3.2 Tripod

Two tripods assembled by the Field Support Group of Coastal Studies Institute of Louisiana State University were deployed 07 August–14 September 2018 at CA dredge pit and 13 June-30 July 2019 at SP dredge pit, each deployment with a duration of approximately 1.5 months. At both dredge pits, tripods were deployed both outside and inside the pits. Tripod deployment stations at CA are identified as CAT1_OUT and CAT2_IN while SP stations are identified as SPT1_OUT and SPT2_IN where T1 and T2 stand for tripod and IN and OUT are for locations. Several acoustic and optical sensors were mounted on each tripod, including an upward-looking ADCP (Acoustic Doppler Current Profiler), HydroCAT, ADV (Acoustic Doppler Velocimeter), and a wave gauge.

During tripod deployments at CA pit, the eye of Hurricane Gordon passed over the Gulf near Mississippi-Alabama border from 3 September to 4 September 2018. Likewise, Tropical Storm Barry passed over the Gulf to Marsh Island, Louisiana from 12 July to 13 July 2019. Unfortunately, no ADV or ADCP data were recovered at station SPT2_IN due to rapid tripod burial by Tropical Storm Barry. Sensors collected temperature, salinity, SSC, DO, chlorophyll a, wave height, and vertical current velocities (Karimpour and Chen, 2017). Analysis methods using MATLAB produced wave induced shear stress, current induced shear stress, and wave-current combined induced shear stress (Soulsby and Dyer, 1981; Wright, 1995; Kim et al., 2000; Whitehouse et al., 2000; Wiberg and Sherwood, 2008; Xu et al., 2016).

3.3 Geophysical Work

An Edgetech 4600 swath bathymetry and sidescan sonar system were used to collect data with a swath width up to 8 times the water depth. The 4600-system produced real-time high-resolution three-dimensional maps of the seafloor while providing co-registered simultaneous sidescan and bathymetric data. Seafloor features, such as pit edges, failure scarps, and bedforms as small as 10-20 cm could be imaged.

3.4 Modeling Work

A 5km coupled hydrodynamic-biological model embedded in the ocean-atmosphere-wave-and-sediment transport (COAWST) modeling system (Warner et al., 2008, 2010) was conducted for the entire Gulf of Mexico (GOM_5km). We focused on biogeochemical and bottom oxygen conditions in the northern Gulf especially area near the Mississippi River plume and the Atchafalaya River plume. We decided to use the GOM_5km model, instead of the nGOM_1km model, due to that 1) the latter was faster in computation due to lower horizontal resolution allowing faster model calibration and validation; 2) hydrodynamics in the northern Gulf region were less affected by boundary effects in the latter model than in the former one; 3) the latter had more vertical layers (36 layers) than the former (18 layers) enabling better estimates in water stratification and vertical dynamics.

The Regional Ocean Modeling System (ROMS; Shchepetkin and McWilliams, 2005; Haidvogel et al., 2008) was used for simulation of hydrodynamics in the GOM; while the biogeochemical model was largely built on the North Pacific Ecosystem Model for Understanding Regional Oceanography (NEMURO; Kishi et al., 2007), which incorporated both nitrogen and silicon flows. We added a phosphorus flow and an oxygen flow into the NEMURO model. Specifically, the oxygen flow included a dissolved oxygen (DO) cycle in water column and a sediment oxygen consumption (SOC) scheme followed Fennel et al.'s (2006) equations. The DO cycle in water column considered oxygen sources terms by photosynthesis of phytoplankton; oxygen sink terms due to respiration of phytoplankton and zooplankton, and aerobic decomposition of particulate and dissolved organic matter by bacteria, and nitrification of ammonium to nitrate; oxygen exchanges between atmosphere and surface ocean. The SOC scheme applied considered a combined effect of remineralization of particulate organic matter, nitrification, and denitrification (detailed formulations could be found at Fennel et al., 2006). Fifteen state variables were included in the model: nitrate, ammonium, phosphate, two types of phytoplankton (small and large), three types of zooplankton (microzooplankton, mesozooplankton and predatory zooplankton), particulate and dissolved nitrogen, particulate and dissolved phosphorus, particulate silica, silicic acid concentration and DO concentration. For better estimates on the biological fields, 63 rivers along the coastal area of the Gulf were added as point sources in the GOM_5km model. They transport horizontal momentums, salinity, temperature, nitrate, ammonium, phosphate, silicic acid, particulate and dissolved nitrogen, particulate and dissolved phosphorus, and DO to the computational domain in a daily interval.

4 Results

4.1 Vessel-based Water Sampling and Profiling

4.1.1 CTD Profiling

CTD casts at both Caminada and Sandy Point pits are summarized in Tables 1 and 2. Profiling results show stable SSC throughout water column and some slight increase in bottom boundary layer (BBL) of several CA stations in May and July (Figure 7). This may indicate that sediment source was likely a result of resuspension of sediment from pit bottom and/or slow settling and accumulation of fine-grained sediment or some organic matter. Likewise, chlorophyll a also increased with depth. The elevated SSC at surface for SP stations is likely due to the turbid Mississippi river plume (Figure 8).

DO was highest in surface waters and lowest in bottom waters for all six stations at CA dredge pit (Figure 7). No hypoxic waters were observed at out of pit stations at CA. Overall, chlorophyll a was lowest at surface and highest near seabed for all CA stations (Figure 7). Likewise, surface waters were more saturated with DO and decreased with depth at SP (Figure 8). There were no major differences in DO levels between inside and outside stations at SP dredge pit (Figure 8). Overall, chlorophyll a concentrations were highest in surface to middle waters for all stations at SP and decreased greatly in waters near seabed (Figure 8).

Furthermore, CA stations contained highest chlorophyll a at lower depths while chlorophyll a at SP was restrained to the upper water column (Figures 7 and 8). These differences are likely due to high SSC at surface associated with the Mississippi River plume and SP's proximity to the Mississippi River Delta. Relatively higher DO measurements at CA8 and CA11 are likely due to the more energetic condition on the shallower crest of Ship Shoal. The lower energy associated with the dredge pit promotes the deposition of finer grained material like organic matter, including phytodetritus, which enhances respiration within the BBL and sediments.

Table 1. CTD casts at Caminada Pit

Station	Date of Year 2018	Depth (m)	Temp (Celsius)	Salinity	Turbidity (NTU)	Chl a (RFU)	DO (mg/L)
CA2_IN 28°54.616" N 90° 37.293" W	5 May	X	X	X	X	X	X
CA2_IN	12 July	X	X	X	X	X	X
CA5_IN 28° 54.744"N 90° 36.654"W	5 May	X	X	X	X	X	X
CA5_IN	12 July	X	X	X	X	X	X
Station	**Date of Year 2018**	**Depth (m)**	**Temp (Celsius)**	**Salinity**	**Turbidity (NTU)**	**Chl a (RFU)**	**DO (mg/L)**
CAEXTRA_IN 28° 54.687" N 90° 36.972" W	5 May	X	X	X	X	X	X
CAEXTRA_IN	12 July	X	X	X	X	X	X
CAT2_IN 28°54.569"N 90°36.924"W	5 May	X	X	X	X	X	X

Station	Date of Year 2018	Depth (m)	Temp (Celsius)	Salinity	Turbidity (NTU)	Chl a (RFU)	DO (mg/L)
CAT2_IN	12 July	X	X	X	X	X	X
CA8_OUT 28° 54.977"N 90° 37.693"W	5 May	X	X	X	X	X	X
CA8_OUT	12 July	X	X	X	X	X	X
CA11_OUT 28° 55.1721"N 90° 36.305"W	5 May	X	X	X	X	X	X
CA11_OUT	12 July	X	X	X	X	X	X
CAT1_OUT 28°56.595"N 90°36.924"W	5 May	X	X	X	X	X	X
CAT1_OUT	12 July	X	X	X	X	X	X

Casting parameters, location, and date at CA dredge pit (x=measured)

Table 2. CTD casts at Sandy Point Pit

Location	Site	Date of Year 2019	Depth (m)	Temp (ºC)	Salinity	Turbidity (NTU)	Chl a (RFU)	DO (mg/L)
Inside	SP3_IN 29° 06.231" N 89° 30.563" W	16 May	x	x	x	x	X	x
Inside	SP3_IN	12 June	x	x	x	x	X	x
Inside	SP3_IN	30 July	x	x	x	o	O	o
Inside	SP3_IN	8 September	o	o	o	o	O	o
Inside	SP5_IN 29° 05.894" N 89° 30.516" W	16 May	x	x	x	x	X	x
Inside	SP5_IN	12 June	x	x	x	x	X	x
Inside	SP5_IN	30 July	x	x	x	o	O	o
Inside	SP5_IN	8 September	x	x	x	x	X	x
Outside	SP4_OUT 29° 06.189" N 89° 30.920" W	16 May	x	x	x	x	X	x
Location	**Site**	**Date of Year 2019**	**Depth (m)**	**Temp (ºC)**	**Salinity**	**Turbidity (NTU)**	**Chl a (RFU)**	**DO (mg/L)**
Outside	SP4_OUT	12 June	x	x	x	x	X	x
Outside	SP4_OUT	30 July	x	x	x	o	O	o
Outside	SP4_OUT	8 September	x	x	x	x	X	x
Outside	SP11_OUT 29° 07.833" N 89° 31.232" W	16 May	x	x	x	x	X	x
Outside	SP11_OUT	12 June	x	x	x	x	X	x
Outside	SP11_OUT	30 July	x	x	x	o	O	o

Location	Site	Date of Year 2019	Depth (m)	Temp (ºC)	Salinity	Turbidity (NTU)	Chl a (RFU)	DO (mg/L)
Outside	SP11_OUT	8 September	x	x	x	x	X	x
Outside	SPT1_OUT 29° 08.361" N 89° 31.287" W	16 May	x	x	x	x	X	x
Outside	SPT1_OUT	12 June	x	x	x	x	X	x
Outside	SPT1_OUT	30 July	x	x	x	o	O	o
Outside	SPT1_OUT	8 September	x	x	x	x	X	x

Casting parameters, location, and date at SP dredge pit (x=measured, o=not measured).

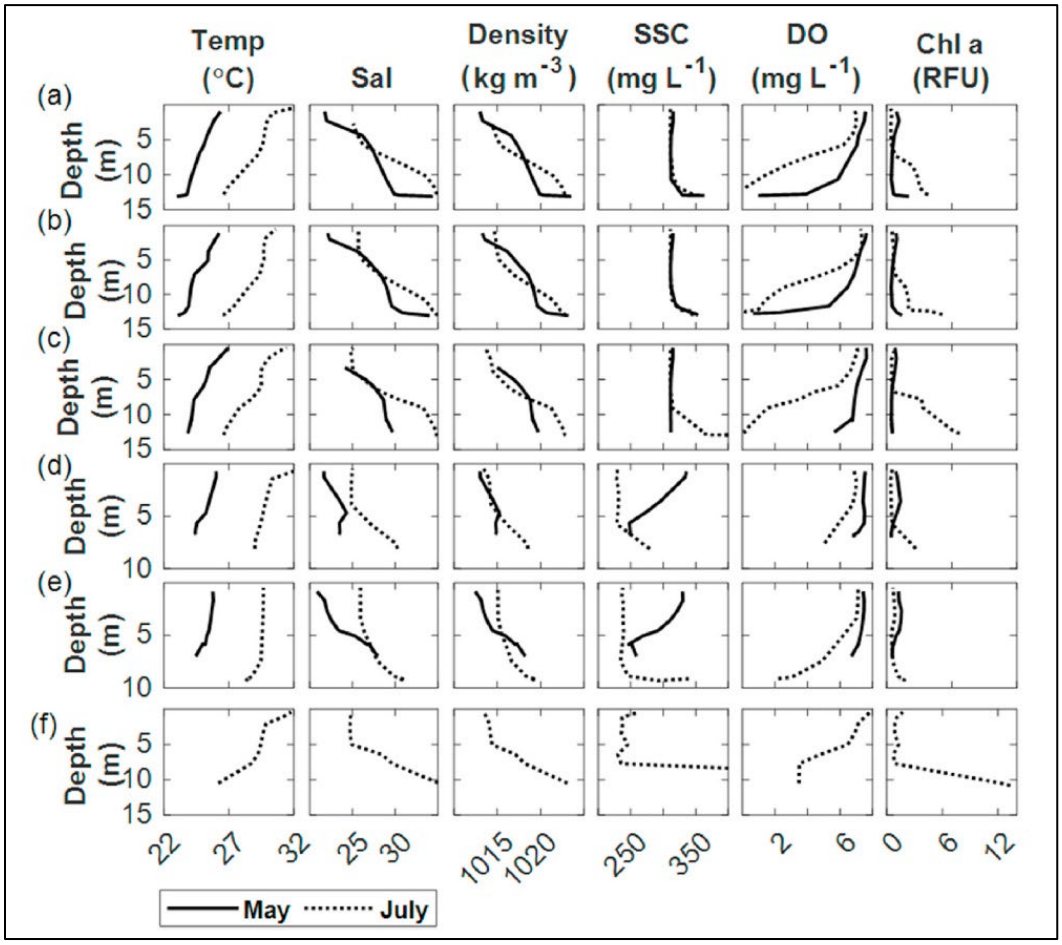

Figure 7. Vertical profiles from Caminada pit.

Vertical profiles of temperature, salinity, density, DO, SSC, and chlorophyll a (in relative fluorescent units (RFU)) from May and July 2018 at stations (a) CA2_IN; (b) CA5_IN; (c) CAT2_IN; (d) CA8; (e) CA11; (f) CAT1 (from Bales et al., 2021).

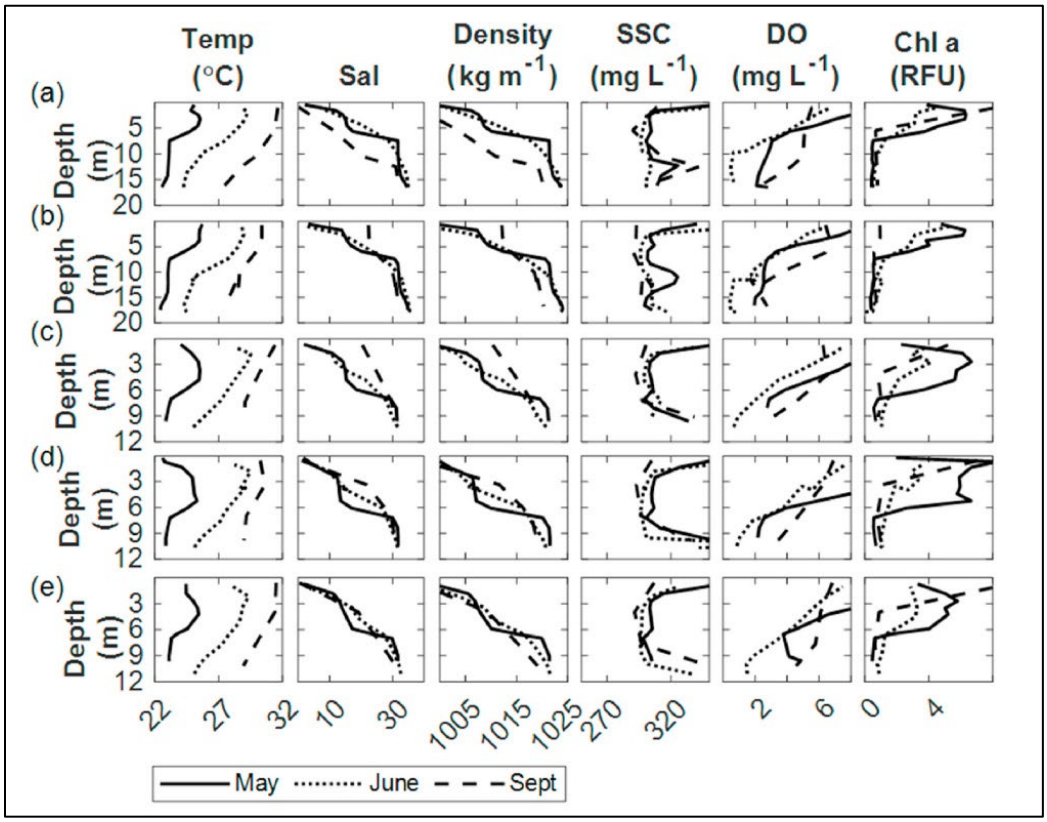

Figure 8. Profiles from Sandy Point dredge pit.

Vertical profiles of temperature, salinity, density, DO, SSC, and chlorophyll a from May, June, and September 2019 at stations (a) SP5_IN; (b) SP3_IN; (c) SPT1; (d) SP11; (e) SP4 (from Bales et al., 2021).

4.1.2 Water Sampling

The Caminada pit had higher spring concentrations of dissolved inorganic nutrients in the surface water samples compared to summer and the opposite was true for the summer, where bottom-water nutrient concentrations were higher than surface waters, shown in Table 3. Nitrate + nitrite ($NO_2 + NO_3$) concentrations for spring were significantly higher in the surface waters when compared to bottom water samples ($p = 0.01$) and no significant differences were detected for summer samples ($p > 0.05$). Ammonium (NH_4) concentrations were significantly higher in the bottom water when compared to surface water for all stations and seasons ($p = 0.005$). Phosphate (PO_4) values were similar between seasons and consistently higher values were detected at depth. Silica (SiO_2) concentrations were higher at the surface water during the spring compared to summer surface concentrations ($p = 0.002$) and remained low in the bottom water in spring at all stations, however, bottom water SiO_2 concentrations significantly increased during the summer inside the pit when compared to outside pit stations ($p = 0.001$) (Table 3).

Table 3. Summary of dissolved inorganic nutrients from the Caminada Dredge Pit

		Spring				Summer			
Station	**Depth**	**NO_2+NO_3 (µM)**	**NH_4 (µM)**	**PO_4 (µM)**	**SiO_2 (µM)**	**NO_2+NO_3 (µM)**	**NH_4 (µM)**	**PO_4 (µM)**	**SiO_2 (µM)**
CA2_IN	Surface	1.89	18.32	0.32	10.33	0.89	14.36	0.26	4.17

		Spring				Summer			
Station	**Depth**	**NO_2+NO_3 (µM)**	**NH_4 (µM)**	**PO_4 (µM)**	**SiO_2 (µM)**	**NO_2+NO_3 (µM)**	**NH_4 (µM)**	**PO_4 (µM)**	**SiO_2 (µM)**
	Bottom	0.24	20.89	0.1	1.82	0.31	27.22	1.68	35.25
CA5_IN	Surface	1.4	bd	0.26	10.02	0	13.96	0.26	6.34
	Bottom	0.28	14.19	0.19	1.84	8.57	18.52	1.29	33.05
CA8	Surface	2.1	7.66	0.29	12.48	0.33	5.68	bd	0
	Bottom	0.49	20.6	0.26	2.91	0.35	13	0.26	0
CA11	Surface	1.37	bd	0.29	10.93	0.06	9.02	0.1	1.89
	Bottom	1.3	14.15	0.32	1.92	1.3	17.72	0.32	1.92

Summary of dissolved inorganic nutrients (µM) from water samples collected during spring and summer of 2018, NO_2+NO_3 = Nitrate + Nitrite, SiO_2= Silica, NH_4= ammonium, 'bd' indicated samples were below detection.

The chl a concentrations in the surface water were higher in the spring at all stations (2.12 ± 0.85 µg chl a L^{-1}) compared to bottom water (0.55 ± 0.07 µg chl a L^{-1}) (Figure 9). Additionally, surface water chl a concentrations were lower in summer compared to the spring for all stations with a mean value of 0.73 ± 0.36 µg chl a L^{-1}. The highest values of bottom water chl a were recorded inside the pit (stations CA2_IN and CA5_IN) during the summer, averaging 4.87 ± 0.15 µg chl a L^{-1}, about four times greater than the bottom values from the spring. Chl a was positively correlated with N+N and SiO_2 in the spring ($p = 0.01$ and $p < 0.001$, respectively), whereas chl a was positively correlated with NH4, SiO_2 and PO_4 in the summer ($p < 0.001$, $p = 0.04$, and $p < 0.001$, respectively).

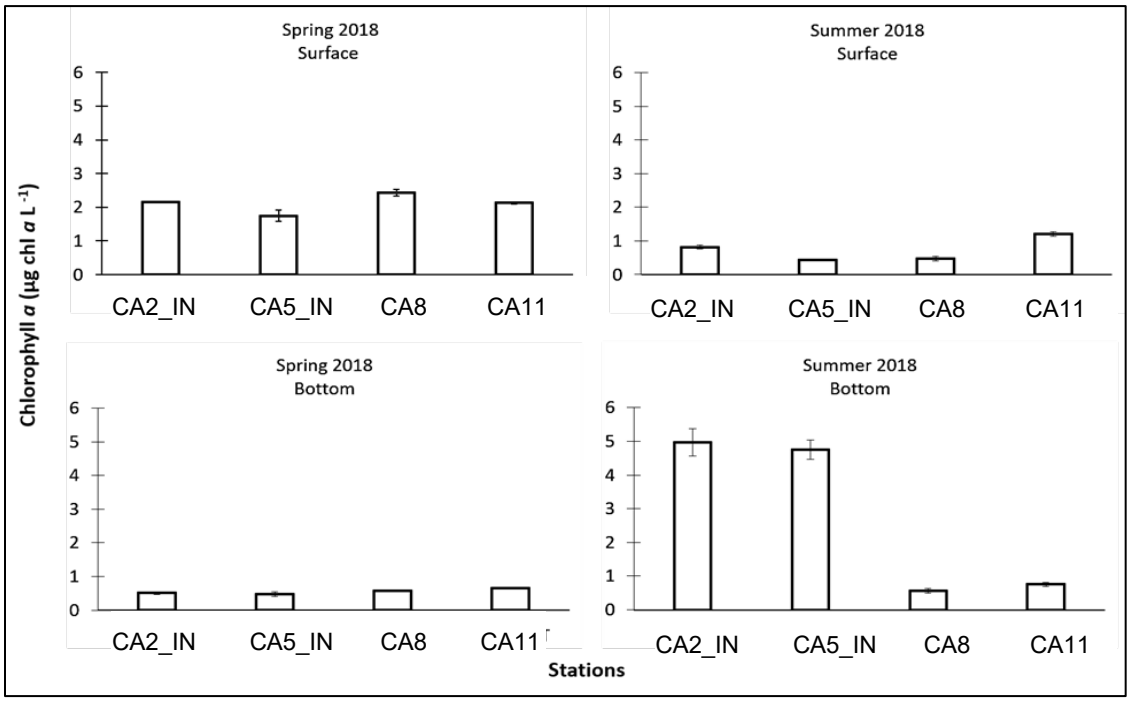

Figure 9. Chlorophyll a (chl a) values from Caminada Dredge Pit.

Chlorophyll a (chl a) values for the water column stations at Caminada between the two seasons, spring and summer of 2018, for surface and bottom water depths.

The phytoplankton community composition by taxonomic groups based on the selected diagnostic pigments indicated that the community inside and outside of the borrow pit were largely made up of

diatoms and cyanobacteria (Figure 10). Diatoms were more abundant in the summer surface water when compared to spring, whereas cyanobacteria were more present in spring. Bottom water samples showed similar patterns between spring and summer but there was an increase in diatoms in the summer for station CA2_IN. Chlorophyte abundance was similar at all stations and among both seasons, except for an increase in abundance at CA11 for the summer in bottom water samples. Microscopy observations revealed the diatom community to be mostly dominated by chain-forming centric diatoms, however no clear distinction was shown in species diversity between inside and outside of the pit.

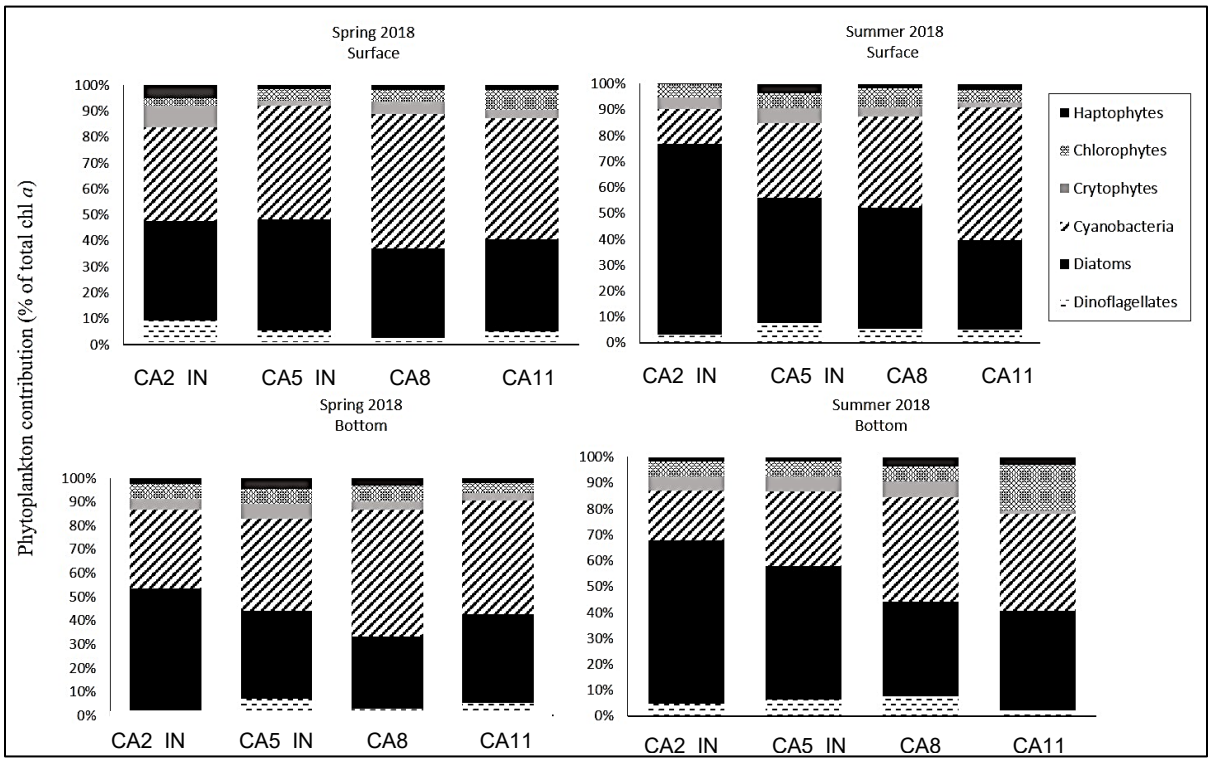

Figure 10. Phytoplankton community composition by taxonomic groups from Caminada Dredge Pit.

Phytoplankton community composition by taxonomic groups based on diagnostic pigments between the two seasons, spring and summer of 2018, for surface and bottom water depths. Most notably diatoms are represented by the solid black fill and cyanobacteria are represented by diagonal line pattern fill.

In general, Sandy Point borrow pit had higher NH_4 and SiO_2 concentrations in the summer when compared to the spring, while $NO_2 + NO_3$ and PO_4 concentrations were variable, shown in Table 4. Overall, $NO_2 + NO_3$ concentrations were higher in spring (25.2 ± 13.5 µM) than summer (5.4 ± 4.8 µM) ($p = 0.002$) (Table 4). Spring surface $NO_2 + NO_3$ concentrations were higher than bottom (32.9 ± 15.7 µM and 17.4 ± 4.7 µM, respectively) and the opposite was true for the summer, where surface concentrations were lower than bottom water (1.3 ± 0.25 µM and 9.6 ± 2.7 µM, respectively). Spring ammonium (NH_4) concentrations were significantly lower in surface water (2.6 ± 2.6 µM) when compared to bottom water (18.3 ± 6.0 µM) for all stations ($p = 0.003$). On the other hand, surface-water NH_4 concentrations significantly increased in summer (36.4 ± 9.6 µM) compared to spring ($p < 0.001$). but were still significantly lower than concentrations detected at depth (49.1 ± 8.0 µM) for the summer. Bottom-water concentrations of NH_4 were higher in the summer when compared to spring ($p < 0.001$). PO4 values were similar between seasons and consistently higher values were detected at depth ($p > 0.05$). Surface PO_4 concentration were 0.3 ± 0.2 µM and 0.1 ± 0.2 µM for the spring and summer, respectively ($p > 0.05$), while bottom PO_4 concentrations were 0.8 ± 0.3 µM and 0.9 ± 1.0 µM for the

spring and summer, respectively ($p > 0.05$). Silica (SiO_2) concentrations were averaging 15.5 ± 3.8 µM in spring and 32.4 ± 8.1 µM in summer. SiO_2 concentrations were higher both at the surface and depth during summer compared to spring for all stations ($p < 0.001$). NH_4 and PO_4 were positively correlated with depth in the spring, while N+N was positively correlated with depth in the summer (Table 4).

Table 4. Summary of dissolved inorganic nutrients from Sandy Point dredge pit

		Spring				Summer			
Station	**Depth**	**NO_2+NO_3 (µM)**	**NH_4 (µM)**	**PO_4 (µM)**	**SiO_2 (µM)**	**NO_2+NO_3 (µM)**	**NH_4 (µM)**	**PO_4 (µM)**	**SiO_2 (µM)**
SP3_IN	Surface	17.1	0.6	0.1	14.6	0.9	27.8	0.4	41.8
SP3_IN	Bottom	18.4	11.4	0.9	15.3	11.3	45.6	0.0	30.2
SP5_IN	Surface	50.0	3.5	0.5	14.2	1.4	44.7	0.0	27.6
SP5_IN	Bottom	10.7	16.0	0.7	13.0	6.3	39.3	0.0	18.7
SP4	Surface	22.3	5.9	0.1	15.9	1.5	28.4	0.1	38.8
SP4	Bottom	18.8	25.5	1.2	22.8	12.3	56.0	2.1	36.9
SP11	Surface	42.0	0.4	0.4	9.9	1.3	44.7	0.0	39.6
SP11	Bottom	21.7	20.3	0.5	18.6	8.6	55.3	1.4	25.9

Summary of dissolved inorganic nutrients (µM) from water samples collected during spring and summer of 2019, NO_2+NO_3 = Nitrate + Nitrite, SiO_2= Silica, NH_4= ammonium, 'bd' indicated samples were below detection.

The surface-water chl a concentrations were higher in the spring at all stations (7.49 ± 0.52 µg chl a L^{-1}) compared to bottom-water chl a concentrations (0.73 ± 0.13 µg chl a L^{-1}) (Figure 11). However, surface-water chl a concentrations were even higher in summer compared to spring for all stations, except SP5_IN, with a mean value of 14.32 ± 1.3 µg chl a L^{-1}. Bottom-water chl a concentrations were slightly higher in the summer compared to spring but remained significantly low compared to surface chl a concentrations ($p = 0.001$). Overall, chl a was positively correlated with temperature and DO and negatively correlated with depth and salinity for both spring and summer. Additionally, chl a concentrations were negatively correlated with NH_4 and PO_4 in the spring, while positively correlated to SiO2 in the summer.

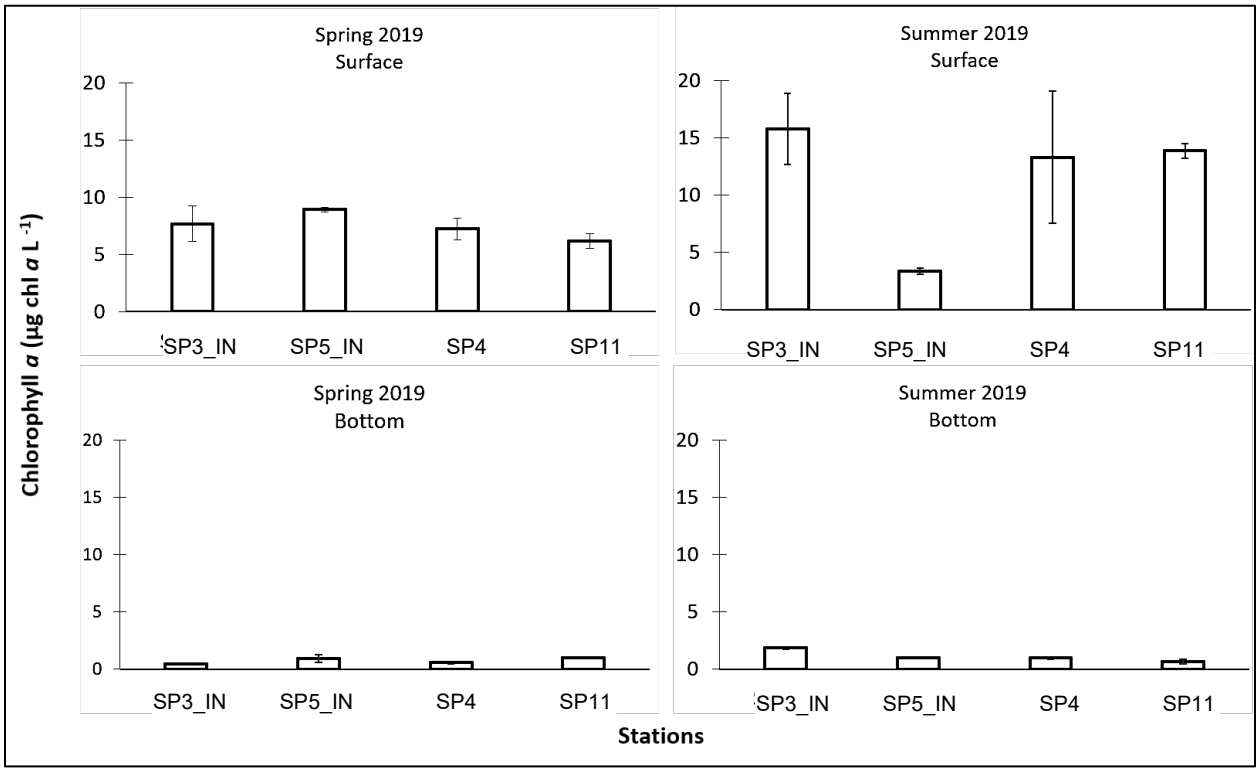

Figure 11. Chlorophyll a (chl a) values from Sandy Point dredge pit.

Chlorophyll a (chl a) values for the water column stations at Sandy Point between the two seasons, spring and summer of 2019, for surface and bottom water depths. Error bars represent standard deviation.

The phytoplankton community composition by taxonomic groups based on the selected diagnostic pigments indicated that the surface community inside and outside of the borrow pit were largely made up of chain forming diatoms in the spring and a mix of cyanobacteria and diatoms in the summer (Figure 12). Bottom-water community composition for all stations during the spring were mostly made up of diatoms and summer samples were a mix of cyanobacteria, dinoflagellates, and diatoms. In general, diatoms were most abundant in the spring at both depths, more visible inside the pit. Chlorophytes were also abundant in the spring surface water but that was replaced with cryptophytes at depth. In summer, diatoms were less abundant compared to spring at both depths and mostly replaced with cyanobacteria, especially at station SP5_IN. Notably, dinoflagellates became also abundant during the summer at depth at all stations.

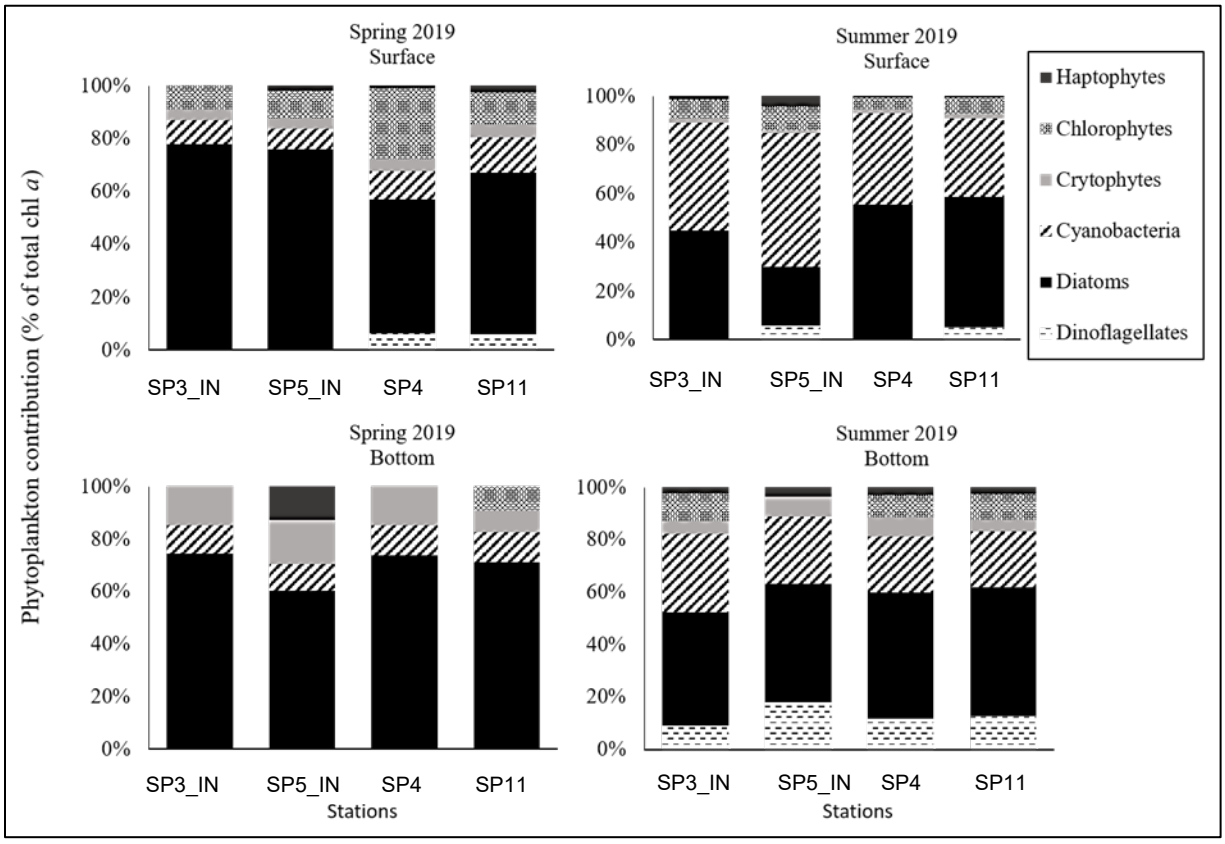

Figure 12. Phytoplankton community composition by taxonomic groups from Sandy Point dredge pit.

Phytoplankton community composition by taxonomic groups based on diagnostic pigments between the two seasons, spring and summer of 2019, for surface and bottom water depths. Most notably diatoms are represented by the solid black fill and cyanobacteria are represented by diagonal line pattern fill.

4.2 Multicoring and Box Coring

4.2.1 Sediment Texture, Radionuclide, and X-Ray

In general, it is evident that sedimentation rates inside both Caminada (CA) and Sandy Point (SP) borrow areas vary seasonally, and these sedimentation rates appear to correspond to varying discharge of the Mississippi and Atchafalaya Rivers (Table 5). For example, in fall 2017, Xue (2019) noted after a 6-month average Mississippi River discharge of ~18,900 m^3/s that 4-12 cm of ^{7}Be-laden sediments were deposited in CA (leading to calculated sedimentation rates of 0.02-0.06 cm/day), while in spring 2018 after a 6-month average Mississippi River discharge of ~20,300 m^3/s, 8-16 cm of ^{7}Be-laden sediment was observed (calculated sedimentation rates were correspondingly greater: 0.05-0.15 cm/day). This seasonal trend continued with fall coring in 2018 by Barley (2020) who observed 2 – 6 cm of ^{7}Be-laden sediment deposited in CA (calculated sedimentation rate was 0.02 – 0.04 cm/day; 6-month average Mississippi River discharge ~18,300 m^3/s; Table 5). Barley (2020) also observed this seasonal variation at SP: in May 2019, approximately 14 – 34 cm of ^{7}Be-laden sediments were deposited, and sedimentation rates were calculated to be 0.1 – 0.5 cm/day (6-month average Mississippi River discharge of ~30,500 m^3/s). An earlier survey in SP borrow area by M. O'Connor (2017) in July 2015, showed although approximately 14 – 28 cm of ^{7}Be-laden sediments were deposited, sedimentation rates were calculated to be lower at 0.08 – 0.26 cm/day, corresponding to a lower 6-month average Mississippi River discharge of ~20,200

m^3/s (Table 5). During repeat coring at SP in September 2019 (when the 6-month average Mississippi River discharge was ~20,300 m^3/s), only 2 – 6 cm of ^{7}Be-laden sediment was deposited, and sedimentation rates were 0.02 – 0.03 cm/day, but we believe this lower sedimentation rate is a function of the passage of Hurricane Barry, which impacted the region in July 2019.

Geophysical surveys identified low-lying topography in CA borrow area, which were preferentially infilling first (see locations in Figures 5 and 6). Grain size analysis from cores in these topographic lows shows that on average, the sediment infill has a median grain size around fine- to coarse-silt, ranging from 12 - 48 μm (4.5 – 6 Φ; see Figure 13). There are coarse silt to fine sand beds and laminations found in the cores, which are better resolved in the x-ray imagery. Outside these topographic lows, but still within the CA borrow area, the grain size was documented in May 2018 as fine sand (~100 μm, see CA5 in Figure 13 as an example), like found outside the pit (interpreted as Ship Shoal sand). However, by September 2018, a thin layer of fine- to coarse-silt was capping the fine sand at this location inside the pit (see Figure 13). Outside the pit remained sandy. It is important to note that the grain size observed infilling CA borrow area is finer than predicted by Nairn et al (2005), and the infilling rate is ~5 times slower than predicted. From these results, we conclude restoration quality sand from this location is deemed not renewable.

At SP borrow areas, no topographic lows were noted, and we observed the sediment infill has a median grain size of very fine- to fine-silt, ranging from 6 – 8.5 μm (~7 Φ), with a few medium- to coarse-silt laminations (see Figure 13). This was like what was previously observed and reported by O'Connor (2017). However, after the passage of Hurricane Barry, it was observed that a more homogenous sediment package was deposited within the borrow area with a distinct fining upward trend (this sediment was also ^{7}Be dead; see Figure 13).

For CA and SP cores, we identified Type 1, 2 and 3 sediment packages as described by O'Connor (2017), as well as two new Types (Type 4 & 5) not previously seen within the borrow areas (see Figure 14). From O'Connor (2017), Type 1 is ^{7}Be laden very fine-grained sediment (predominantly silt), interpreted to be from the Mississippi and/or Atchafalaya Rivers during rising and high discharge (see Figure 15). Type 2 is ^{7}Be dead slightly coarser grained sediment (coarse silt to fine sand) deposited as thin beds or laminations, interpreted to result from high energy events on the continental shelf, such as passage of winter storms. Type 3 is ^{7}Be laden sediment, but finer grained (more clay content) and lower ^{7}Be concentrations, interpreted to be from the Mississippi and/or Atchafalaya Rivers during low discharge summer. Type 4 was only observed at CA borrow area, and is characterized as ^{7}Be dead very fine sand, interpreted to result from local infill from pit wall failure/readjustment, and was only occasionally observed in the cores (see Figure 14). Type 5 was only observed at SP borrow area and was characterized by ^{7}Be dead homogenous sediment that had a distinct fining upward grain size (Figure 14), interpreted to represent rapid deposition following Hurricane Barry.

Using these sediment Type packages and average sedimentation rate models, we quantified that winter storms deposited ~ 12 – 20% of the annual infill seen within SP cores collected in May 2019 (see Table 6). In comparison, we estimate that ~ 66 – 73% of annual infill within CA cores collected in May 2018 was from winter storms. We attribute the greater portion of Type 2 sediment relative to annual infill at CA to the lack of proximal fluvial-sediment source at this borrow area.

Volumetric analysis of infill at CA and SP yielded significantly different times to total infill from those predicted by Nairn et al. (2005). For CA, we predict the pit will infill within ~60 years, slower than the 5 years predicted by Nairn's model for sandy dredge pits and more quickly than volumetric analysis from Liu et al. (2019) suggests. We predict SP is infilling at ~ 235,000 m^3/yr, with a time to total infill of ~ 15 – 20 years, just a few years longer than predicted by Nairn et al (2005) and Obelcz et al (2017). We recommend further research is needed to better understand how seasonal infilling from river discharge vs

winter storms vs hurricanes affects borrow area sedimentation in different hydrodynamic regions of the Louisiana continental shelf and models adjusted accordingly.

Multicore samples for x-ray analysis were retrieved using a Plexiglas x-ray tray (dimensions ~ 60 cm × 8 cm × 2 cm) carefully inserted into the core to preserve sedimentary structures. X-ray samples were returned to the lab at LSU and refrigerated for processing. This methodology has also been successfully used in previous studies on the Louisiana continental shelf (O'Connor, 2017; Obelcz et al., 2018). Cores were imaged using a Thales Flashscan 35 digital X-ray detector illuminated by Medison Acoma portable X-ray. These X-radiographs were then digitized to visually analyze the sedimentary structures within each core using the software ImageJ. Brightness and contrast of images was adjusted for clarity. For all cores >30 cm in length, two digitized x-radiographs were imaged and stitched together to visualize the core in its entirety.

X-ray images of multicores taken at CA showed predominantly very fine-grained mud (silt and clay) infilling the pit with a few coarser beds and laminations (see Figure 16 for annotated example from September 2018). In these images, light colors represent higher density and larger grain size (i.e., coarse silts & very fine sand), and darker colors represent lower density and smaller grain size (i.e., fine silts and clay). Other than the coarser grained beds (> 1 cm) and laminations (<1 cm) observed throughout the cores, a few other sedimentary structures can be observed: burrow holes, loaded bedding, shells, etc. X-ray images of multicores taken at SP also showed predominantly very fine-grained mud (silt and clay) infilling the pit with a few coarser beds and laminations, however the imagery results were not as clear due to x-ray imagery resolution issues. These images were used to corroborate the identification of sediment Type packages discussed in the previous section, and the presence of macro-infauna inside and outside the borrow areas.

Table 5. Geotechnical summary for ^{7}Be and sedimentation rate

Retrieval Month	Core Location	Depth of 7Be Penetration (cm)	7Be Inventory (dpm cm^{-2})	Sedimentation Rate (cm day^{-1})	R^2	MR Discharge (m^3 s^{-1})	AR Discharge (m^3 s^{-1})
Oct 2017	CA2	12	3.673	0.059	0.6813	18,931	8,197
Oct 2017	CA3	8	2.125	0.0057	0.7853	18,931	8,197
Oct 2017	CA4	4	0.613	0.019	0.019	18,931	8,197
Oct 2017	CA5						
Oct 2017	CA11						
May 2018	CA2	14	2.614	0.145	0.686	20,358	8,921
May 2018	CA3	8	2.603	0.052	0.9112	20,358	8,921
May 2018	CA4	16	2.854	>0.08		20,358	8,921
May 2018	CA5						
May 2018	CA11						
Sep 2018	CA2	4	0.599	0.02 ± 0.01	0.984	18,228	7,876

Retrieval Month	Core Location	Depth of 7Be Penetration (cm)	7Be Inventory (dpm cm^{-2})	Sedimentation Rate (cm day^{-1})	R^2	MR Discharge (m^3 s^{-1})	AR Discharge (m^3 s^{-1})
Sep 2018	CA3						
Sep 2018	CA4	4	1.243	0.04 ± 0.02	0.7914	18,228	7,876
Sep 2018	CA5	2	2.304				
Sep 2018	CA11						
Jul 2015	SP1	28		0.26	0.57	20,232	8,958
Jul 2015	SP2	24		0.08	0.81	20,232	8,958
Jul 2015	SP3	18		0.16	0.42	20,232	8,958
Jul 2015	SP4						
Jul 2015	SP5	14		0.08	0.79		8,958
Jul 2015	SP11						
May 2019	SP1	34	3.065	0.51 ± 0.27	0.2191	30,559	13,263
May 2019	SP2	30	2.428	0.22 ± 0.036	0.7987	30,559	13,263
May 2019	SP3	14	0.548	0.12 ± 0.076	0.3362	30,559	13,263
May 2019	SP4						
May 2019	SP5	28	2.993	0.40 ± 0.018	0.358	30,559	13,263
May 2019	SP11	4	0.479	0.06 ± 0.09	0.3888	30,559	13,263
Sep 2019	SP1	6	0.416	0.017 ± 0.001	0.9954	30,775	13,880
Sep 2019	SP2	2	0.177				
Sep 2019	SP3	2	0.144				
Sep 2019	SP4						

Retrieval Month	Core Location	Depth of 7Be Penetration (cm)	7Be Inventory (dpm cm^{-2})	Sedimentation Rate (cm day^{-1})	R^2	MR Discharge (m^3 s^{-1})	AR Discharge (m^3 s^{-1})
Sep 2019	SP5	4	0.52	0.026 ± 0.01	0.9422	30,775	13,880
Sep 2019	SP11	4	0.349	0.068 ± 0.015	0.244	30,775	13,880

^{7}Be penetration, inventory, calculated sedimentation rate and fluvial discharge average over 6 months prior to sampling for the Mississippi and Atchafalaya rivers. SP=Sandy Point; CA = Caminada; Average fluvial discharge data downloaded from Rivergauges.com for USGS stations 07295100 (Mississippi River, Tarbert Landing, MS) and 07381490 (Atchafalaya River, Simmesport, LA). Data sources are from O'Connor (2017), Xue (2019), Barley (2020) and this study.

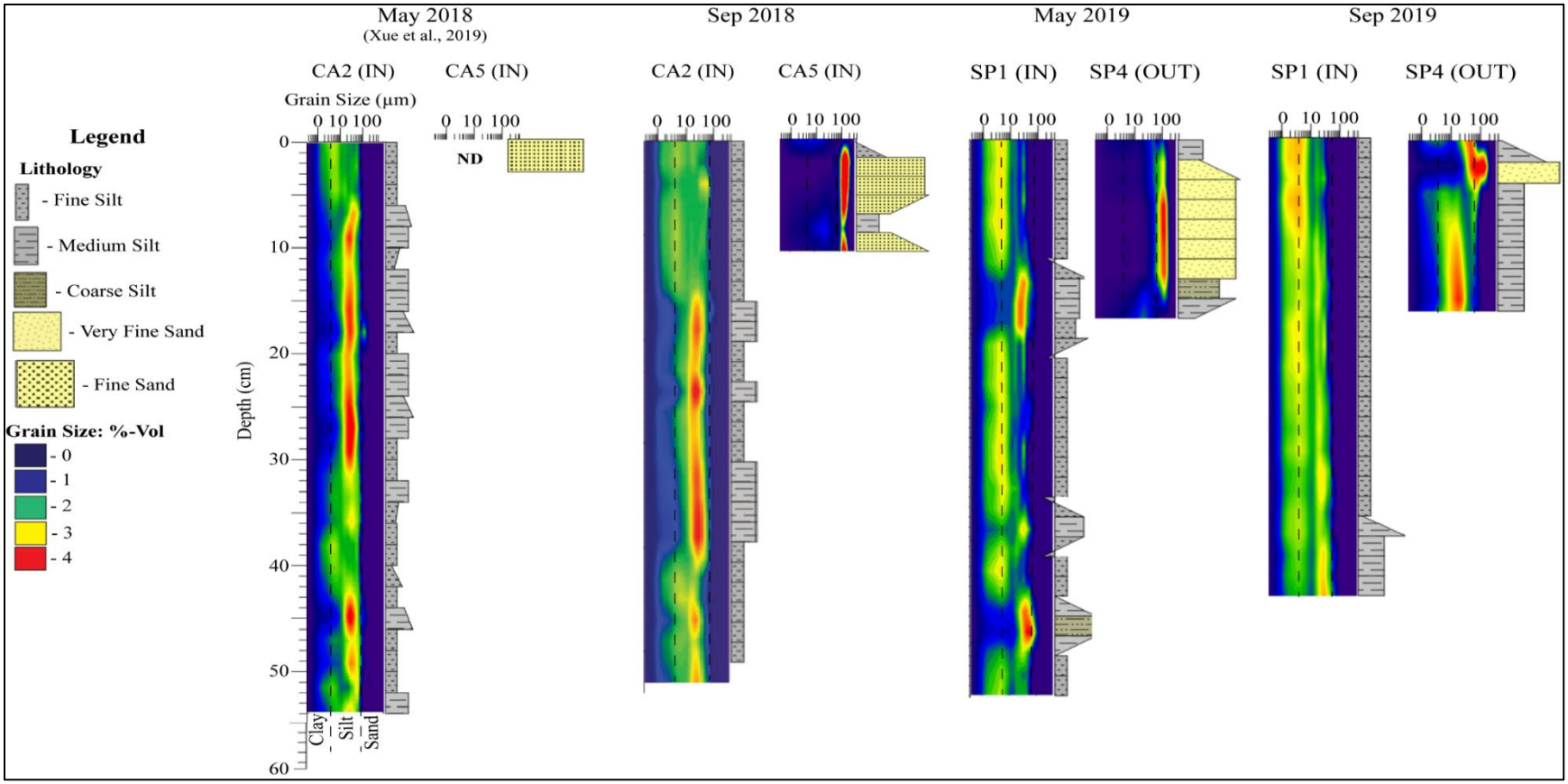

Figure 13. Grainsize frequency contour plots of multicores from Caminada and Sandy Point Dredge Pits.

Grain-Size frequency contour plots with stratigraphic profiles for representative multicores collected from Caminada BA (CA) and Sandy Point BA (SP) in May and September 2018, and May and September 2019, respectively. CA outside pit locations are comparable to CA5 (IN) from May 2018. Vertical dashed lines represent the divisions between clay, silt and sand sized sediments. Grain sizes within the BAs is predominately fine silts and clays, with occasional coarse silt and fine sand laminations and beds. ND = Insufficient data to create frequency plot. All core data are compiled from Xue et al. (2021) and Barley (2020).

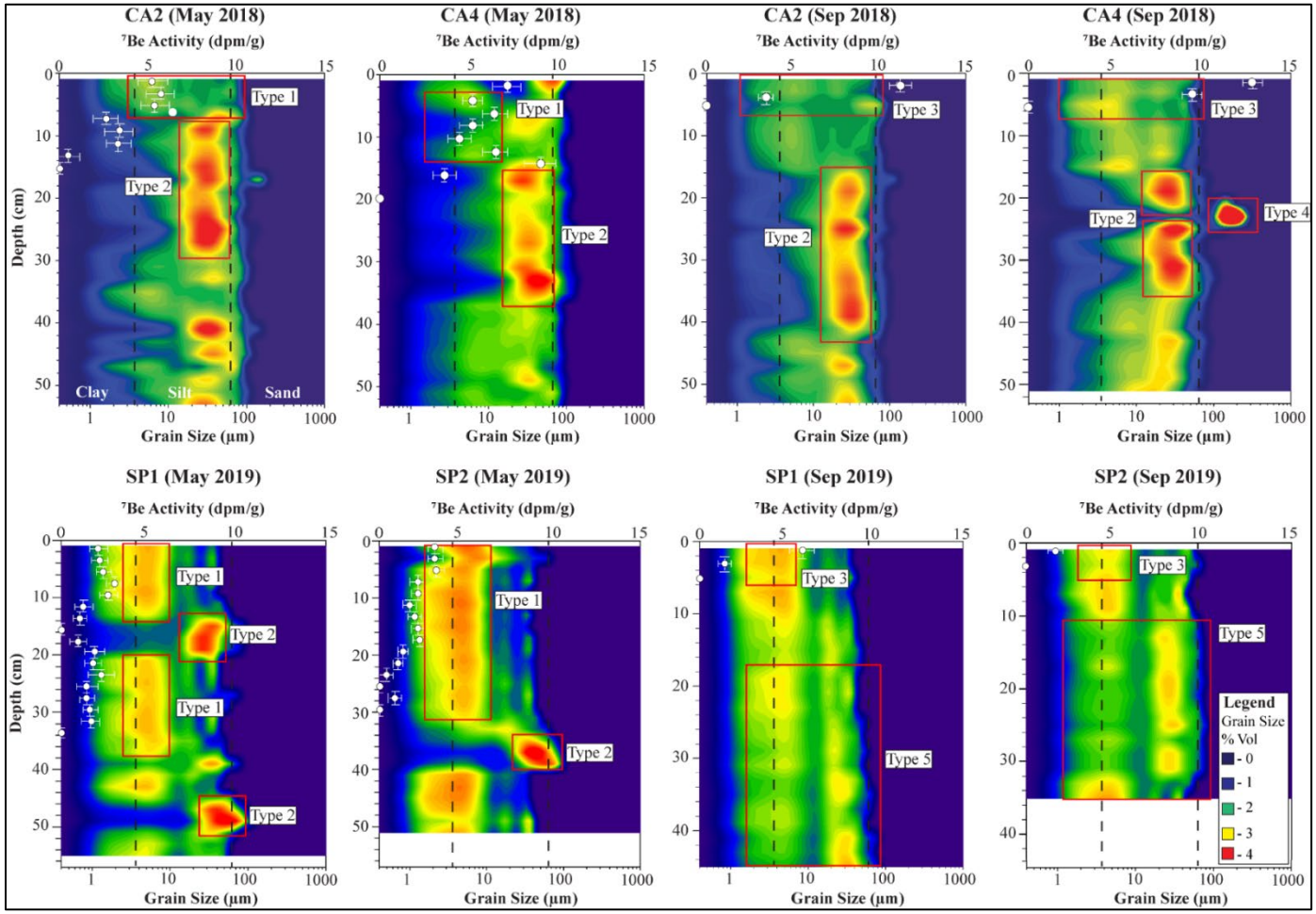

Figure 14. ^{7}Be activity overlying grainsize frequency contour plots from Caminada and Sandy Point Dredge Pits

Grain size frequency contour plots with ^{7}Be activity (dpm/g) overlain on top (white circles) for Caminada BA Sites 2 and 4 and Sandy Point BA Sites 1 and 2. Types 1,2 and 3 sediments are similar to those seen by O'Connor (2017) for cores collected at Sandy Point BA in July 2015. Type 4 sediment is a newly identified type seen only at Caminada BA, while Type 5 is only seen at Sandy Point BA and interpreted to represent hurricane Barry sedimentation. All core data are compiled from Xue et al. (2021) and Barley (2020).

Table 6. Percent of sediment types for cores collected at Caminada and Sandy Point Dredge Pits

Dredge Pit	Core Site	Date Sampled (mm/yyyy)	% Type 1 & 3	% Type 2	%Type 4	% Type 5
Caminada	CA2	05/2018	27	73	0	0
Caminada	CA4	05/2018	33	66	0	0
Caminada	CA2	09/2018	66	33	0	0
Caminada	CA4	09/2018	80	13	7	0
Sandy Point	SP1	05/2019	80	20	0	0
Sandy Point	SP2	05/2019	88	12	0	0
Sandy Point	SP1	09/2019	17	0	0	83
Sandy Point	SP2	09/2019	21	0	0	79

Percentage sediment type found during different seasons by dividing the thickness of sediment types by the annual infill for selected coring locations (~ 0.3 m yr^{-1} for Caminada and ~ 0.5 m yr^{-1} for Sandy Point). Type 1 and 3 are combined as they represent fluvial-derived material, Type 2 is inferred to be sediment delivered from winter storms, Type 4 is from pit wall failure/readjustment, and Type 5 is from Hurricane Barry (see also Figure 13 and 14). Core data for May 2018 taken from Xue M.S. thesis (2019), all others are from M. Barley M.S. thesis (2020). See Figure 11 for coring locations.

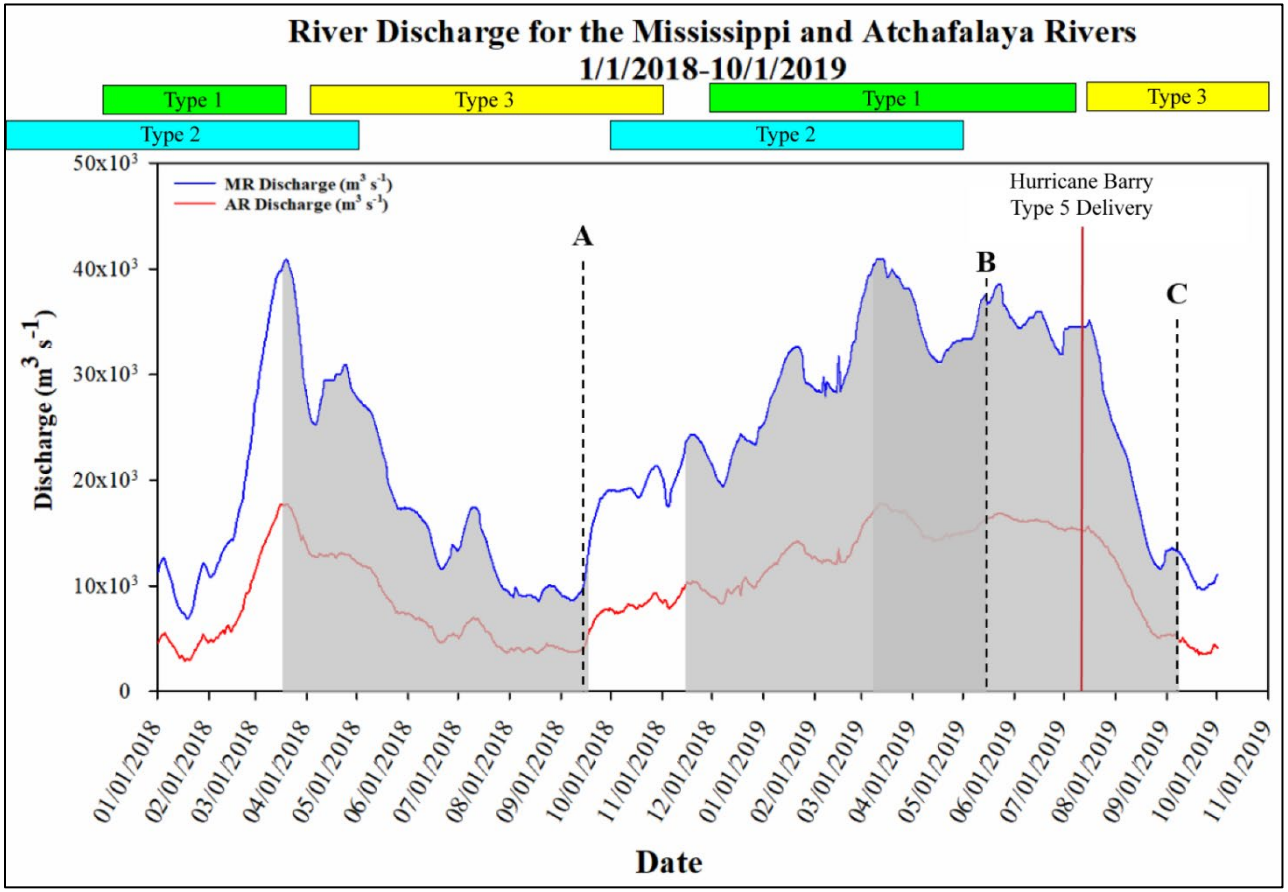

Figure 15. Mississippi and Atchafalaya River discharge.

Discharge data from the US Army Corps of Engineers Website (rivergauges.com) for the Mississippi River at Talbert Landing, and the Atchafalaya River at Simmesport, LA. Shaded areas represent 6 months leading up to multicoring done for (A) Caminada Borrow Area in September 2018, (B&C) Sandy Point Borrow Area in May and September 2019, respectively. Horizontal bars above the graph represent expected Types of sediment delivery during certain river discharge periods. Rapid Type 5 depositions in denoted by a vertical red line at the time of Hurricane Barry.

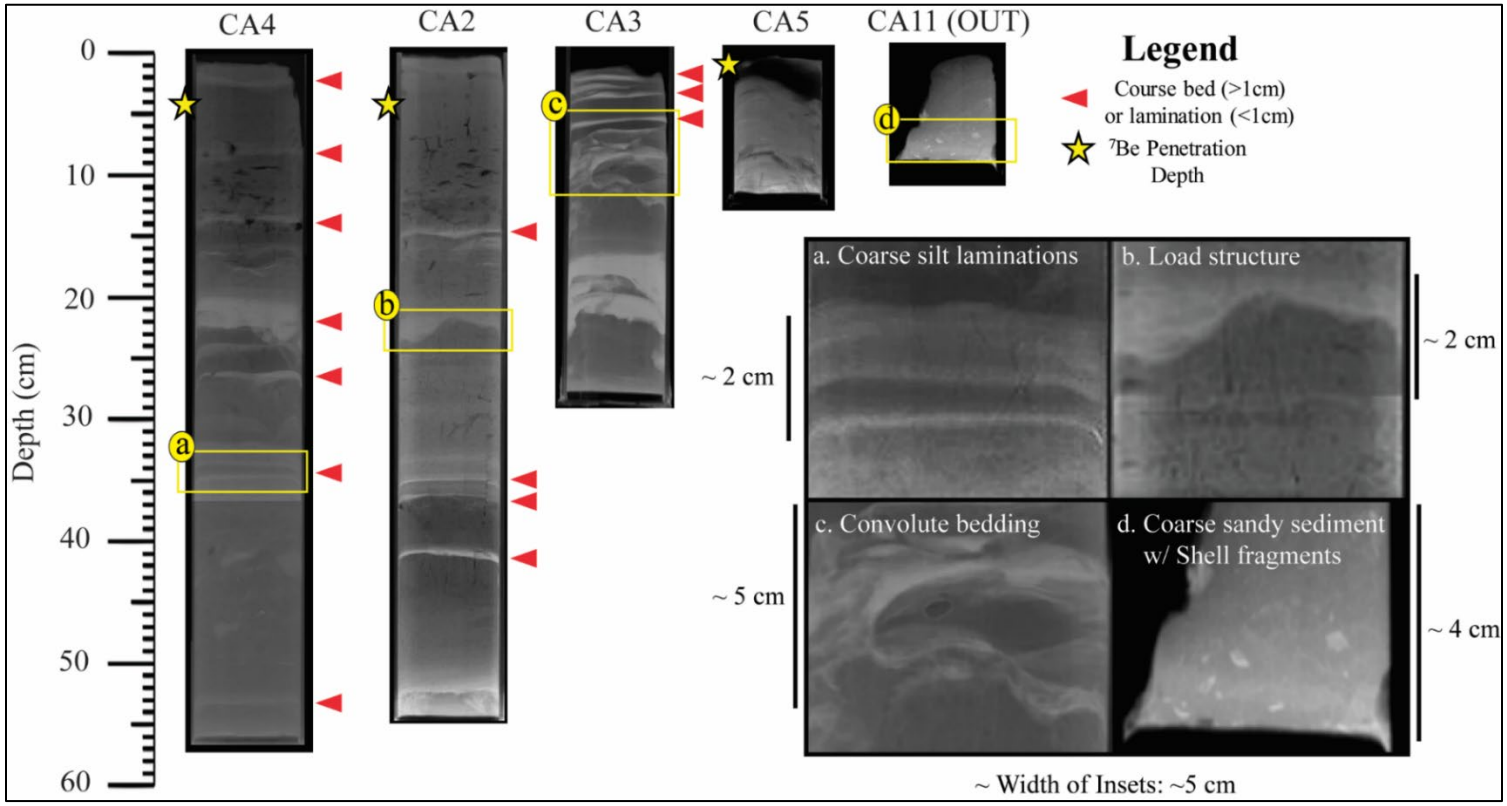

Figure 16 X-Ray images of multicores from Caminada Dredge Pit.

Annotated x-ray images of multicores taken at Caminada BA in September 2018 showing predominantly very fine-grained mud (silt and clay) infilling the pit with a few coarser beds and laminations (red arrows). Light colors represent higher density and larger grain size (i.e., coarse silts & very fine sand). Areas boxed in yellow are enlarged to highlight a few observed sedimentary structures. All core data are compiled from Xue et al. (2021) and Barley (2020).

4.2.2 Core Biological Analysis

Total organic carbon and total nitrogen analyses were performed for all 2 cm subsamples for each core. The average was taken for the whole 10 cm core due to no significant differnce found when the top 2 cm section was compared tosubsequent downcore samples ($p > 0.05$). Overall, there was low organic matter in the sediment outside of the pit compared to sediment inside the pit stations (Figure 17). Muddier sediment was found inside the pit versus outside the pit and differences were observed *in situ* during core slicing. Total N (TN) is defined as the sum of NO_2+NO_3 and NH4 here. Most stations experienced a decrease in %TOC and %TN from spring to summer apart from station CA1_IN, which showed the opposite trend. Higher percentage organic carbon values were recorded at station CA1_IN with 1.80 %TOC and 2.59 %TOC for spring and summer, respectively. Percent total nitrogen for all stations were similar (%TN < 0.1%) except for station CA1_IN where percentage were 0.25 %TN and 0.35 %TN for spring and summer, respectively. Chl a concentrations decreased from 17.37 ± 0.81 μg m^{-2} to 11.26 ± 13.77 μg m^{-2} for spring and summer, respectively, for station CA1_IN (Figure 18). However, chl a concentrations increased from 1.05 ± 0.13 μg m^{-2} in the spring to 45.82 ± 2.70 μg m^{-2} in the summer for station CA2_IN. Overall, chl a concentrations decreased at outside stations from 14.36 ± 5.60 μg m^{-2} to 7.68 ± 7.08 μg m^{-2} for spring to summer, respectively.

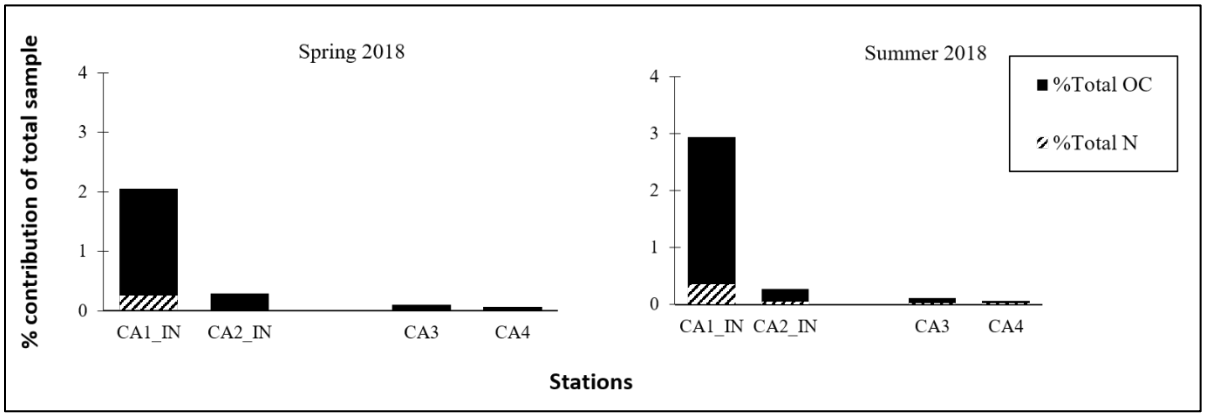

Figure 17. Percent total organic carbon and total nitrogen at Caminada Dredge Pit.

Percent total organic carbon and total nitrogen from sediment samples at all four stations at Caminada between inside and outside stations and amongst seasons, spring and summer of 2018.

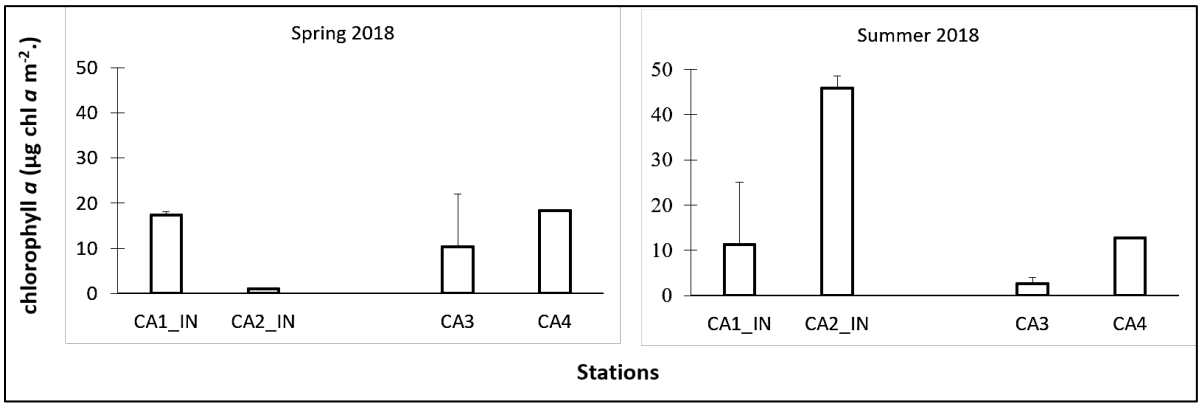

Figure 18. Sediment chlorophyll a at Caminada Dredge Pit.

Chlorophyll a from sediment samples at all four stations at Caminada between inside and outside stations and amongst seasons, spring and summer of 2018.

Microscope images of MPB show two distinct communities residing inside the pit versus those residing outside of the pit. The diatom community inside the pit was comprised of mostly single-cell centric

diatoms, whereas the outside pit stations were mostly single-cell pennate diatoms (Figure 19). No differences were seen between spring versus summer. Centric diatom *Coscinodiscus* spp. dominated the MPB community at stations CA1_IN and CA2_IN, while a mixture of pennate diatoms was found at outside stations, CA3 and CA4 (Figure 19).

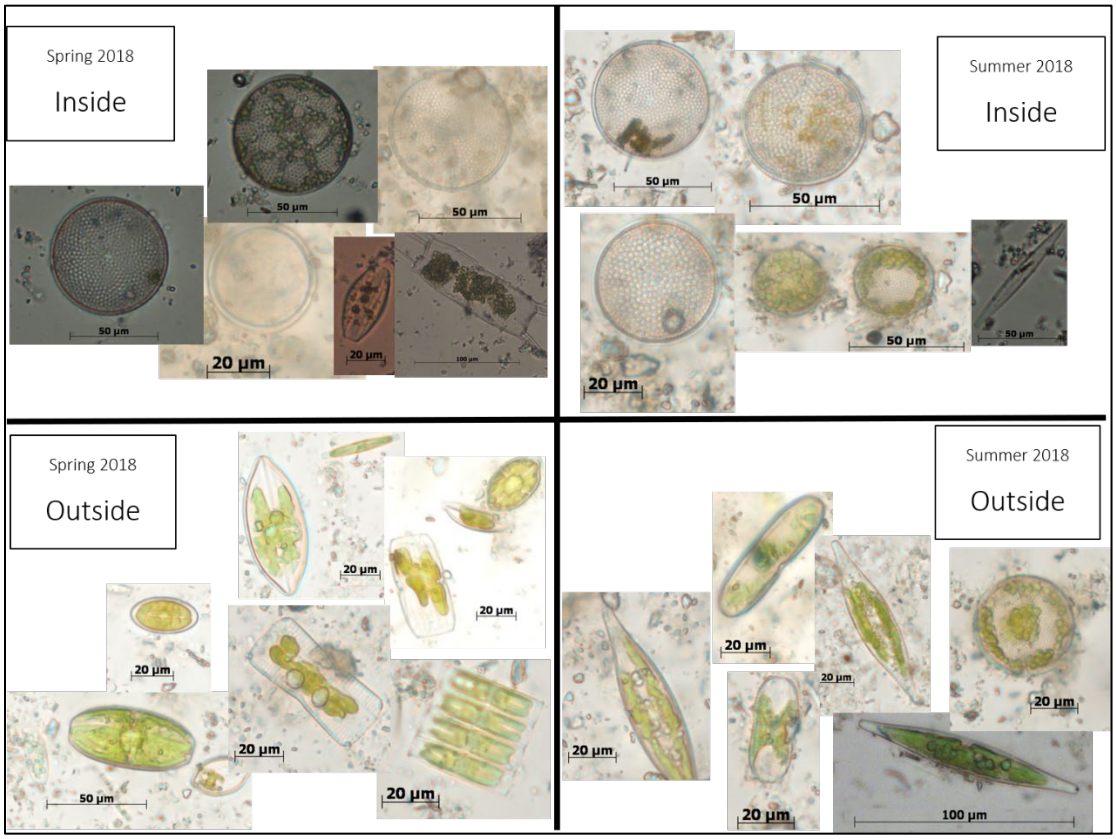

Figure 19. Microscope images of microphytobenthos at Caminada Dredge Pit.

Example microscope images of microphytobenthos show two distinct communities residing inside the pit, images on the top, compared with those residing outside of the pit, images on the bottom. Images on the left side were from samples collected during the spring 2018 while those on the right were collected during the summer 2018.

Total organic carbon and total nitrogen analyses were performed for all 2 cm subsamples for each core. The average was taken for the whole 10 cm core due to no significant difference found when the top 2 cm section was compared to subsequent downcore samples ($p > 0.05$). Overall, there was low organic matter in the sediment outside of the pit (1.03 %TOC and 0.12 %TN) compared to sediment inside the pit stations (2.02 %TOC and 0.21%TN) for both seasons combined (Figure 20). All stations experienced a decrease in %TOC (1.63 to 1.42 %) and %TN (0.17 to 0.14 %) from spring to summer ($p = 0.006$ and $p = 0.03$, respectively), apart from station SP3, which showed the opposite trend. Differences in sediment type were not observed from sediment cores taken at Sandy Point at stations inside and outside of the borrow pit.

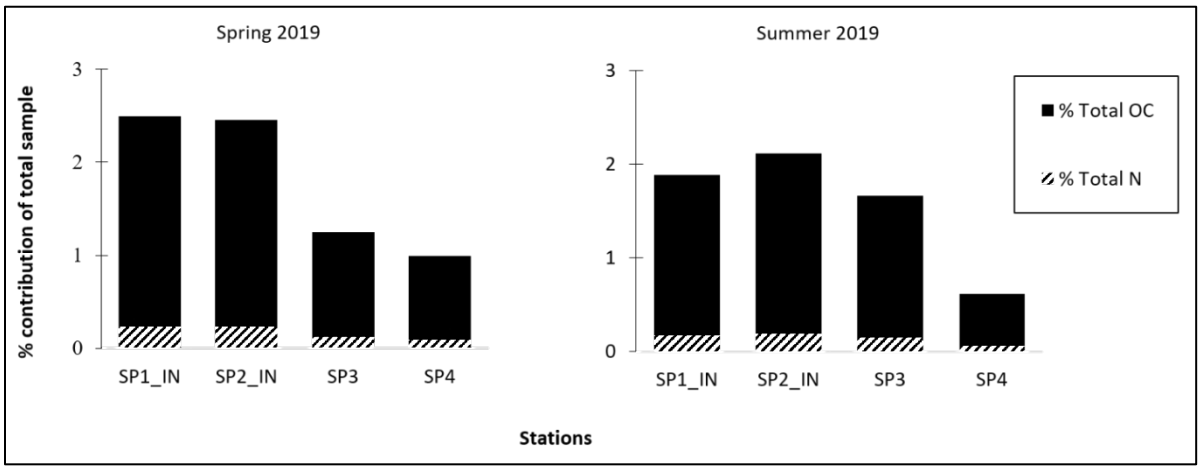

Figure 20. Percent total organic carbon and total nitrogen at Sandy Point Dredge Pit.

Percent total organic carbon and total nitrogen for sediment samples at all four stations at Sandy Point between inside and outside stations and among seasons, spring and summer of 2019.

Sediment chl a concentrations decreased from 20.05 ± 1.3 µg m^{-2} in the spring to 1.81 ± 0.41 µg m^{-2} in the summer for station SP1_IN. However, sediment chl a concentrations increased from 3.44 ± 0.27 µg m^{-2} in the spring to 15.08 ± 7.83 µg m^{-2} in the summer for station SP2_IN (Figure 21). Sediment chl a concentrations at outside stations decreased from spring to summer (13.94 ± 1.75 µg m^{-2} to 9.40 ± 5.47 µg m^{-2} respectively). Microscopy observations of MPB showed a mix of diatoms residing inside and outside of the borrow pit (Figure 22). No differences were seen between spring versus summer or amongst stations. Centric diatom *Coscinodiscus* spp. dominated the MPB community at all stations (Figure 22). Table 7 shows a summary of common ecological conditions at both Caminada and Sandy Point Dredge pits.

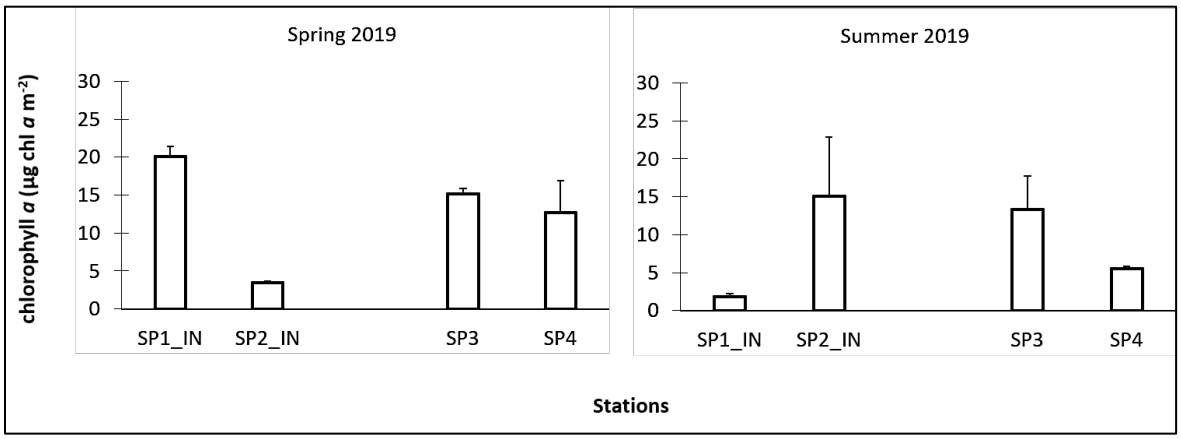

Figure 21. Sediment chlorophyll a at Sandy Point Dredge Pit.

Chlorophyll a values from sediment samples at all four inside and outside stations for spring and summer for 2019.

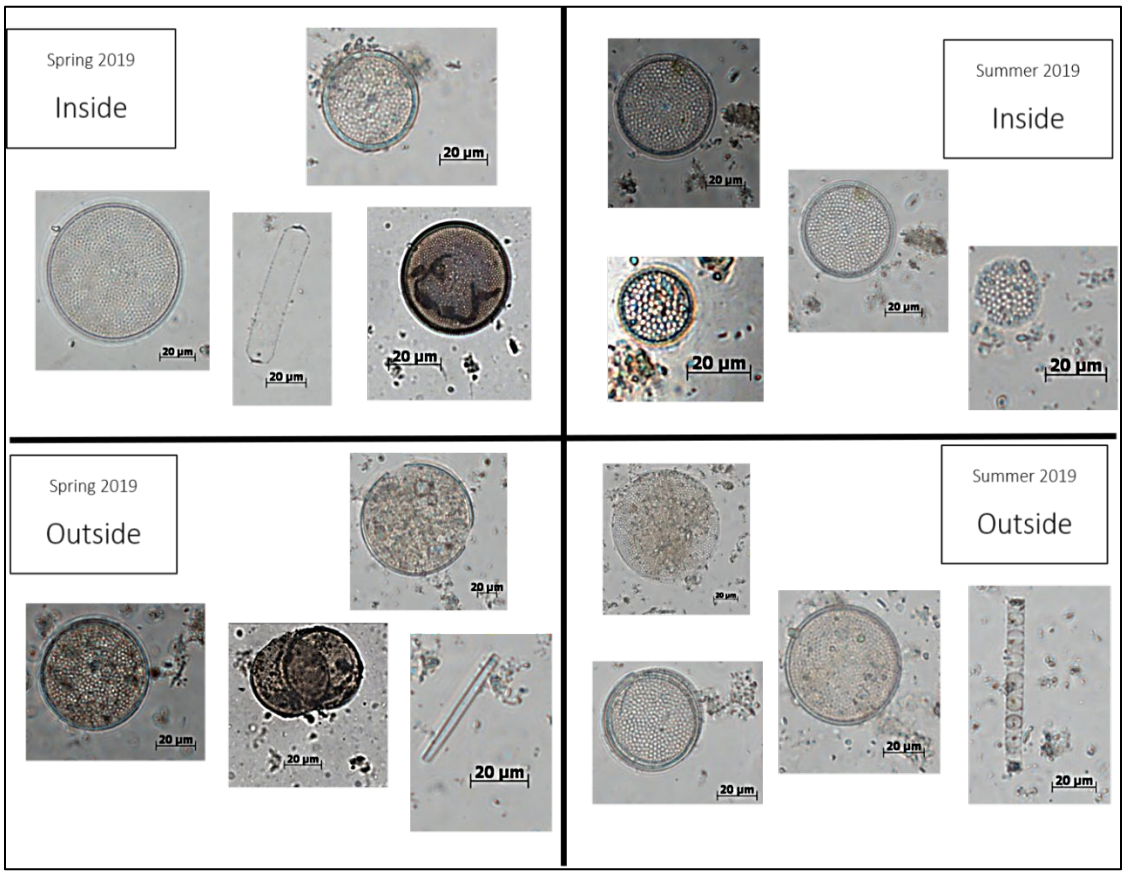

Figure 22. Microscope images of microphytobenthos at Sandy Point Dredge Pit.

Example microscope images of microphytobenthos show a mix of diatoms residing both inside and outside of Sandy Point borrow pit during the spring and summer of 2019. Images on the left side were from samples collected during the spring while those on the right were collected during the summer.

Table 7. Summary of common ecological conditions at Caminada and Sandy Point Dredge Pits

Ecological Condition	Caminada (2018)	Sandy Point (2019)
Year when sand was dredged	2013-2016	2012
Water depth	Outside: 7.82 m Inside: 12.68 m	Outside: 10.05 m Inside: 16.65 m
Bottom DO	Outside: 6.73 ± 1.17 mg L^{-1} Inside: 1.56 ± 0.25 mg L^{-1}	Outside and Inside: 3.1 ± 1.1 mg L^{-1}
Mississippi River Discharge	May 2018: 22,155 m^3 s^{-1} July 2018: 13,887 m^3 s^{-1}	May 2019: 33,074 m^3 s^{-1} September 2019: 10,479 m^3 s^{-1}

Ecological Condition	Caminada (2018)	Sandy Point (2019)
Surface dissolved inorganic nutrients	May 2018: $NO_2 + NO_3$: 1.69 ± 0.36 µM NH_4: 12.99 ± 7.54 µM PO_4: 0.29± 0.03 µM SiO_2: 10.94 ± 1.10 µM July 2018: $NO_2 + NO_3$: 0.32 ± 0.41 µM NH_4: 10.76 ± 4.16 µM PO_4: 0.20 ± 0.09 µM SiO_2: 3.10 ± 2.75 µM	May 2019: $NO_2 + NO_3$: 32.9 ± 15.68 µM NH_4: 2.60 ± 2. µM PO_4: 0.30 ± 0.20 µM SiO_2: 13.7 ± 2.60 µM July 2019: $NO_2 + NO_3$: 1.30 ± 0.25 µM NH_4: 36.40 ± 9.61 µM PO_4: 0.10 ± 0.20 µM SiO_2: 37.00 ± 6.36 µM
Phytoplankton biomass (chl a)	Surface: May 2018: 2.11 ± 0.28 µg L^{-1} July 2018: 0.55 ± 0.07 µg L^{-1} Bottom: May 2018: 0.73 ± 0.36 µg L^{-1} July: 2018: 2.76 ± 2.43 µg L^{-1}	Surface: May 2019: 7.49 ± 1.13 µg L^{-1} July 2019: 0.73 ± 0.25 µg L^{-1} Bottom: May 2019: 11.58 ± 5.59 µg L^{-1} July: 2019: 1.12 ± 0.51 µg L^{-1}
Dominant phytoplankton taxa	Surface: Diatoms and cyanobacteria Bottom: Diatoms and cyanobacteria	Surface: Diatoms and cyanobacteria Bottom: Diatoms and cyanobacteria
MPB biomass (chl a)	Outside: 11.03 ± 6.49 µg m^{-2} Inside: 18.87 ± 19.18 µg m^{-2}	Outside: 11.09 ± 8.89 µg m^{-2} Inside: 10.09 ± 4.22 µg m^{-2}
Dominant MPB taxa	Outside: Pennate diatoms Inside: Centric diatoms	Outside and Inside: Centric diatoms

Common ecological conditions summarized over two seasons-inside and outside - observed at two borrow pits, Caminada and Sandy Point during 2018 and 2019.

4.2.3 Core Biogeochemical Analysis

This study shows there was no significant difference in dredge pit SOC across different seasons. Sediment oxygen consumption rates did vary among season and in most cases, SOC increased from spring to summer as expected, however no station from either dredge pit experienced significant seasonal differences in SOC, with the exception of Caminada outside station CA11 ($p = 0.039$). The SOC at station CA11 increased by factor of three (19 mmol O_2 m^{-2} d^{-1}) from spring to summer. The adjacent outside station CA8 also demonstrated an increasing trend from spring to summer, but the increase was not significant ($p = 0.067$). There was not enough data to determine seasonal differences in Caminada inside station CA5_IN, but SOC rates at the other inside station CA2_IN were similar between the two seasons (51 to 52 mmol O_2 m^{-2} d^{-1}) with bottom water being consistently hypoxic from spring to summer. Overall, only outside station CA11 showed a significant difference, whereas inside the pit there were no seasonal differences in SOC rates. This is surprising given that no station experienced significant differences in sediment TOC content between spring and summer, except for inside station CA5_IN ($p = 0.009$). This points to the fact that SOC in sediment is a complex interplay between temperature, quantity, and quality of organic matter present in sediments, and bottom O_2 conditions, among other factors. The observed increase in SOC (Figure 23) outside the pit from spring to summer can be partly attributed to the observed higher temperatures in summer at these sites compared to spring, which promotes higher microbial activity (Lomas et al., 2002). The Mississippi River discharge peaked in March 2018 and declined thereafter which is likely reflected by concurrent increase in bottom water salinity changes between spring and summer (Table 8). Thus, the spring bloom associated with biological productivity from the river plume that supplies fresh organic matter to the sediment may have a smaller impact on sediment organic matter content in spring than in the summer, when the bloom is declining and hence supplying

more organic matter to the seafloor. The same factors should also impact on the inside pit stations but that is contrary to our data which shows no significant change in SOC inside the pit. However, the bottom water inside the pit was consistently low in dissolved O_2 from spring to summer, suggesting that the inside of the pit is persistently stratified, leading to hypoxic environment for extended periods of time. This persistently low O_2 condition inside pit bottom will lead to very shallow O_2 penetration depth inside the sediments (Cai et al., 1996; Rowe et al., 2008; Glud, 2008) resulting in more pronounced anaerobic respiration (Sorensen, 1982; Lehrter et al., 2012).

The SOC rates for Sandy Point also showed increasing trends from spring to summer, but these increases were not significant. This scenario is different from Caminada, where there was a seasonal difference outside the pit but not inside. The same factors mentioned above for lack of significant seasonal variability inside the pit at CA is equally applicable for this site. However, one important factor that can exert additional influence is the proximity of SP to Mississippi River outflow. Sandy Point is located about 20 km northwest from the Southwest Pass, which is one of the main discharge channels for the Mississippi River and is located within a clockwise gyre of the Louisiana Bight that advects the river plume over Sandy Point (Walker et al., 1996; Obelcz et al., 2018). During our sampling season of 2019, the river discharge was high in February, peaked in March, and finally began to decline in August after an unusually long period of flood stage discharge thus Sandy Point could have been continuously influenced by energetic currents and fresh organic matter over the course of both seasons. Salinities at all stations were higher in spring compared to summer, supporting that the high freshwater influence during spring continued until summer months. Temperatures at all stations warmed from spring to summer, however temperatures between inside and outside stations were similar, differing only 1.5 °C or less each season. Bottom water dissolved O_2 concentrations at inside station SP5_IN and outside station SP4 decreased by ~0.5 mg L^{-1}, while inside station SP3_IN and outside station SP11 experienced increases from spring to summer by almost 1.0 mg L^{-1}. All stations experienced decreases in TOC content from spring to summer, except for SP11 which increased, however, this increase was not significant due to variability (Figure 24). This increase in TOC was unexpected due to SP11 having the smallest increase in SOC of ~1.5 mmol O_2 m^{-2} d^{-1} between seasons, while all other stations increased at least 7 mmol O_2 m^{-2} d^{-1} or more between seasons. Although inside stations SP3_IN and SP5_IN significantly decreased from spring to summer ($p = 0.0006$ and $p = 0.003$, respectively), TOC inside the pit remained substantial throughout both seasons. Similar to CA, increases in SOC along with decreases in TOC between seasons rely on the factors of bottom water dissolved O_2 availability, temperature, and substrate quality. In addition, the continuous freshwater river influence in 2019 provided energetic currents and promoted a well-mixed water column at SP, contributing to the increased TOC at station SP11 and allowing the inside stations to have high organic matter between seasons.

Bottom water nitrate concentration inside CA remained consistently low from spring to summer ranging from 0.35 to 0.37 µM, although outside concentrations were higher at 1.51 µM in spring and 0.66 µM in summer (Table 8). Nitrate concentrations at SP were notably higher in the spring compared to summer, at ~15 µM inside the pit and roughly 21.5 µM outside the pit, which later decreased to concentrations below 1.0 µM NO_3 (Table 8). Nitrate fluxes for all stations were consistently negative throughout sampling seasons (Figure 25), indicating a flux of NO_3 into the sediment due to denitrification. CA fluxes were generally minor, with all stations experiencing fluxes below 0.10 mmol m^{-2} d^{-1} and minimal increases or decreases between seasons (Figure 24b). SP experienced high NO_3 fluxes into the sediment in spring, ranging -4.55 ± 0.32 to -2.14 ± 0.24 mmol m^{-2} d^{-1}, which decreased to a range of -0.24 ± 0.02 to -0.02 ± 0.01 to mmol m^{-2} d^{-1} in summer (Figure 25).

Ammonium in CA bottom water was below detection in both inside and outside stations during spring, but in the summer showed an increase of 19.4 µM NH_4 inside and 9.71 µM NH_4 outside the pit (Table 8). Ammonium inside SP ammonium was <1 µM or below detection in spring, however due to a lack of NH_4 data in summer, comparisons of seasonal changes cannot be made (Table 8). The NH_4 concentrations

inside CA were the highest reported among all sampling stations. Ammonium fluxes were mostly negative throughout all sampling locations (Figure 24c), indicating that sediment acts an overall sink for NH_4. Inside stations CA2_IN and CA5_IN were the only exception, with a release of ammonium from the sediment during both seasons (Figure 24c). Outside station CA8 also experienced a small flux into the overlying water column, although only in spring. The biggest sink of NH_4 into the sediments at CA dredge pit occurred at CA11. All SP stations experienced negative NH_4 flux rates, which all decreased from spring to summer, with station SP3_IN having the highest flux during both seasons, and SP4 having the lowest flux during both seasons (Figure 25). Systems such as the northern Gulf hypoxic region, where stratification and low oxygen (or no oxygen) bottom waters occur, suggest the importance of oxygen for coupled nitrification and denitrification processes (Seitzinger et al., 2006). Thus, the oxygen availability in these sediments is ultimately controlled by O_2 diffusion into sediments and SOC, along with the nitrification processes necessary for N removal (Seitzinger et al., 2006). Bottom O_2 concentrations in this study ranged from 0.44 to 6.88 mg L^{-1}. There were no significant differences in bottom O_2 between the inside CA and SP dredge pit stations. However, only CA inside stations experienced a significant difference when bottom O_2 inside the pit was compared locally to the outside stations ($p = 0.01$), due to the saturated bottom O_2 recorded outside at CA8 and CA11. Inside stations CA2_IN and CA5_IN were persistently hypoxic for the period of this study, and consequently, NO_3 concentrations inside CA were the lowest recorded within this study, even when NH_4 was available in bottom water at concentrations up to 20 µM (Table 8). In fact, NH_4 fluxes found in this study ranged from -2.29 ± 0.24 to 0.16 ± 0.03 mmol m^{-2} d^{-1}, with the only positive fluxes found at CA (Figure 25) which were significantly different from outside station fluxes ($p = 0.01$). This suggests that due to persistent low oxygen conditions, nitrification processes may be inhibited leading to a buildup of NH_4, allowing a positive flux of ammonium into the overlying water column at these inside CA stations (Lehrter et al., 2012; McCarthy et al., 2008). In some studies, high NH_4 concentrations postulate dissimilatory nitrate reduction to ammonium (DNRA) and thus should be considered as a potential source of ammonium (e.g., McCarthy et al., 2015; Lehrter et al., 2012; Childs et al., 2002; Gardner et al., 2006, McCarthy et al., 2008).

Benthic nitrate removal was higher when overlying bottom water NO_3 concentrations were higher ($p = 1.5 \times 10^{-6}$, $r^2 = 0.64$). However, not all nitrate fluxes reflect the rates at which denitrification occurred because of additional microbial processes acting as source or sink of nitrate (Figure 25). Further, CA inside and outside stations were not similar in bottom O_2 concentrations, with inside stations being persistently hypoxic and outside stations maintaining above hypoxic levels. This indicates the complexity associated with denitrification which is affected by the interplay of many factors such as O_2, NO_3, and NH_4 availability, organic matter, and temperature and does not have a simple relationship with bottom water O_2 and NO_3 (Table 8). It is possible in systems with low oxygen and low nitrate, denitrification may still be evident although NO_3 is limiting, suggesting nitrification-derived NO_3 may play a less significant role in driving denitrification (McCarthy et al., 2008). Thus, NO_3 may be taken up quickly if it is available and may not be replenished as fast as it undergoes denitrification. (Figure 25). Sulfide inhibits nitrification and denitrification processes, as many sulfate reducers can fix N (Joye et al., 1995; Gardner et al., 2006; McCarthy et al., 2015). Hydrogen sulfide (H_2S) accumulation in surface sediments is likely during hypoxia and has been measured in this sediment, and thus is an important factor when determining N fluxes (McCarthy et al., 2008). Compared to all other stations, SP had the highest NO_3 availability, highest NO_3 fluxes into the sediment, low NH_4 presence, and only one station, SP3_IN, was hypoxic (1.70 mg O_2 L^{-1}) during spring sampling (Figure 25; Table 8). This suggests that denitrification was driven by the availability of NO_3 and O_2 and thus nitrification could occur. Based on similarities between inside and outside stations, high river discharge during spring sampling of SP, and the proximity to the Mississippi River delta, the water column SP was probably mixed and the availability of O_2 could fuel the nitrification process. In fact, the differences in NO_3 fluxes from spring to summer were significant ($p = 0.0004$), with fluxes decreasing over 10x at all stations between seasons.

Phosphate concentrations inside CA were below detection throughout spring and summer seasons. Similarly, outside PO_4 stations had below detection phosphate in spring and increased to 0.23 µM PO_4 in summer (Table 8). Spring concentrations at SP is 0.81 µM inside the pit and 0.74 µM outside the pit. At CA phosphate release was overall low, at below 0.1 mmol m^{-2} d^{-1}, except for CA2_IN which released PO_4 at a rate of 0.59 ± 0.07 mmol m^{-2} d^{-1} in spring, which decreased to 0.48 ± 0.03 mmol m^{-2} d^{-1} in summer (Figure 25). At SP, there were no stations found to release phosphate in spring, except SP4 which released phosphate at a rate of 0.01 ± 0.00 mmol m^{-2} d^{-1}. By summer, every SP station experienced an increase in phosphate release from the sediments (Figure 25).

Significant positive correlations of P release rates and Fe/Al bound P have been found in NGOM sediments (Adhikari et al., 2015; Zhang et al., 2012), which were driven specifically by the release of iron bound P due to the reduction of Fe^{3+} to Fe^{2+} (Zhang., et al 2012). In this present study, the overall phosphate concentrations in bottom water were low at all stations, <1.50 µM, and were frequently below the detection levels. The PO_4 fluxes, ranged from -0.26 to 0.84 mmol P m^{-2} d^{-1}. The highest recorded phosphate release occurred inside dredge pits, specifically at inside station CA2_IN in spring and summer and inside stations SP3_IN and SP5_IN in spring, and not at adjacent outside pit stations. The difference between phosphate fluxes at these inside stations and both outside pit stations was significant (CA $p = 0.004$, SP $p = 0.000$). However, there was no significant correlation between bottom O_2 concentration and PO_4 flux. This is surprising due to low oxygen conditions in coincidence with high SOC rates ranging 23.7 to 59.0 mmol O_2 m^{-2} d^{-1}. Even so, the dynamic of sedimentary P is multifaceted, as benthic P fluxes also widely depend upon iron cycling, carbon oxidation, and oxygen penetration in sediments (McManus et al., 1997). There is abundant evidence supporting positive P fluxes in low oxygen environments (Ingall and Jahnke, 1994; Ghiasas et al., 2015; Adhikari et al., 2015), however, low carbon oxidation may play a prominent role in inhibiting the release of P from sediments as iron oxyhydroxides form near the sediment surface (McManus et al., 1997). Shelf sediments exclusively incubated under anaerobic conditions by Adhikari et al. (2015), experienced higher flux rates of phosphate release, ranging 0.6 to 142.4 mmol P m^{-2} d^{-1}. Thus, low oxygen observed inside the pit maybe responsible for the remobilization of iron bound phosphate in these sediments.

Silica concentrations at CA were higher in spring compared to summer, starting at 2.46 µM Si inside and 11.7 µM Si outside and decreasing to below detection inside and 3.44 µM Si outside the pit (Table 8). SP stations had overall higher Si concentration than CA, however the inside and outside SP stations showed different trends. Si inside SP increased from 16.1 to 57.8 µM between seasons, while outside SP decreased from 28.7 to 10.7 µM between seasons.

Silica fluxes were variable among seasons (Figure 25). Station CA2_IN had the highest rate among CA stations, and most notable change in flux rate from spring to summer, with a rate of 6.73 ± 0.71 mmol m^{-2} d^{-1} which decreased to 2.92 ± 0.05 mmol m^{-2} d^{-1} in summer (Figure 25). CA8 was the only station to experience a negligible bSi flux in spring. At SP, every station experienced an increased in bSi flux from spring to summer, with notably high Si fluxes in summer (Figure 25). Between seasons, the Si fluxes at SP increased by at least 3.5 mmol m^{-2} d^{-1} up to almost 6.0 mmol m^{-2} d^{-1}. SP3_IN was the only station at SP to experience a negative flux of -0.54 ± 0.25 mmol m^{-2} d^{-1}, occurring in spring.

Silica fluxes presented in a recent study by Berelson et al. (2019) using in situ benthic chambers found benthic silica fluxes ranging from 0.8 to 11.8 mmol m^{-2} d^{-1}, which is higher compared to the flux rates found in this study ranging, -0.54 to 6.93 mmol m^{-2} d^{-1} (Figure 25). Si fluxes and biogenic Si deposition has shown consistently positive correlations in the past (Berelson et al., 2003, 2013, 2019) and evidence of diatom pigment accumulation in sediment, such as fucoxanthin and chlorophyll, have been observed in the NGOM hypoxic zone (Rabalais et al., 2004), which further points to the direct correlation between benthic silica flux and %TOC. However, in this study bSi in sediment was not measured and the correlation between %TOC and Si fluxes, was not significant. Inside dredge pit station CA2_IN and

outside dredge pit station SP4 were found to have the highest Si fluxes of this study, with rates of 6.73 ± 0.71 and 6.93 ± 0.38 for CA2_IN and SP4, respectively. Conversely, these stations were not found to have the highest %TOC, with %TOC <1.0. Instead, stations CA5_IN, SP3_IN, and SP5_IN, all inside pit stations, were found to have consistently higher %TOC, greater than 1.50%, throughout sampling seasons compared to outside pit stations. A notable seasonal trend in silica flux was found at SP ($p = 1.7 \times 10^{-7}$) which may be attributed to high river discharge during spring of 2019, however the same trend was not observed with %TOC between seasons, with inside stations SP3_IN and SP5_IN decreasing from spring to summer.

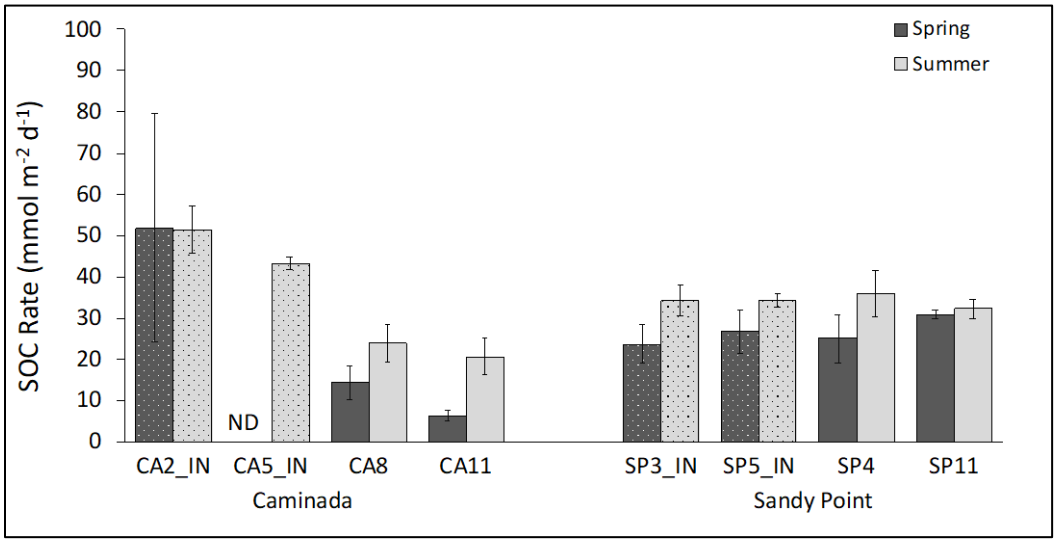

Figure 23. SOC rates from Caminada and Sandy Point.

Comparison of SOC rates from Caminada and Sandy Point sediment core incubations. Inside stations are displayed with a diagonal line pattern fill, and outside stations are displayed without a pattern fill. 'ND' indicates no data was collected (from Thompson et al., 2021).

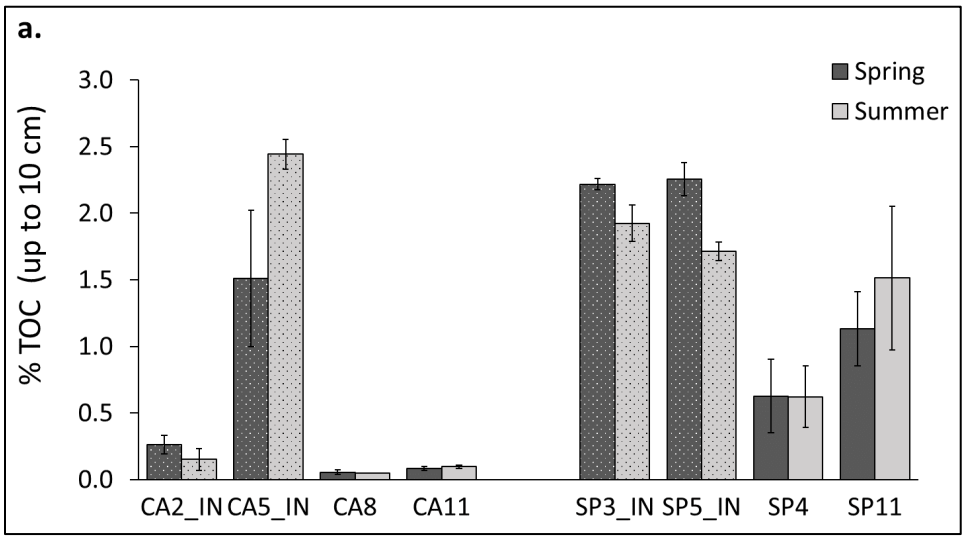

Figure 24. TOC from Caminada and Sandy Point Dredge Pits.

Total organic carbon (TOC) from Caminada and Sandy Inside pit stations are displayed with a pattern fill. 'ND' indicates no data was collected (from Thompson et al., 2021).

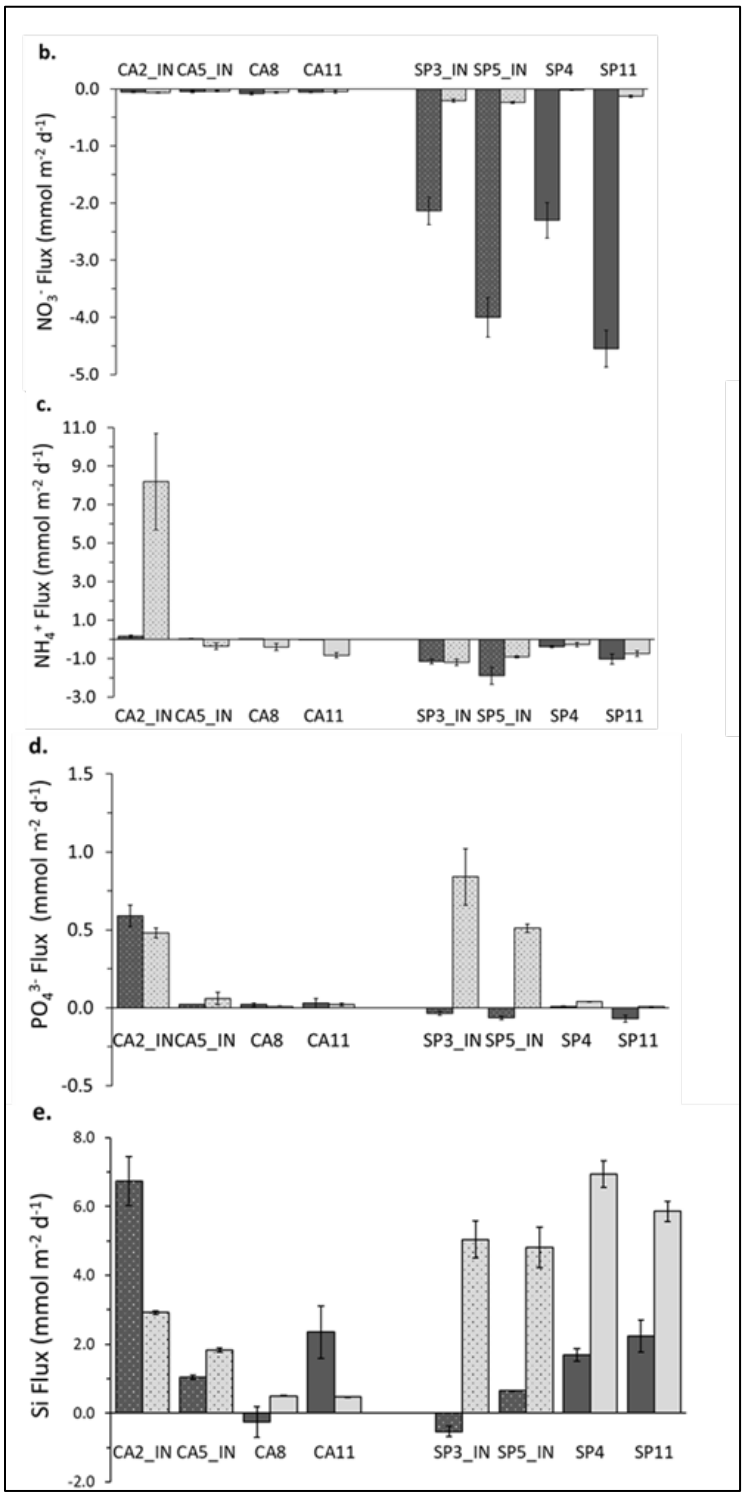

Figure 25. Nutrient flux rates from Caminada and Sandy Point Dredge Pits.

Nutrient flux rates for dredge pits presented in mmol m^{-2} d^{-1} for NO_3 , NH_4, PO_4 and Si. “ND” indicates no data.

Table 8. Bottom water conditions at Caminada and Sandy Point Dredge Pits

Station	Month	Depth (m)	Temp (°C)	%TOC	O_2	NO_3	NH_4	PO_4	Si
CA2_IN	May 2018	13.1	22.9	0.26 ± 0.07	1.93	0.35	0.00	0.00	2.46
CA2_IN	July 2018	12.9	26.6	0.15 ± 0.08	1.46	0.37	19.40	0.00	0.00
CA5_IN	May 2018	13.1	23.1	1.51 ± 0.51	1.43	0.35	0.00	0.00	2.46
CA5_IN	July 2018	13.2	26.7	2.44 ± 0.11	1.42	0.37	19.40	0.00	0.00
CA8	May 2018	7.0	25.5	0.06 ± 0.02	6.88	1.51	0.00	0.00	11.70
CA8	July 2018	8.1	29.0	0.05 ± 0.00	5.46	0.66	9.71	0.23	3.44
CA11	May 2018	7.0	24.5	0.08 ± 0.01	6.71	1.51	0.00	0.00	11.70
CA11	July 2018	9.3	28.5	0.10 ± 0.01	3.50	0.66	9.71	0.23	3.44
SP3_IN	May 2019	17.3	22.5	2.22 ± 0.04	1.79	15.50	0.00	0.81	16.10
SP3_IN	Sep 2019	16.7	27.5	1.92 ± 0.14	2.75	0.53			57.80
SP5_IN	May 2019	16.7	22.6	2.25 ± 0.12	2.81	15.50	0.00	0.81	16.10
SP5_IN	Sep 2019	16.5	27.4	1.71 ± 0.07	2.32	0.53			57.80
SP4	May 2019	10.6	23.1	0.63 ± 0.28	4.92	21.90	0.78	0.74	28.70
SP4	Sep 2019	10.8	28.9	0.62 +0.23	4.56	0.33			10.70
SP11	May 2019	10.4	22.9	1.13 ± 0.28	2.36	21.90	0.78	0.74	28.70
SP11	Sep 2019	10.3	29.0	1.51 ± 0.54	3.03	0.33			10.70

Summary of conditions at study sites. Months April-May are referred as 'spring' and July-September are referred as 'summer'. Units for bottom water nutrients are reported in µM, except for dissolved oxygen reported in mg L^{-1}. Caminada is represented as CA and Sandy Point is represented as "SP".

4.3 Tripod

Tripod time series results are shown in Figures 26, 27, 28, 29 and 30. Temperatures at CAT1_OUT fluctuated from 26.45 to 29.89 ºC and salinity varied from 32.02 to 35.61 until the passage of TS Gordon where both stabilized around 28.47 ºC and 33.59, respectively (Figure 26e and 26f). Inside bottom water temperature was steady between 26.98 and 29.02 ºC and salinity remained between 33.72 and 35.42. Wave height was similar at both stations. At SPT1_OUT, temperatures varied from 24.85 to 29.93 ºC and salinity ranged from 15.95 to 34.75 (Figure 27e and 27f). Both parameters fluctuated the most from 18 June to 26 June 2019 when wave heights were around 1 m and combined shear stress varied from 0.5 to >2.0 Pa.

Overall, temperature and salinity at CAT1_OUT and CAT2_IN were relatively stable in comparison to SPT1_OUT. Both parameters fluctuated gradually at Caminada dredge pit, with few rapid changes. However, SPT1_OUT experienced prompt variations of salinity and temperature, especially in middle to late June. The range of temperature was similar at CAT1_OUT, CAT2_IN, and SPT1_OUT. Conversely, the range of salinity was much greater at SPT1_OUT, extending from less than 16 to more than 34. The rapid fluctuations of both parameters and large range of salinity at SPT1_OUT are likely due to the proximity to the mouth of the Mississippi River and possibly wave forces enhancing mixing of the water column.

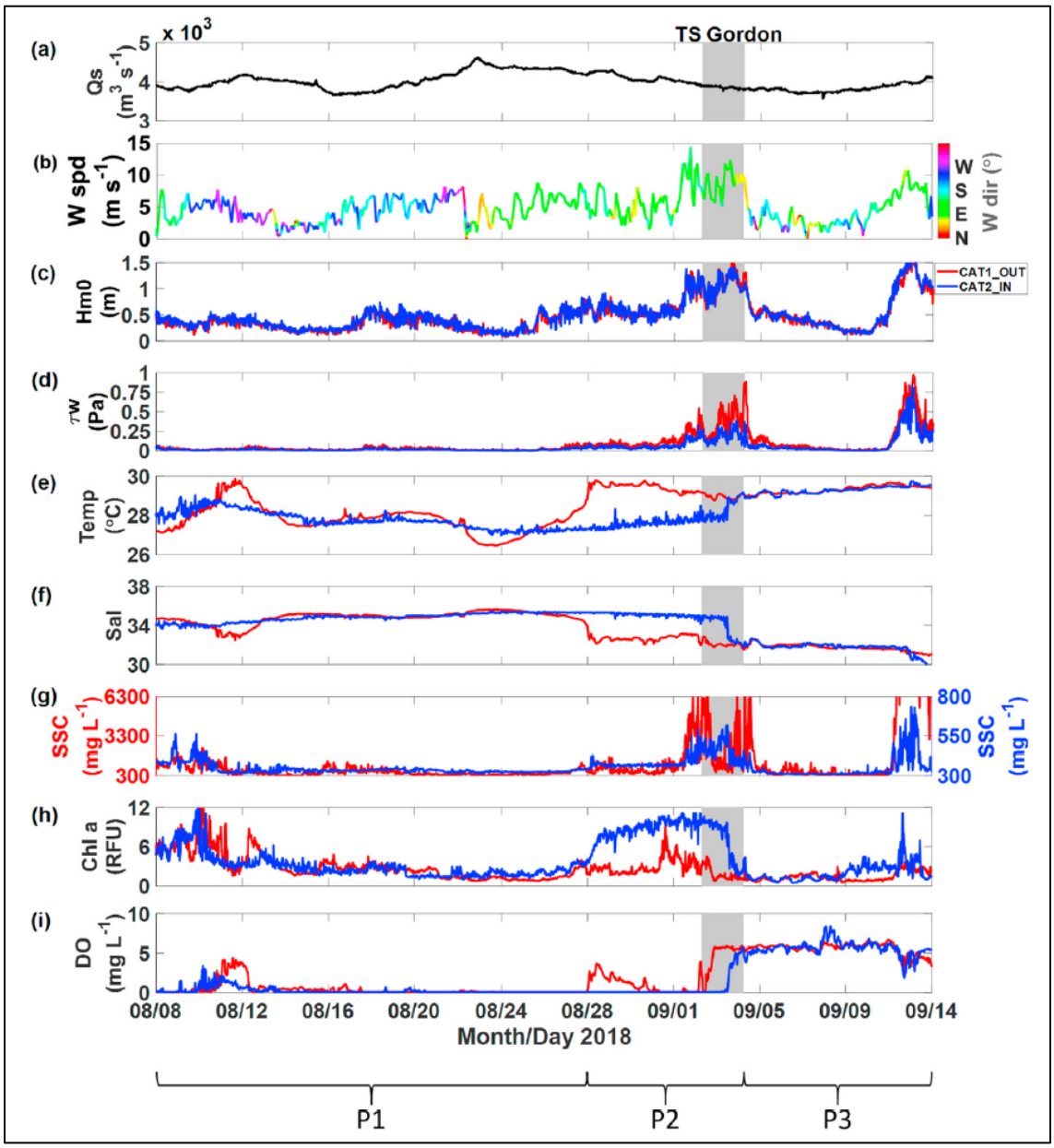

Figure 26. Time series results from Caminada Dredge Pit.

Time series results outside (red line) and inside (blue line) of CA dredge pit: (a) Atchafalaya river discharge (Qs) measured every 15 min at USGS station, Simmesport, LA; (b) wind speed (black line) and wind direction (colors) (averaged hourly) at NOAA station SPLL1, South Timbalier Block 52, LA; (c) wave height; (d) wave-induced bed shear stress; (e) temperature; (f) salinity; (g) near bed SSC; (h) chlorophyll a; (i) DO (from Bales et al., 2021).

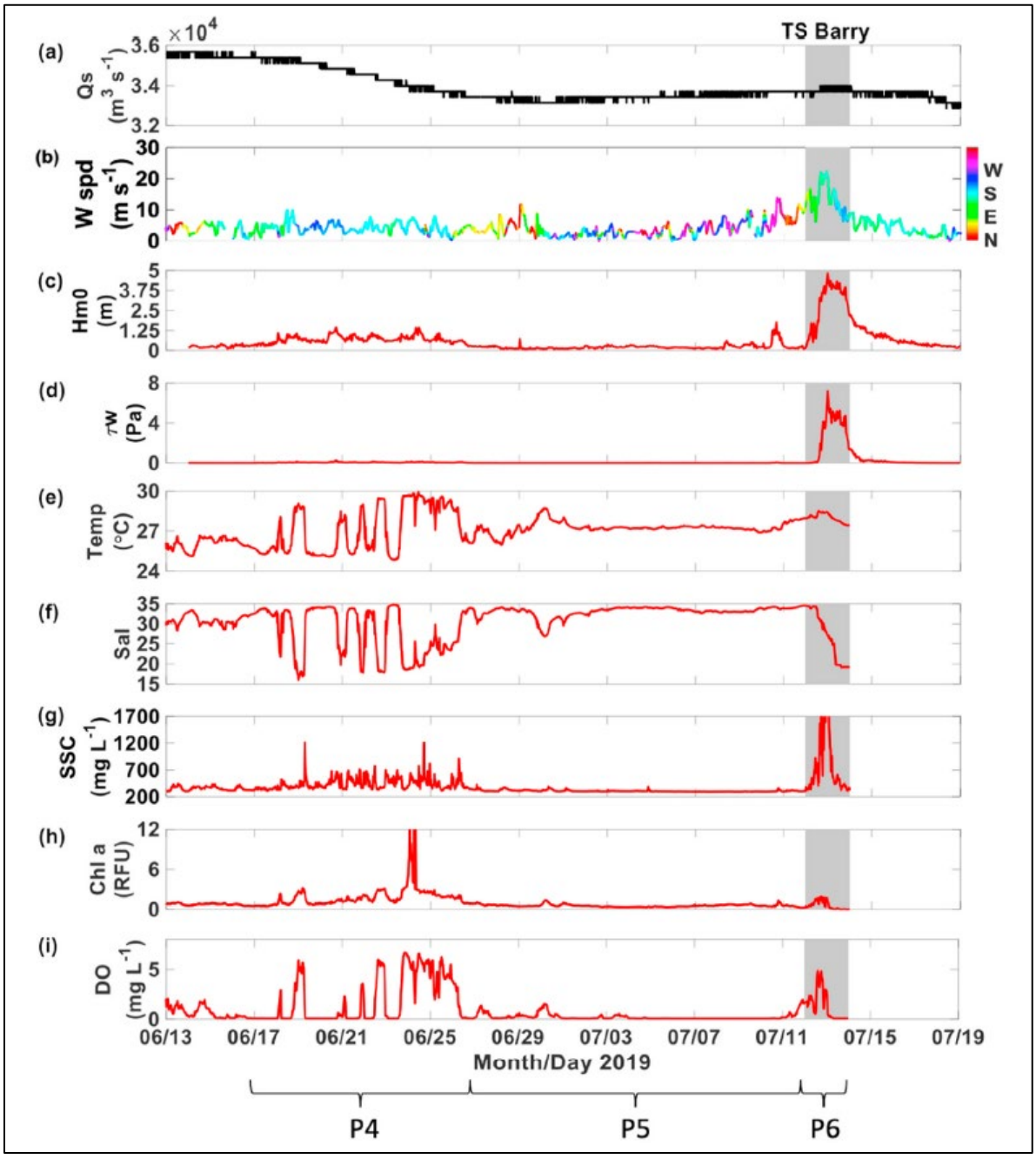

Figure 27. Times series results from Sandy Point Dredge Pit.

Time series results outside SP dredge pit (inside SP dredge pit was not recovered): (a) Mississippi river discharge (Qs) measured every 15 min at USGS station, Baton Rouge, LA; (b) wind speed (averaged hourly) at NOAA station PSTL1, pilot's station east, SW pass, LA; (c) wave height; (d) wave-induced shear stress; (e) temperature; (f) salinity; (g) near bed SSC; (h) chlorophyll a; (i) DO (from Bales et al., 2021).

Near bed SSC outside CA dredge pit were much higher than inside pit, fluctuating between 300 and >6,300 mg L^{-1} (Figure 26g). Suspended sediment near seabed generally remained between 290 to 450 mg

L^{-1} outside SP dredge pit (Figure 27g). Suspended sediment concentrations generally varied with combined shear stress.

Greatest amounts of suspended sediment concentrations were associated with increased shear stress at all locations. SSC near seabed at SPT1_OUT reached higher levels than SSC at CAT2_IN. The contribution of riverine sediments from the nearby Mississippi River mouth may further explain this difference.

Overall, near seabed chlorophyll a values were lower at SPT1_OUT in comparison to CAT1_OUT and CAT2_IN. Vertical profiling data confirms that the chlorophyll a distribution throughout the water columns at CA and SP were different. CA stations contained highest chlorophyll a at lower depths while chlorophyll a at SP was restrained to the upper water column. At CA dredge pit, CAT2_IN experienced longer periods of hypoxic conditions. Fluctuations in DO concentrations in the BBL at CA and SP were dominantly associated with changes in water masses. At CA dredge pit, increased SSC was occasionally associated with decreased DO which may imply a biogeochemical control on hypoxia of bottom waters near CA dredge pit.

The currents at CAT1_OUT and CAT2_IN, measured using ADCP and ADV, were highly variable with eastward and westward being most dominant directions (Figures 28c, 28d, 29c, and 29d). Mean current velocities of surface and middle waters were slightly higher at CAT2_IN. The slight increase in current velocities over eastern Ship Shoal likely resulted from maintaining continuous flow (Kobashi and Jose, 2018).

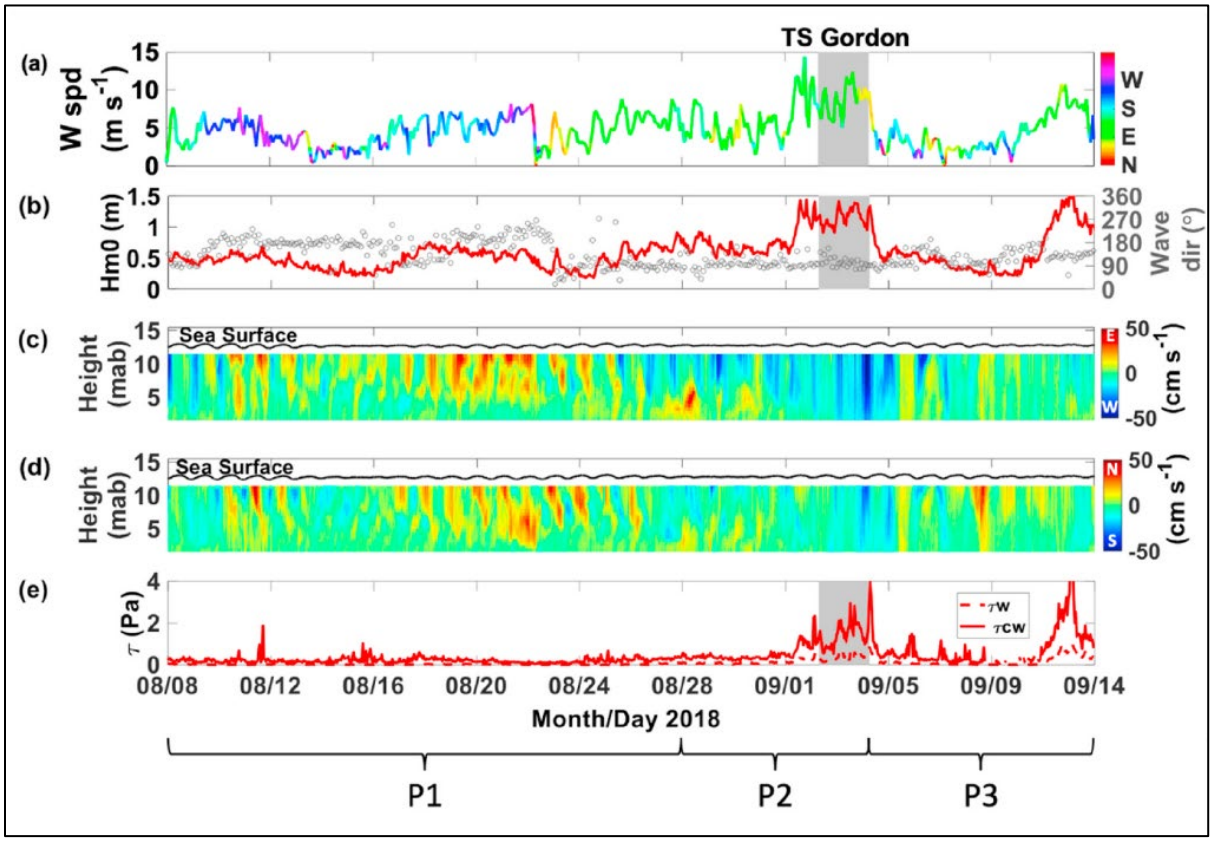

Figure 28. Times series results from outside Caminada Dredge Pit.

Time series results outside CA dredge pit (CAT1_OUT): (a) wind speed and direction (averaged hourly) at NOAA station SPLL1, South Timbalier Block 52, LA; (b) wave height (red line) and wave direction (grey circles); (c) vertical profile of east (+)/west (-) current velocities; mab is meters above bed; (d) vertical profile of north (+)/south (-) current velocities; (e) wave-induced bed shear stress (dashed red line) and combined wave-current bed shear stress (solid red line) (from Bales et al., 2021).

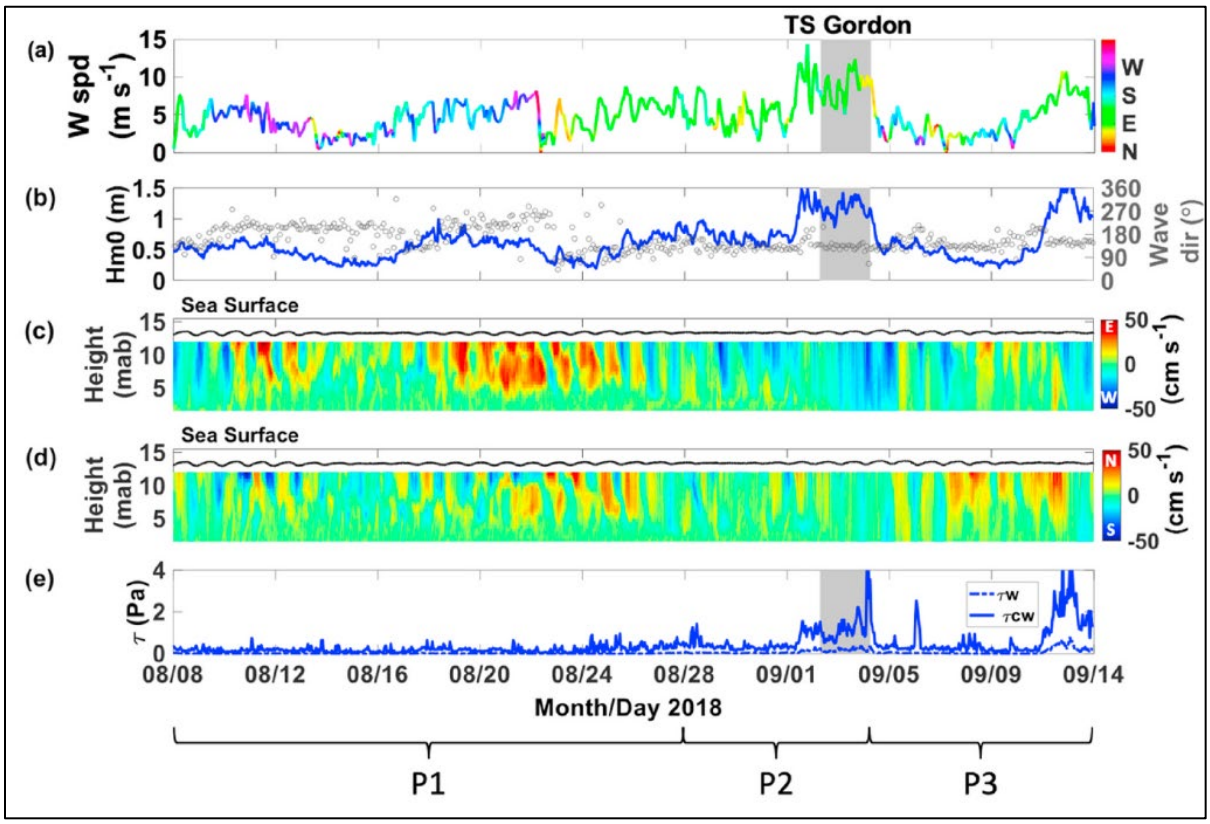

Figure 29. Time series results from inside Caminada Dredge Pit.

Time series results inside CA dredge pit (CAT2_IN): (a) wind speed and direction (averaged hourly) at NOAA station SPLL1, South Timbalier Block 52, LA; (b) wave height (solid blue line) and wave direction (grey circles); (c) vertical profile of east (+)/west (-) current velocities; mab is meters above bed; (d) vertical profile of north (+)/south (-) current velocities; (e) wave-induced bed shear stress (dashed blue line) and combined wave-current bed shear stress (solid blue line) (from Bales et al., 2021).

Current profiles outside SP dredge pit collected using ADCP showed prominent stratification where surface currents flowed in opposite directions as middle and bottom water currents (Fig 30c and 30d). For most of the observation period, surface currents flowed northwestward and middle to bottom water currents flowed southeastward, generating a horizontal current shear. The opposite flow directions of shallow and deep-water masses at SPT1_OUT have been previously observed in stratified water columns (Lentz, 2001). Surface currents at SPT1_OUT were dominantly controlled by wind direction, while deeper currents followed the pattern of the clockwise gyre associated with the Louisiana Bight.

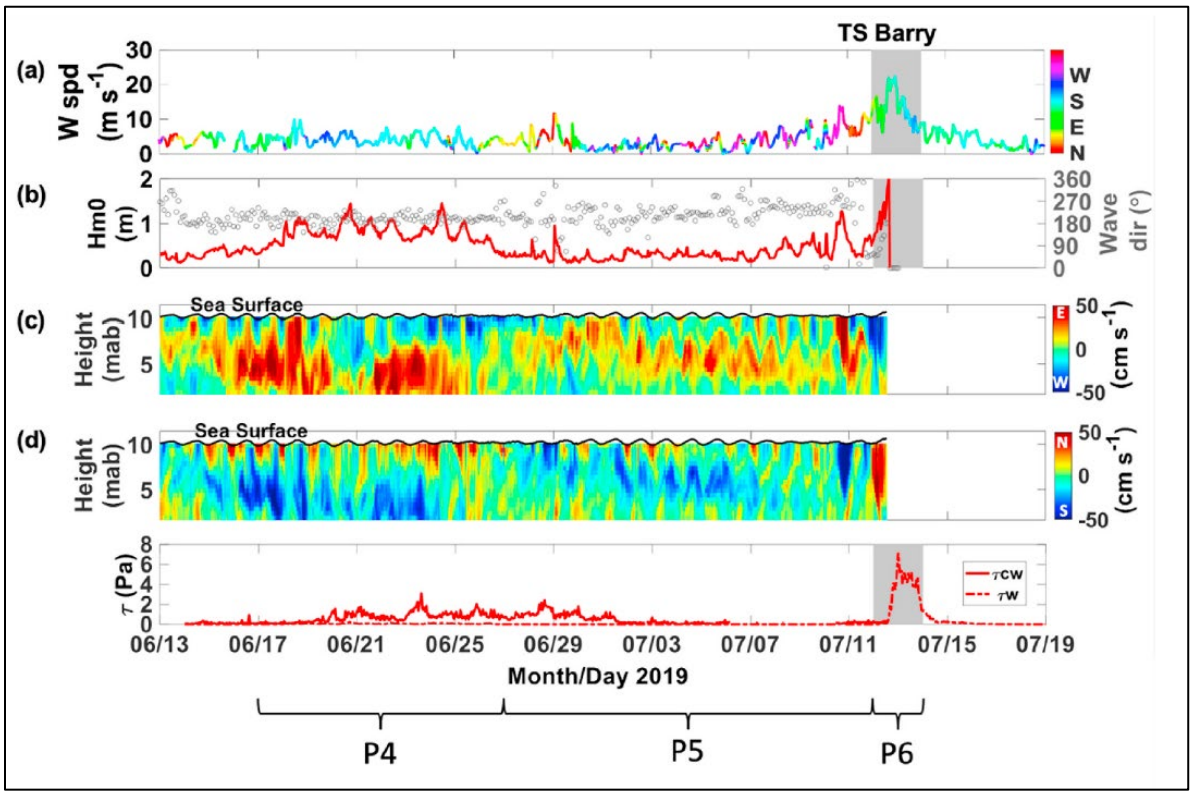

Figure 30. Times series results (ADCP) from outside Sandy Point Dredge Pit.

Time series results outside SP dredge pit (SPT1_OUT): (a) wind speed (solid black line) and wind direction (grey circles) averaged hourly at NOAA station PSTL1, Pilot's Station East, SW Pass, LA; (b) wave height and wave direction; (c) vertical profile of east (+)/west (-) current velocities; mab is meters above bed; (d) vertical profile of north (+)/south (-) current velocities; (e) wave-induced bed shear stress (dashed red line) and combined wave/current-induced bed shear stress (solid red line) (from Bales et al., 2021).

The vertical structure of current velocities inside CA dredge pit was affected by the coupling of increased depth of the pit and the topography of eastern Ship Shoal. While the vertical current structure near SP dredge pit was controlled mainly by interactions among clockwise gyre, direction-variable surface winds and Mississippi River plume.

4.4 Geophysical Work

Figure 31 shows the bathymetric changes in Caminada pit from 2016 to 2017 and from 2017 to 2018. It can be seen that there were minimal outward pit wall migrations and a thin layer of sediment accumulation in pit bottom (Figure 31E).

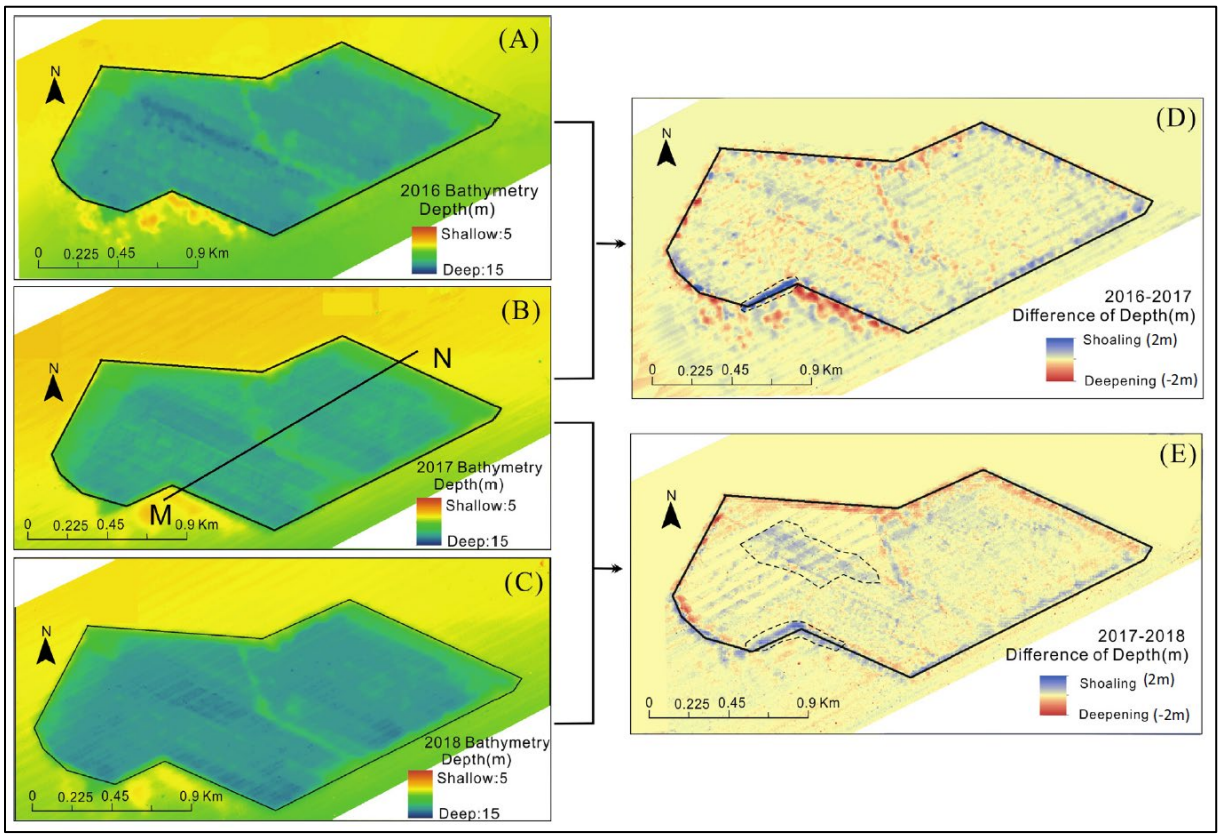

Figure 31. Bathymetry, side-scan, and gradient map of Caminada dredge pit in August 2018.
Bathymetry map of Caminada (South Pelto) dredge pit in three different surveys from 10/2016, 07/2017, and 08/2018 (From Liu et al. 2022).

4.5 Modeling Work

We followed Shropshire et al.'s (2020) biological parameterizations in our GOM_5km model. Two tests were carried out from August 1, 2005 to December 31, 2008 and from August 1, 2018 to December 31, 2019, respectively. There were 1,270 nutrient profiles (i.e., NO3, PO4, $SiOH_4$) and DO profiles observed from January 1, 2006 to December 31, 2008 by the World Ocean Database (WOD) (Figure 32e). Modeled nutrient profiles agree well with the WOD observations (Figure 32a~c). Relatively high nutrient concentrations were detected at near surface layers due to that only profiles near the Mississippi River plume and the Atchafalaya River plume were compared. The two river plumes diverted a considerable amount of nutrients to the northern Gulf annually. Surprisingly, the GOM_5km model well captured the shape of DO profiles with relatively high values at sub-surface and surface layers, but low concentrations at bottom layer when water depth was shallower than 30 meters.

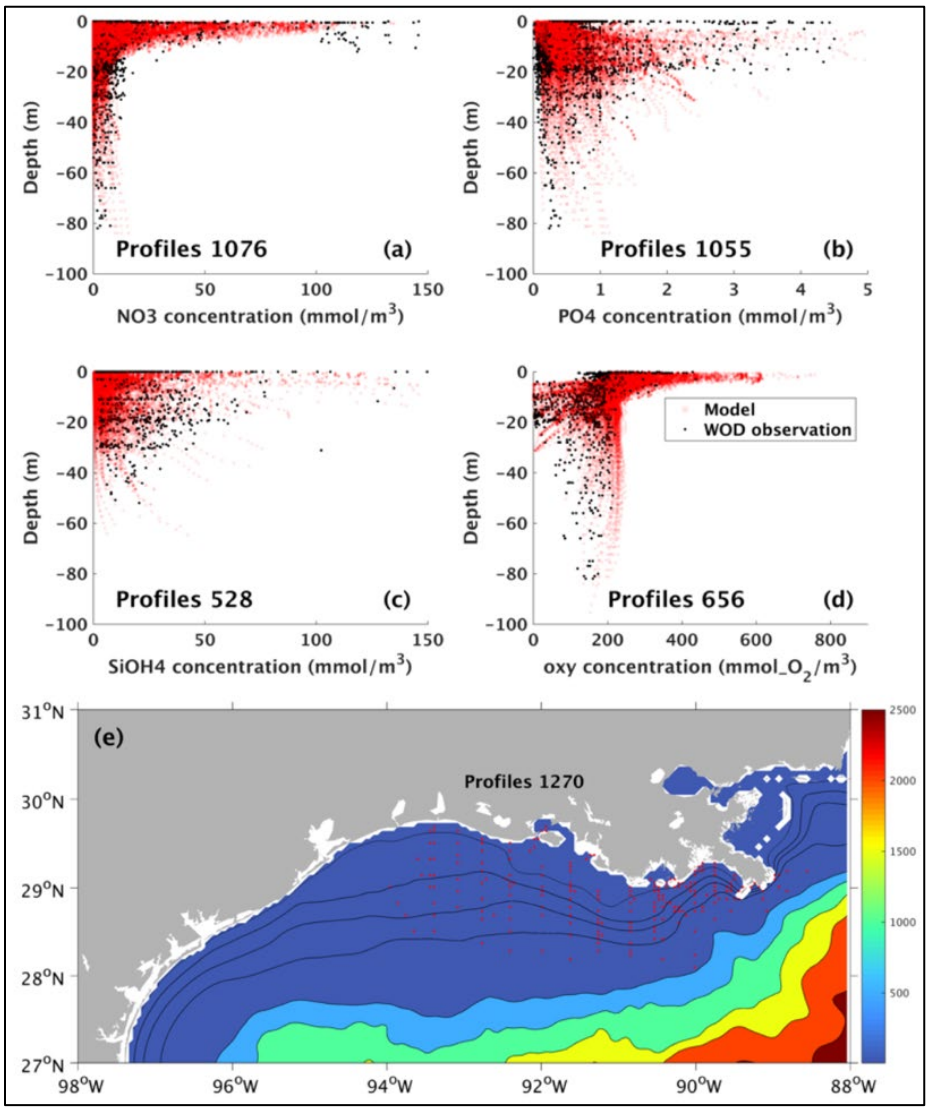

Figure 32. Modeled vs. observed NO_3, PO_4, and $SiOH_4$ profiles.

Comparisons between modeled and observed profiles for (a) NO_3, (b) PO_4, (c) $SiOH_4$, and (d) dissolved oxygen. (e) Bathymetry contours (color) and locations of profiles observed (red dots). The observations were provided by the World Ocean Database (WOD) (https://www.nodc.noaa.gov/OC5/WOD/pr_wod.html).

Surface chlorophyll a concentration patterns were also well reproduced near the two river plumes comparing with the MODIS-Aqua and MODIS-Terra chlorophyll *a* estimate (Figures 33 and 34). However, our model overestimated the chlorophyll a concentrations right at the river months which served as source points in the model. The unrealistically high values were driven by the relatively high nutrient loads from the source points. More sensitivity tests were needed to suppress the simulated chlorophyll a around river mouths, for example, the half saturation coefficients for nutrients uptake by phytoplankton groups were critical for controlling the nutrients dynamics. Another reason why remote sensing estimate were much lower than the model simulation was that the former ignored the estimates at estuarine area and river mouth regions due to the colored dissolved organic matter (CDOM) effects while our model covered such areas. On the shelf area, the modeled chlorophyll *a* concentrations were close to the remote sensing estimates.

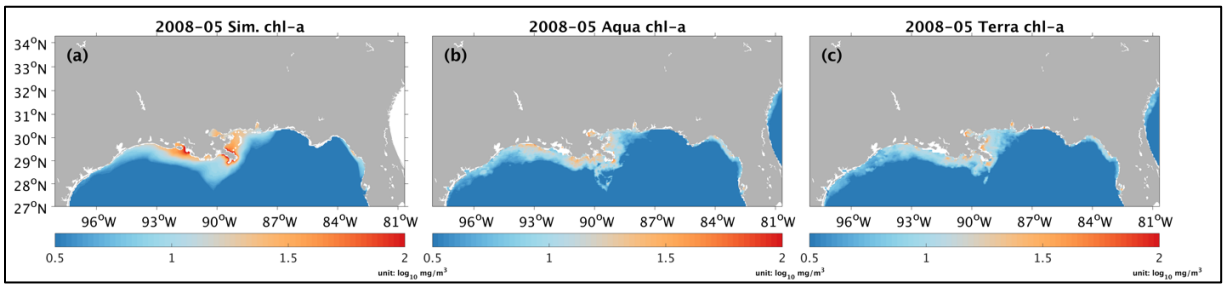

Figure 33. May 2008 modeled, MODIS-Aqua, and MODIS-Terra surface chlorophyll a.

Monthly averaged (a) Modeled, (b) MODIS-Aqua, and (c) MODIS-Terra surface chlorophyll a concentrations in the northern Gulf of Mexico for May 2008. Note that the unit shown was in $\log_{10}$ mg/m^3.

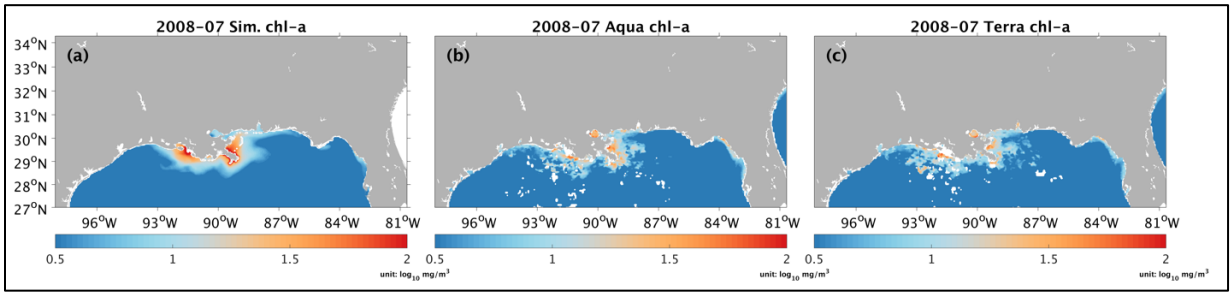

Figure 34. July 2008 modeled, MODIS-Aqua, and MODIS-Terra surface chlorophyll a.

Monthly averaged (a) Modeled, (b) MODIS-Aqua, and (c) MODIS-Terra surface chlorophyll a concentrations in the northern Gulf of Mexico for July 2008. Note that the unit shown was in $\log_{10}$ mg/m^3.

Hypoxic water was found in 2008 summer and 2019 summer both from DO measurements by the SEAMAP Groundfish Survey (Figure 35b, 35d) and the Shelf-wide cruise (Figure 36b, 36d). However, hypoxic area was larger in 2008 summer than in 2009 summer. Such difference could also be detected from the numerical results (Figures 35a, 35c, 36a, 36c). The modeled bottom DO concentration could capture a feature that the biggest hypoxic area occurred in July rather than other summer months (i.e., June and August) which corresponded to the measurements. Nevertheless, bottom DO concentration was about 1mg/L greater than the SEAMAP cruise and Shelf-wide cruise observations, leading to underestimated hypoxic areas. More sensitivity tests should be carried out related to sinking velocity of particulate organic nitrogen, and oxygen consumption rate due to remineralization and nitrification at the bottom layer of water column. Our next step is to fine tune the GOM_5km coupled hydrodynamic-biological model in terms of bottom DO concentration.

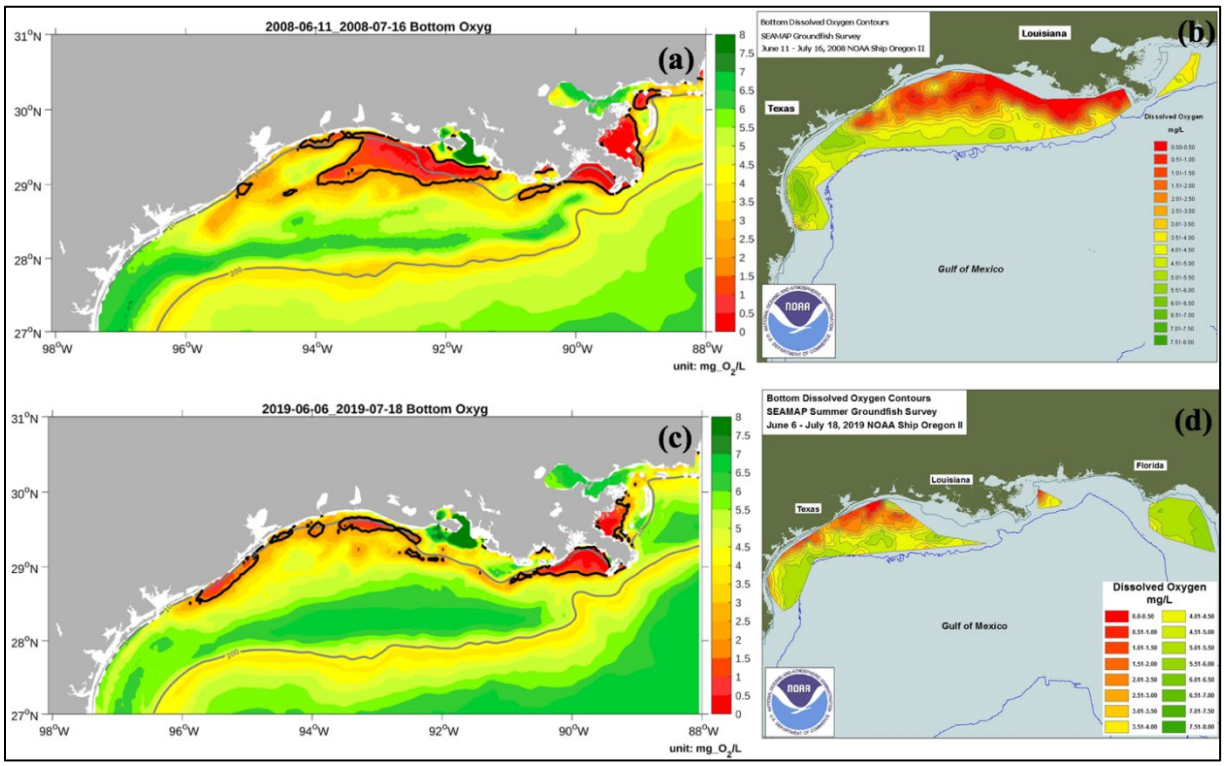

Figure 35. Simulated and averaged bottom DO concentrations in June-July of 2008 and 2019.

Simulated bottom dissolved oxygen concentration averaged (a) from June 11, 2008 to July 16, 2008 and (c) from June 6, 2019 to July 18, 2019. Measured bottom dissolved oxygen concentration averaged (b) from June 11, 2008 to July 16, 2008 and (d) from June 6, 2019 to July 18, 2019 by the Southeast Area Monitoring and Assessment Program's (SEAMAP) Groundfish Survey (see https://www.ncei.noaa.gov/products/hypoxia-watch). Two grey curves in (a) and (c) represent isobath of 10 m and 200 m, respectively. Black solid lines in (a) and (c) are contour lines of oxygen concentration of 2 mg/L, below which water masses are considered hypoxia.

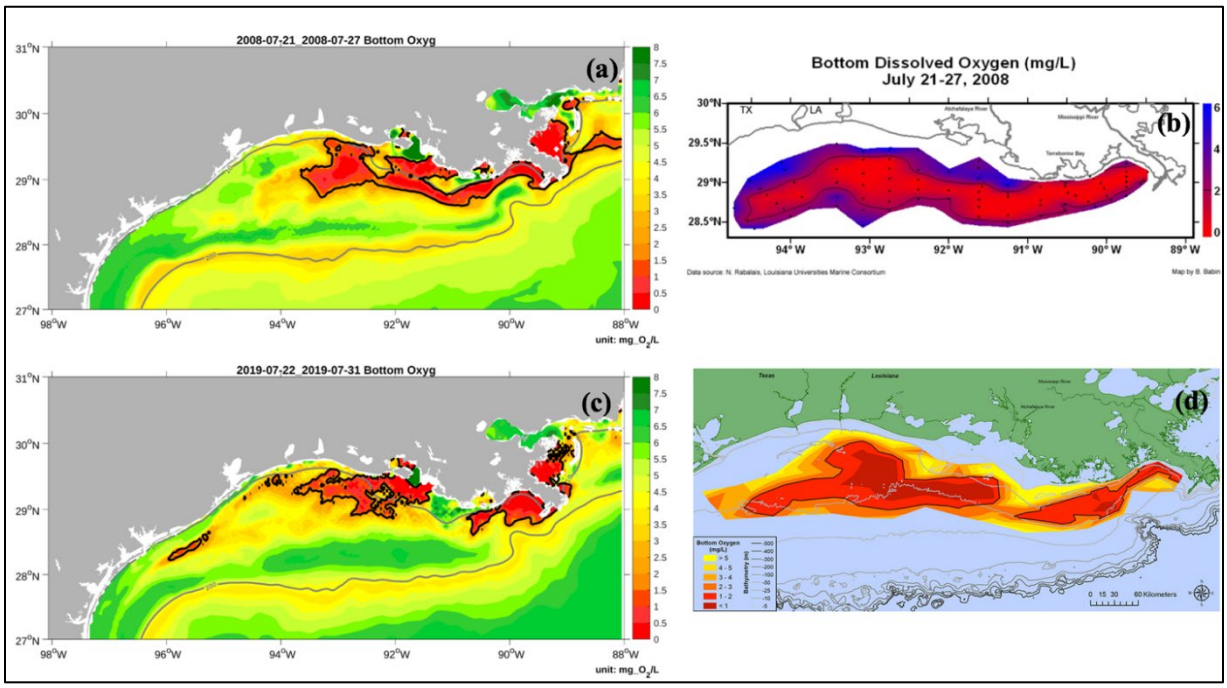

Figure 36. Simulated and averaged bottom DO concentrations in late July of 2018 and 2019.

Simulated bottom dissolved oxygen concentration averaged (a) from July 21, 2008 to July 27, 2008 and (c) from July 22, 2019 to July 31, 2019. Measured bottom dissolved oxygen concentration averaged (b) from July 21, 2008 to July 27, 2008 and (d) from July 22, 2019 to July 31, 2019 by the Shelf-wide cruise (details can be found at https://gulfhypoxia.net/research/shelfwide-cruise). The black solid lines in (b) and (d) indicate oxygen concentration of 2 mg/L.

5 Discussion and Conclusions

5.1 Physical and Geological Processes

The following section summaries the major findings from Xue et al. (2021), Bales et al. (2021) and Liu et al. (2021). Bales et al. (2021) reported that bottom waters inside Caminada dredge pit experienced fewer variations in water masses, lower DO conditions, and lower SSC when comparing to outside Caminada pit throughout the tripod deployment. Fewer changes in bottom water masses inside Caminada pit were likely due to is the location further offshore. Bottom water masses outside Caminada pit were more exposed to less saline waters from the coast. DO conditions at both locations were dominantly associated with changes in bottom water masses which suggests strong physical control on DO conditions at these locations. Bales et al. (2021) also suggested that a resuspension event at the end of the 2018 observational period was accompanied by a decrease in DO levels at both stations. This may suggest some biogeochemical control on DO conditions as well. Highest SSC at both locations related to periods of greatest wave-current induced shear stress. As shown by the profiling data, the water column at shoal crest stations CA8 and CA11 were less stratified and bottom waters were most saturated with DO. These locations were most likely more affected by wave energy, which promoted physical mixing of the water column. Bales et al. (2021) then compared physical conditions between Caminada with Sandy Point dredge pit. Bottom waters outside Sandy Point dredge pit experienced more extreme temperature and salinity changes when comparing to Caminada due to the Mississippi River plume's influence. Vertical profiling data also shows an extreme density gradient at Sandy Point stations that results from the Mississippi River plume. The vertical current structure at Sandy Point was greatly affected by a combination of the Mississippi River plume, the clockwise gyre associated with the Louisiana Bight, and daily meteorological activity.

Based on coring and sediment radionuclide studies, Xue et al. (2021) found that sediment infilling at the Caminada dredge pit is not dominated by ambient Ship Shoal sand, as there is an evident lack of sand within the infilled material of the interior of the dredge pit. Results from this study suggest that mainly fine to medium silts are deposited within the dredge pit, punctuated by laminations of coarser silt with few very fine sand laminations. Based on the presence of sediments containing ^{7}Be and grain size analysis of the cores taken within Caminada dredge pit, Xue et al. (2021) determined the sediments within this sandy dredge pit are sourced from a combination of the Atchafalaya and Mississippi River plumes. In addition, storms could be resuspending fine grained material along the shelf and local bays, delivering it to the dredge pit. Xue et al. (2021) also suggested that Caminada dredge pit is infilling at a slower rate (~ 5 times) than numerical modeling predicted (Nairn et al. 2005; Liu et al. 2020b). Nairn et al. (2005) suggested sandy dredge pits would exhibit an increased sedimentation rate compared to paleo-channels with mud overburden due to bedload transport of sand outside the pit and subsequent deposition inside the pit. In contrast to this model prediction, from 2017 to 2018, Xue et al. (2021) found an increase in area covered by fine sediments overlaying the original Ship Shoal. Xue et al. (2021) suggested that new infilling models are needed for future coastal restoration work, particularly for sandy dredge pit environments. Furthermore, due to the dredge pit infilling with finer-grained sediments, sandy shoal restoration quality sand resources are not renewable in this location.

Based on geophysical data, Liu et al. (2021) concluded that bathymetric maps of three post-dredging surveys indicate that nearly no new net sediments deposited outside of the Caminada pit but new sediment was deposited inside the pit. Liu et al. (2021) found that Caminada pit is presently filling at an average rate of 0.15 (±0.05) m/yr. The topography of the seafloor inside the pit has a direct relationship with the patchy mud distribution. Side-scan mosaic maps showed that the troughs inside pit infilled with mud within two years post dredging. Caminada Dredge Pit is under the combined controls of the supply of far-field river plume suspended sediments, the erosion of adjacent seabed sediments by waves and currents,

sediments produced by pit wall failure, and sediments deposited during and after hurricanes and tropical storms.

5.2 Biogeochemical Process

Seasonality did not widely affect dredge pit conditions, but there were differences in SOC between the inside and outside stations of Caminada and Sandy Point. Caminada sediment oxygen consumption data demonstrated significant differences between inside and outside stations. In spring, SOC rate of inside station CA2_IN was not significantly higher than outside stations CA8 and CA11 ($p = 0.113$), probably due to an outlier replicate core that was 2-fold lower that other two replicate cores, which when removed, shows that inside is significantly different than outside ($p = 0.0001$). On average SOC rates in spring were 5-fold higher inside the pit compared to outside, and similarly in summer, SOC rates were significantly higher inside the pit than outside stations ($p = 0.00001$), by a factor of two. Sediment TOC content was higher inside the pit compared to outside, but only station CA5_IN had significantly higher TOC than outside stations in spring and summer ($p = 0.003$ and 0.00001, respectively). The CA5_IN station also had higher TOC content than CA2_IN although both located inside the pit, suggesting variability in in TOC and sediment distribution inside the pit. However, despite higher TOC content at CA5_IN, higher SOC rates were observed at station CA2_IN. This points to the fact that SOC in sediment is not just a function of sediment TOC content but other variables like bottom O_2 concentration and efficiency of reoxidation of reduced species (Lehrter et al., 2012). Further, this complex relationship suggests that other anaerobic processes could be driving organic matter remineralization and O_2 consumption, such as nitrification, particularly ammonia oxidation (Campbell et al., 2019; Pakulski et al., 2000; Nunnally et al., 2014), and oxidation of other reduced species such as hydrogen sulfide oxidation (Brooks and Mahnken, 2003; Lee et al., 2019). Hydrogen sulfide oxidation has been observed in previously studied dredge pits (Graca, 2009), as well as reduced iron and manganese oxidation (Lehrter et al., 2012; Jorgensen, 1982; Sampou and Oviatt, 1991; Aller et al., 1996; Jones et al., 2015). Overall, the larger differences in SOC rates inside versus outside the pit does impact the overlying bottom water O_2 conditions. The stations inside Caminada had consistently low O_2 compared to outside stations, about 2 times lower, suggesting that sluggish bottom water current coupled with high SOC inside the pit is responsible for the persistent hypoxic conditions inside the pit (Johnston 1981; Nairn et al., 2004; Flocks and Franze, 2002; Graca, 2009).

The sediment oxygen consumption rates at Sandy Point did not show statistically significant differences between inside and outside stations. In spring, SOC inside and outside the pit stations fell within the same range, with outside station SP11 having the highest SOC. Similarly, summer SOC rates of inside and outside stations fell within the same range, with outside station SP4 having the highest SOC. %TOC was significantly higher inside SP compared to outside ($p = 0.02$), however, all SP stations were relatively higher in TOC than CA stations, except CA5_IN. This is contrary to our expectations of higher SOC inside the pit driven by higher organic matter accumulations, which differs from what was observed in CA. However, closer comparisons of bottom O_2 variabilities inside versus outside the two different pits shows interesting patterns. CA shows dramatic bottom O_2 differences inside versus outside, whereas SP does not (Table 8). This suggests that SP, which has much more energetic setting than CA, replenishes bottom water at a faster rate. In fact, ADV based bottom current velocities were found to be consistently higher inside Sandy point pit with respect to Caminada pit (Bales et al., 2019). Overall, inside CA stations had significantly higher (~2x higher) SOC rates than inside SP stations for both spring and summer ($p=0.04$ and $p=0.001$, respectively). This does not support the hypotheses, that the mud-capped dredge pit Sandy Point will have higher SOC rates compared to the sandy dredge pit Caminada due to higher rates of organic matter supply. It is likely that Caminada was less energetic and more stratified than Sandy Point as a result of its proximity to the Mississippi River delta, suggesting that prevailing physical processes may play a more dominant role in determining dredge pit O_2 dynamics than sediment biogeochemistry.

The high organic matter deposition coupled with the low-flow environment found in the bottom of dredge pit at Caminada limited the release of inorganic nutrients back to water column and fueled a unique and healthy MPB community. High concentration of ammonium and high sediment chl a concentration found inside the dredge pit at Caminada were not detected at Sandy Point. Sandy Point dredge pit can be characterized as a highly productive and energetic environment that had persistently high chl a concentration in the surface waters during spring and summer that were not seen at depth nor in sediment samples. Diatoms were more abundant in the summer surface water when compared to spring, whereas cyanobacteria were more present in spring. Microscopy observations revealed the diatom community to be mostly dominated by chain-forming centric diatoms, however no clear distinction was shown in species diversity between inside and outside of the pit. MPB diversity was also similar between the two dredge pits, however, the biomass differed greatly. Caminada dredge pit had higher chl a concentration observed in sediment samples (18.9 ± 19.2 μg m^{-2}) when compared to Sandy Point (10.1 ± 8.88 μg m^{-2}). Sandy Point was comparable to other studies from that region that reported the MPB production to be small when compared to that of phytoplankton in the overlying water column at stations west of the Mississippi River bird-foot delta (Lehrter et al. 2014). Interestingly, both dredge pits allowed for the establishment of unique sediment MPB community, mainly consisting of Coscinodiscus spp. Coscinodiscus spp. is a unique, single cell centric diatom commonly found in the northern Gulf that is well adapted to low light and low oxygen conditions (Baustian et al. 2013). This study suggests that this species was abundant inside the dredge pit at Caminiada due to this special adaptation to low light and low oxygen and present at all stations at Sandy Point given that all stations experienced frequent mixing that hindered light reaching the sediment floor. Previous studies have reported the MPB of sandy shoals, like seen in Caminada stations outside the dredge pit, to be mostly pennate diatoms and filamentous cyanobacteria that are not associated with the water column (Grippo et al. 2009, 2010, Baustian et al., 2013). The discovery of these well-established, diatom dominated MPB communities within the dredge pits can also potentially aid in the stabilization of sediments during infill as diatom dominated biofilms have been to stabilize soil (Valentine and Mariotti 2020).

5.3 Summary

The setback buffer distance from pits to oil/gas infrastructure currently being used by BOEM ranges from 500 feet for wells to 1,000 feet for pipelines.. Our results show that pit walls of both CA and SP were relatively stable. Due to its cohesive nature, paleo river channel dredge pits (like Sandy Point) have fairly stable pit walls with minimal migration. Similarly, Liu et al. (2021) reported that sandy Caminada pit walls became slightly gentler two years after dredging and localized sediment erosion and deposition were found near the walls. Less than a few meters of outer migration of the walls of Caminada pit indicate that current setback buffer distances of 1000 ft from planned pipelines is adequate. Since it will take several more years to fill up CA and SP pits, long-term continuous morphological monitoring of bathymetry, sidescan and subbottom is needed. In particular, sidescan data are very valuable in detecting seabed reflectivity and identifying the types of muds and sands of infilling sediments on pit bottom.

Temperature, salinity, turbidity, and dissolved oxygen are fundamental water quality parameters in the dredge pits areas. Turbidity plays a key role in controlling light attenuation and impacting photosynthesis. Dissolved oxygen is critical to marine animals living in both water column and seabed surface. As shown in this study, hypoxic conditions were found in both CA and SP pits. Despite the fact that CA pit is on top of energetic and sandy Ship Shoal, dissolved oxygen in CA pit was below 2 mg/L for a fairly long period: two to three weeks (Figure 26). The impact of low oxygen on benthos should be monitored continuously so that the recovery of benthos over time can be tracked. Time-series tripod observation and vessel-based profiling used in this project are two effective and complementary methods. Tripod or buoy observation is limited to one station but can provide data with excellent temporal resolution (hours to minutes), especially during events like cold fronts or hurricanes. Vessel-based profiling can be performed in

multiple targeted stations to get great spatial coverage (both inside and outside pits) but is limited to the short duration of a few days during research cruises.

Sediment oxygen consumption, total organic carbon, phytoplankton biomass and its dominant taxa, microphytobenthos and its dominant taxa, as well as nutrients are key biological and chemical parameters/data in the dredge pit areas. In this project, due to limited budget, parameters were mainly collected in spring and summer in CA pit in one year and in spring and summer in SP pit in another year. It is recommended that parameters in all four seasons of the whole year should be collected so that the impacts from physical parameters (like temperature, stratification, river discharge, winds, waves, and pit infilling) can be fully captured. In the long term, intra-annual variability should also be considered in dredge pit studies. In addition to the above biological and chemical parameters, future research can also be performed on the impact of dredge pits on turtle, fish, bird, and benthos.

When designing new dredge pits, the cutting depths should be planned carefully. For instance, a deep pit will likely develop a sluggish environment which tends to develop hypoxia whereas a shallow pit will likely have less impact on hydrodynamics and dissolved oxygen. Future water quality modeling work can be focused on the threshold of cutting depth in triggering hypoxia conditions. In other words, is there a critical depth to significantly increase the probability of low dissolved oxygen in dredge pits? Moreover, how does the geometry of dredge pits (elongated vs. rounded) impact the development of low dissolved oxygen? Since hypoxia tends to develop in summer, if budget is limited, dissolved oxygen profiles and bottom sediment sampling in summer should be high priorities. Our results show that the sediment infilling at both CA and SP pits were lower than the past modeling predictions. Future modeling effort should be focused on how to calibrate the parameters used in this model and how to add new processes (such as biogeochemical cycle and event-driven degassing/consolidation) to improve future model predictions.

Works Cited

Adhikari PL, White JR, Maiti K, Nguyen N. 2015. Phosphorus speciation and sedimentary phosphorus release from the Gulf of Mexico sediments: implication for hypoxia. Estuarine Coast Shelf Sci. 164:77–85.

Aller RC, Blair NE, Xia Q, Rude PD. 1996. Remineralization rates, recycling, and storage of carbon in Amazon shelf sediments. Cont Shelf Res. 16 (5–6):753–786.

Bales R, Xu K, Li G, Maiti K, Liu H. 2021. Hydrodynamics, sediment transport, and water quality of two contrasting dredge pits on the Louisiana shelf. Cont Shelf Res. 230, 104569.

Bales, R. 2020. Hydrodynamics, sediment transport, and water quality of two contrasting dredge pits on the Louisiana Shelf [thesis]. Baton Rouge (LA): Louisiana State University. 84 p.

Barley, M. 2020. Seasonal infilling and sedimentary characteristics in sandy versus muddy coastal borrow areas on the Louisiana Continental Shelf, USA [thesis]. Baton Rouge (LA): Louisiana State University. 84 p.

Baskaran M, Coleman CH, Santschi PH. 1993. Atmospheric depositional fluxes of 7Be and 210Pb at Galveston and College Station, Texas. J Geophys Res D: Atmos. 98 (D11): 20555–20571.

Baustian MM, Rabalais NN, Morrison WL, Turner RE. 2013. Microphytobenthos along the Louisiana continental shelf during mid–summer hypoxia. Cont Shelf Res. 52:108–118.

Berelson WM, McManus J, Severmann S, Reimers CE. 2013. Benthic flux of oxygen and nutrients across Oregon/California shelf sediments. Cont Shelf Res. 55:66–75.

Berelson WM, McManus J, Severmann S, Rollins N. 2019. Benthic fluxes from hypoxia influenced Gulf of Mexico sediments: impact on bottom water acidification. Mar Chem. (209):94–106.

Berelson W, McManus J, Coale K, Johnson K, Burdige D et al. 2003. A time series of benthic flux measurements from Monterey Bay, CA. Cont Shelf Res. 23 (5):457–481.

Bianchi TS, DiMarco SF, Cowan JH, Hetland RD, Chapman P, Day JW, Allison MA. 2010. The science of hypoxia in the Northern Gulf of Mexico: a review. Sci Total Environ. 408 (7):1471–1484.

Brooks KM, Mahnken CV. 2003. Interactions of Atlantic salmon in the Pacific Northwest environment: III Accumulation of zinc and copper. Fish Res. 62 (3):295–305.

Cai WJ, Sayles FL. 1996. Oxygen penetration depths and fluxes in marine sediments. Mar Chem. 52 (2):123–131.

Campbell LG, Thrash, JC, Rabalais NN, Mason OU. 2019. Extent of the annual Gulf of Mexico hypoxic zone influences microbial community structure. PloS one. 14(4):e0209055.

Childs CR, Rabalais NN, Turner RE, Proctor LM. 2002. Sediment denitrification in the Gulf of Mexico zone of hypoxia. Mar Ecol Prog Ser. 240:285–290.

Couvillion BR, Beck H, Schoolmaster D, Fischer M. 2017. Land area change in coastal Louisiana (1932 to 2016), pamphlet to accompany Scientific Investigation Map 3381. Washington (DC): US Geological Survey. 16 p. https://doi.org/10.3133/sim3381.

[CPRA] Coastal Protection and Restoration Authority of Louisiana. 2017. Louisiana's comprehensive master plan for a sustainable coast. 93 p. Baton Rouge (LA): Coastal Protection and Restoration Authority of Louisiana.

Dalsgaard T, ed. 2000. Protocol handbook for NICE—nitrogen cycling in estuaries: a project under the EU research programme: marine science and technology (MASTIII). Silkeborg (DK): National Environmental Research Institute. 62 p.

Fennel K, Wilkin J, Levin J, Moisan J, O'Reilly J, Haidvogel, D. 2006. Nitrogen cycling in the Middle Atlantic Bight:rResults from a three–dimensional model and implications for the North Atlantic nitrogen budget. Global Biogeochem Cycles. 20:1–14.

Flocks F, Franze C. 2002. Environmental issues–dredge pit characterization, environmental atlas of the Lake Pontchartrain Basin. In: Penland S, Beall A (University of New Orleans, LA; Kindinger J, US Geological Survey) Environmental atlas of the Lake Pontchartrain Basin. New Orleans (LA): US Geological Survey. USGS Open File Report 02-206. [accessed 4 Oct 2023]; https://pubs.usgs.gov/of/2002/of02-206/env-issues/pit-characterization.html

Gardner WS, McCarthy MJ, An S, Sobolev D, Sell KS, Brock D. 2006. Nitrogen fixation and dissimilatory nitrate reduction to ammonium (DNRA. support nitrogen dynamics in Texas estuaries. Limnol Oceanogr, 51(1):558–568.

Ghaisas NA, Maiti K, White JR. 2019. Coupled iron and phosphorus release from seasonally hypoxic Louisiana shelf sediment. Estuarine Coast Shelf Sci. 219:81–89.

Glud RN. 2008. Oxygen dynamics of marine sediments. Mar Biol Res. 4 (4):243–289.

Graca B. 2009.The Puck Bay as an example of deep dredging unfavorably affecting the aquatic environment. Oceanol Hydrobiol Stud. 38 (2):109–127.

Graca B, Burska D, Matuszewska K. 2004.The impact of dredging deep pits on organic matter decomposition in sediments. Water Air Soil Pollut. 158 (1):237–259.

Grippo MA, Fleeger JW, Rabalais NN, Condrey R, Carman KR. 2010. Contribution of phytoplankton and benthic microalgae to inner shelf sediments of the north–central Gulf of Mexico. Cont Shelf Res. 30(5):456–466.

Grippo M, Fleeger JW, Condrey R, Carman KR. 2009. High benthic microalgal biomass found on Ship Shoal, north–central Gulf of Mexico. Bulletin of Mar Sci. 84(2):237–256.

Haidvogel DB, Arango H, Budgell WP, Cornuelle BD, Curchitser E et al. 2008. Ocean forecasting in terrain–following coordinates: formulation and skill assessment of the Regional Ocean Modeling System. J Comput Phys. 227:3595–3624.

Hedges JI, Turin HJ, Ertel JR. 1984. Sources and distributions of sedimentary organic matter in the Columbia River drainage basin, Washington and Oregon. Limnol Oceanogr. 29(1):35–46.

Heiri O, Lotter AF, Lemcke G. 2001. Loss on ignition as a method for estimating organic and carbonate content in sediments: reproducibility and comparability of results. J Paleolimnol. 25(1):101–110.

Hopkinson CS, Giblin AE, Tucker J, Garritt RH. 1999. Benthic metabolism and nutrient cycling along an estuarine salinity gradient. Estuaries. 22(4):863–881.

Ingall E, Jahnke R. 1994. Evidence for enhanced phosphorus regeneration from marine sediments overlain by oxygen depleted waters. Geochim Cosmochim Acta. 58 (11):2571–2575.

Johnston SA. 1981. Estuarine dredge and fill activities: a review of impacts. Environ Manag. 5(5):427–440.

Jørgensen BB. 1982. Mineralization of organic matter in the sea bed—the role of sulphate reduction. Nature. 296(5858):643.

Joye SB, Hollibaugh JT. 1995. Influence of sulfide inhibition of nitrification on nitrogen regeneration in sediments. Science. 270(5236):623–625.

Jutte PC, Van Dolah RF, Gayes PT. 2002. Recovery of benthic communities following offshore dredging, Myrtle Beach, South Carolina. Shore & Beach. 70 (3):25–30.

Karimpour A, Chen Q. 2017.Wind wave analysis in depth limited water using OCEANLYZ, A MATLAB toolbox. Comput Geosci. 106:181–189.

Kaste JM, Baskaran M. 2011. Meteoric 7Be and 10Be as process tracers in the environment. In: Baskaran M, editor. Handbook of environmental isotope geochemistry. Berlin (DE): Springer-Verlag. p. 61–85.

Keller G, Bentley SJ, Xu K, Maloney J, Miner M, Georgiou I. 2016. River–plume sedimentation and 210Pb/7Be seabed delivery on the Mississippi River delta front. Geo-Mar Lett. 37: 259–272.

Khalil SM, Finkl CW, Roberts HH, Raynie RC. 2010. New approaches to sediment management on the inner continental shelf offshore coastal Louisiana. J Coast Res. 26 (4):591–604.

Kim SC, Friedrichs, CT, Maa JY, Wright LD. 2000. Estimating bottom stress in tidal boundary layer from acoustic Doppler velocimeter data. J Hydraul Eng. 126 (6)399–406.

Kishi MJ, Kashiwai M, Ware DM, Megrey BA, Eslinger DL et al. 2007. NEMURO—a lower trophic level model for the North Pacific marine ecosystem. Ecol Modell. 202:12–25.

Kobashi D, Jose F. 2018. Potential Impacts of Sand Mining on Hydrodynamics and Fine Sediment Suspension and Deposition on an Inner–shelf Shoal. J Coast Res. 81:76–85.

Lee T, Kim HC, Son YB. 2019. Sediment oxygen consumption and hydrogen sulfide release in hypoxic areas of Gamak Bay, Korea. Appl Ecol Environ Res. 17(2):3199–3214.

Lehrter JC, Beddick DL, Devereux R, Yates DF, Murrell MC. 2012. Sediment–water fluxes of dissolved inorganic carbon, O2, nutrients, and N2 from the hypoxic region of the Louisiana continental shelf. Biogeochemistry. 109 (1–3):233–252.

Lehrter JC, Murrell MC, Kurtz JC. 2009. Interactions between freshwater input, light, and phytoplankton dynamics on the Louisiana continental shelf. Cont Shelf Res. 29 (15):1861–1872.

Lehrter J, Fry B, Murrell M. 2014.Microphytobenthos production potential and contribution to bottom layer oxygen dynamics on the inner Louisiana continental shelf. Bulletin of Mar Sci. 90(3):765–780.

Lentz SJ. 2001.The influence of stratification on the wind–driven cross–shelf circulation over the North Carolina shelf. J Phys Oceanogr,. 31(9):2749–2760.

Liu B, D'Sa E, Joshi I. 2019. Floodwater impact on Galveston Bay phytoplankton taxonomy, pigment composition and photo-physiological state following Hurricane Harvey from field and ocean color. Biogeosci Discuss. 1–29.

Liu H, Xu K, Li B, Han Y, Li G. 2019. Sediment identification using machine learning classifiers in a mixed–texture dredge pit of Louisiana Shelf for coastal restoration. Water. 11(6):1257.

Liu H, Xu K, Wilson C, Bentley S, Xue Z, Zhang Z. 2021. Geomorphologic response and patchy mud infilling in a sandy dredge pit in Ship Shoal, Louisiana shelf, USA. Geomorphology. 107983.

Lomas MW, Glibert PM, Shiah FK, Smith EM. 2002. Microbial processes and temperature in Chesapeake Bay: current relationships and potential impacts of regional warming. Global Change Biol. 8 (1):51–70.

Manap N, Voulvoulis N. 2016. Data analysis for environmental impact of dredging. J Cleaner Prod. 137:394–404.

McCarthy MJ, Carini SA, Liu Z, Ostrom NE, Gardner WS. 2013. Oxygen consumption in the water column and sediments of the northern Gulf of Mexico hypoxic zone. Estuarine Coast Shelf Sci. 123:46–53.

McCarthy MJ, McNeal KS, Morse JW, Gardner WS. 2008. Bottom–water hypoxia effects on sediment–water interface nitrogen transformations in a seasonally hypoxic, shallow bay (Corpus Christi Bay, TX, USA). Estuaries Coasts. 31(3):521–531.

McManus J, Berelson WM, Coale KH, Johnson KS, Kilgore TE. 1997. Phosphorus regeneration in continental margin sediments. Geochim Cosmochim Acta. 61(14):2891–2907.

Moore LJ, Patsch K, List JH, Williams SJ. 2014. The potential for sea–level–rise–induced barrier island loss: insights from the Chandeleur Islands, Louisiana, USA. Mar Geol. 355:244–259.

Nairn RB, Lu Q, Langendyk SK (Baird & Associates, Madison, WI; Research Planning, New Orleans, LA). 2005. A study to address the issue of seafloor stability and the impact on oil and gas infrastructure in the Gulf of Mexico. New Orleans (LA): US Department of the Interior, Minerals Management Service. Obligation No.: 1435-01-04-CT-335085. Report No.: OCS Study MMS 2005-043.

Nairn R, Johnson JA, Hardin D, Michel J. 2004. A biological and physical monitoring program to evaluate long–term impacts from sand dredging operations in the United States outer continental shelf. J Coast Res. 20(1):126–137.

Nunnally CC, Quigg A, DiMarco S, Chapman P, Rowe GT. 2014. Benthic–pelagic coupling in the Gulf of Mexico hypoxic area: Sedimentary enhancement of hypoxic conditions and near bottom primary production. Cont Shelf Res. 85:143–152.

O'Connor M. 2017. Sediment infilling of Louisiana Continental–shelf dredge pits: a record of sedimentary processes in the northern Gulf of Mexico [thesis]. Baton Rouge: Louisiana State University. 64 p.

Obelcz J, Xu K, Bentley SJ, O'Connor M, Miner MD. 2018. Mud–capped dredge pits: An experiment of opportunity for characterizing cohesive sediment transport and slope stability in the northern Gulf of Mexico. Estuarine Coast Shelf Sci. 208:161–169.

Obelcz J, Xu K, Georgiou IY, Maloney J, Bentley SJ, Miner MD. 2017. Subdecadal submarine landslides are important drivers of deltaic sediment flux: Insights from the Mississippi River Delta Front. Geology. 45 (8):703–706.

Otvos EG. 2012. Coastal barriers—Nomenclature, processes, and classification issues. Geomorphology. 139:39–52.

Paerl HW, Valdes LM, Pinckney JL, Piehler MF, Dyble J, Moisander PH. 2003. Phytoplankton photopigments as indicators of estuarine and coastal eutrophication. BioScience. 53(10):953–964.

Pakulski JD, Benner R, Whitledge T, Amon R, Eadie B, Cifuentes L, Stockwell D. 2000. Microbial metabolism and nutrient cycling in the Mississippi and Atchafalaya River plumes. Estuarine Coast Shelf Sci. 50(2):173–184.

Palmer TA, Montagna PA, Nairn, RB. 2008.The effects of a dredge excavation pit on benthic macrofauna in offshore Louisiana. Environ Manag. 4(4):573–583.

Penland S, Suter JR. 1988. Barrier island erosion and protection in Louisiana: A coastal geomorphological perspective. Gulf Coast Assoc Geol Soc Trans., 38:331–342

Penland S, Boyd R, Suter JR. 1988. Transgressive depositional systems of the Mississippi Delta plain; a model for barrier shoreline and shelf sand development. J Sediment Res. 58(6):932–949

Pinckney JL, Millie DF, Vinyard BT, Paerl HW. 1997. Environmental controls of phytoplankton bloom dynamics in the Neuse River estuary (North Carolina, USA). Can J Fish Aquat Sci. 54:2491–2501.

Pinckney JL, Paerl HW, Harrington MB, Howe KE. 1998. Annual cycles of phytoplankton community structure and bloom dynamics in the Neuse River Estuary, North Carolina. Mar Biol. 131:371–382.

Rabalais NN, Atilla N, Normandeau C, Turner ER. 2004. Ecosystem history of Mississippi River–influenced continental shelf revealed through preserved phytoplankton pigments. Mar Pollut Bull. 49(7):537–547.

Restreppo GA, Bentley SJ, Wang J, Xu K. 2019. Riverine sediment contribution to distal deltaic wetlands: Fourleague Bay, LA. Estuaries Coasts. 42(1):55–67.

Robichaux P, Xu K, Bentley SJ, Miner MD, Xue ZG. 2020. Morphological evolution of a mud–capped dredge pit on the Louisiana shelf: Nonlinear infilling and continuing consolidation. Geomorphology. 354:107030.

Rowe GT, Morse J, Nunnally C, Boland GS. 2008. Sediment community oxygen consumption in the deep Gulf of Mexico. Deep Sea Res Part II. 55(24–26):2686–2691.

Sampou P, Oviatt CA. 1991. A carbon budget for a eutrophic marine ecosystem and the role of sulfur metabolism in sedimentary carbon, oxygen and energy dynamics. J Mar Res. 49 (4):825–844.

Santschi PH, Presley BJ, Wade TL, Garcia–Romero B, Baskaran M. 2001. Historical contamination of PAHs, PCBs, DDTs, and heavy metals in Mississippi River Delta, Galveston Bay and Tampa bay sediment cores. Mar Environ Res. 52(1):51–79.

Seitzinger S, Harrison JA, Bohlke JK, Bouwman AF, Lowrance R, Peterson B, Tobias C, Van Drecht G. 2006. Denitrification across landscapes and waterscapes: a synthesis. Ecol Appl. 16:2064–2090.

Shchepetkin AF, McWilliams JC. 2005. The regional oceanic modeling system (ROMS) A split–explicit, free–surface, topography–following–coordinate oceanic model. Ocean Model. 9:347–404

Shropshire TA, Steven LM, Chassignet PC, Bozec A, Coles VJ, Landry MR, Swalethorp R, Zapfe G Stukel MR. 2020. Quantifying spatiotemporal variability in zooplankton dynamics in the Gulf of Mexico with a physical–biogeochemical model. Biogeosciences. 17(13):3385–3407.

Sørensen J. 1982. Reduction of ferric iron in anaerobic, marine sediment and interaction with reduction of nitrate and sulfate. Appl Environ Microbiol. 43(2):319–324.

Soulsby RL, Dyer KR.1981.The form of the near-bed velocity profile in a tidally accelerating flow. J Geophys Res: Oceans. 86(C9):8067–8074.

Stone GW, McBride RA. 1998. Louisiana barrier islands and their importance in wetland protection: forecasting shoreline change and subsequent response of wave climate. J Coast Res. 14(3):900–915.

Stone GW, Pepper DA, Xu J, Zhang X. 2004. Ship Shoal as a prospective borrow site for barrier island restoration, Coastal south–central Louisiana, USA: Numerical wave modeling and field measurements of hydrodynamics and sediment transport. J Coast Res. 20(1):70–88

Strickland JDH, Parsons TR. 1972. Determination of reactive silicate. A practical handbook of seawater analysis. Fish Res Board Can. Bulletin 167, 65–70.

Szymelfenig M, Kotwicki L, Graca B. 2006. Benthic re–colonization in post–dredging pits in the Puck Bay (Southern Baltic Sea). Estuarine Coast Shelf Sci. 68(3–4):489–498

Thompson L, Maiti K, White JR, Dufore CM, Liu H. 2021. The impact of recently excavated dredge pits on coastal hypoxia in the northern Gulf of Mexico shelf. Mar Environ Res. (163): 105199. doi: https://doi.org/10.1016/j.marenvres.2020.105199.

Turner RE, Rabalais NN, Justic D. 2008. Gulf of Mexico hypoxia: alternate states and a legacy. Environ Sci Technol. 42(7):2323–2327.

Upreti K, Maiti K, Rivera–Monroy, VH. 2019. Microbial mediated sedimentary phosphorus mobilization in emerging and eroding wetlands of coastal Louisiana. Sci Total Environ. 651:122–133.

Valentine K, Mariotti G. 2020. Does eutrophication affect the ability of biofilms to stabilize muddy sediments? Estuarine Coast Shelf Sci. 232: 106490.

Walker ND. 1996. Satellite assessment of Mississippi River plume variability: causes and predictability. Remote Sens Environ. 58(1):21–35.

Wang J, Xu K, Li C, Obelcz J. 2018.Forces driving the morphological evolution of a mud–capped dredge pit, northern Gulf of Mexico. Water. 10(8):1001.

Wang SQ, Ishizaka J, Hirawake T, Watanabe Y, Zhu YL, Hayashi M, Yoo S. 2015. Remote estimation of phytoplankton size fractions using the spectral shape of light absorption. Optics Express. 23 (8):10301–1031

Warner JC, Armstrong B, He R, Zambon JB. 2010. Development of a Coupled Ocean–Atmosphere–Wave–Sediment Transport (COAWST) modeling system. Ocean Model. 35(3): 230–244.

Warner JC, Sherwood CR, Signell, RP, Harris CK, Arango HG. 2008. Development of a three–dimensional, regional, coupled wave, current, and sediment–transport model. Comput Geosci. 34 (10): 1284–1306.

Whitehouse RJS, Soulsby RL, Roberts W, Mitchener HJ. 2000. Dynamics of estuarine muds: a manual for practical applications. London (GB): Thomas Telford.

Wiberg PL, Sherwood CR. 2008. Calculating wave–generated bottom orbital velocities from surface–wave parameters. Comput Geosci. 34(10):1243–1262.

Wright LD, Sherwood CR, Sternberg RW. 1997. Field measurements of fair-weather bottom boundary layer processes and sediment suspension on the Louisiana inner continental shelf. Mar Geol. 140(3–4):329–345.

Xu KH, Bentley SJ, Robichaux P, Sha X, Yang H. 2016. Implications of texture and erodibility for sediment retention in receiving basins of Coastal Louisiana diversions. Water. 8(1): 26. doi:10.3390/w8010026.

Xue Z, Wilson C, Xu K, Bentley S, Liu H. 2021. Sandy Borrow Area sedimentation—characteristics and processes within South Pelto Dredge Pit on Ship Shoal, Louisiana Shelf, USA. Estuaries Coasts. 4: 658–676. https://doi.org/10.1007/s12237-021-00975-6.

Xue, Z. Sandy dredge pit sedimentation – characteristics and processes in Caminada Borrow Area, Ship Shoal, Louisiana Shelf, USA [thesis]. Baton Rouge: Louisiana State University. 71 p.

Zhang JZ, Ortner PB, Fischer CJ. 1997. EPA Method 353.4: Determination of nitrate and nitrite in estuarine and coastal waters by gas segmented continuous flow colorimetric analysis. Revision 2.0 September 1997. Cincinnati (OH):US Environmental Protection Agency. Report No.: DCEPA–600–R–97–072.

Zhang W, White JR, DeLaune RD. 2012. Diverted Mississippi River sediment as a potential phosphorus source affecting coastal Louisiana water quality. J Freshwater Ecol. 27 (4):575–586.

Department of the Interior (DOI)

The Department of the Interior protects and manages the Nation's natural resources and cultural heritage; provides scientific and other information about those resources; and honors the Nation’s trust responsibilities or special commitments to American Indians, Alaska Natives, and affiliated island communities.

BOEM
Bureau of Ocean Energy Management

Bureau of Ocean Energy Management (BOEM)

The mission of the Bureau of Ocean Energy Management is to manage development of U.S. Outer Continental Shelf energy and mineral resources in an environmentally and economically responsible way.

BOEM Environmental Studies Program

The mission of the Environmental Studies Program is to provide the information needed to predict, assess, and manage impacts from offshore energy and marine mineral exploration, development, and production activities on human, marine, and coastal environments. The proposal, selection, research, review, collaboration, production, and dissemination of each of BOEM’s Environmental Studies follows the DOI Code of Scientific and Scholarly Conduct, in support of a culture of scientific and professional integrity, as set out in the DOI Departmental Manual (305 DM 3).